TITOLO TESI

Experimental and Numerical Evaluation of Impact Damage Tolerance in composite materials

Presentata da: Falaschetti Maria Pia

Index

Introduction

Composite materials have always been part of humankind history, but only with industrial application, a deep improvement was obtained. Since '70s, advanced composite materials were introduced in many fields: aerospace, aeronautics, automotive, sports, etc. Different kinds of resins and fibres were studied and developed, in order to achieve several aims and to take advance of the most important composites usefulness, i.e. their adaptability to various load and structure conditions.

At the same time, however, composites drawbacks were acknowledged: due to their 'multiple' nature, load bearing, damage evolutions and external environment influence, are completely far from metal materials, which have been studied for ages. Therefore, aerospace and aeronautic industry, due to the necessity of lighter and safer structures, started a deep research on composite behaviour under operative conditions to be able to overcome material issues.

Aeronautic field is mostly interested in Polymer Matrix Composites due to their high strength, high stiffness, fatigue resistance, low weight and corrosion resistance. In particular, their better strength to weight ratio, compared to metals (Figure 1-2), is probably the main reason that boosted their application.

Many studies were performed to better understand composite mechanical characteristics and their response to operative environment. This allowed this kind of material usage in wide sections of airplane structures, where, as known, safety is the most important issue for builders (Figure 3-4).

Only few characteristics are still unknown and, therefore, safety factors higher, than those theoretically necessary, are needed. In particular, predicting composite vulnerability to an impact is a major issue. Many events could cause an impact on an aeronautic structure: bird strike, hail, luggage loading, handling service, etc. Each one of these causes results in a different kind of impact and a damage more or less detectable (Figure 5).
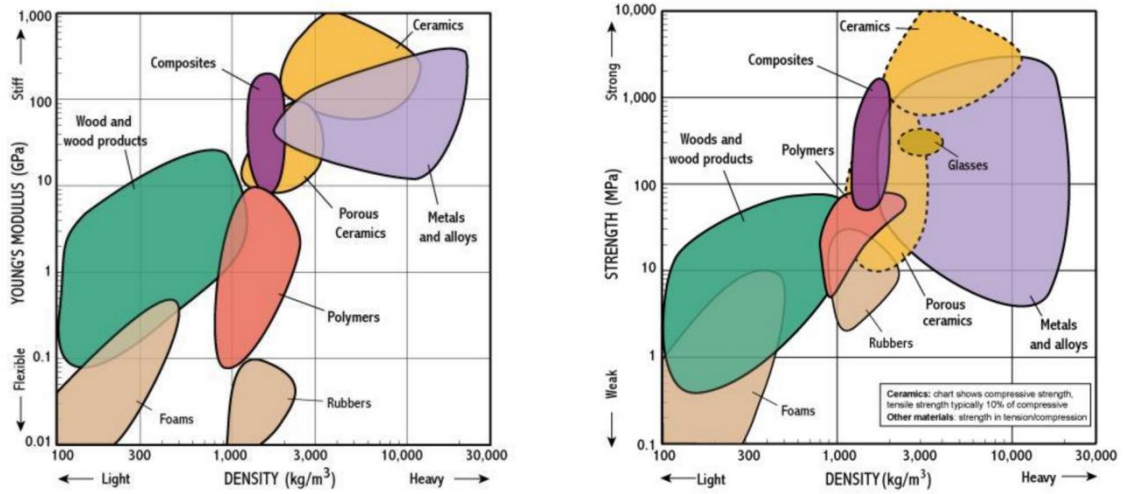
Figure 1: materials strength and Young moduli values referring to density
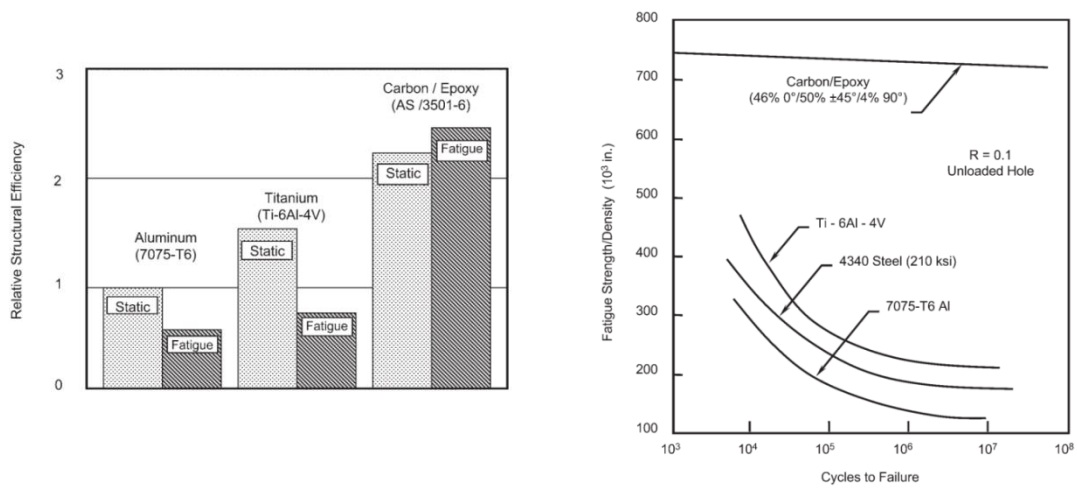
Figure 2: comparison between metals and composites fatique characteristics
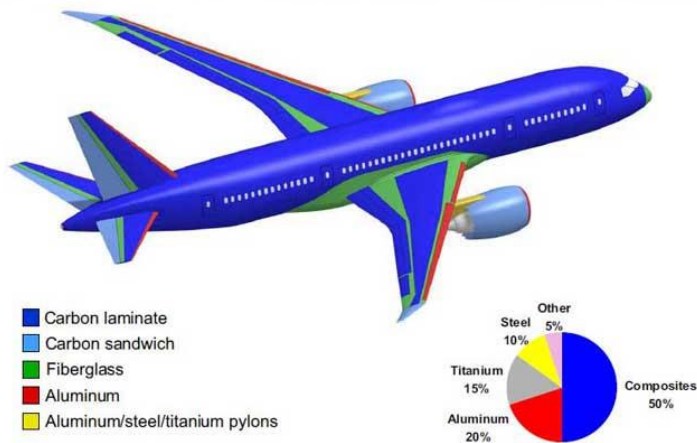
Figure 3: Boeing 787 dreamliner: materials distribution
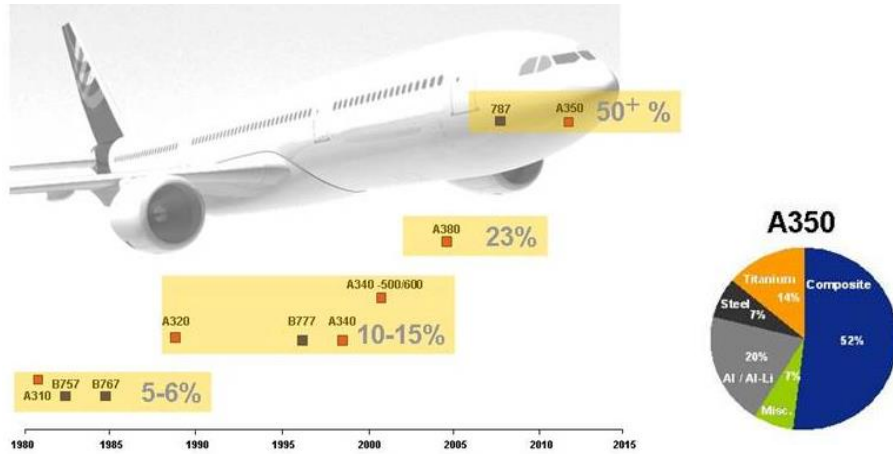
Figure 4: Airbus A350: material content by weight
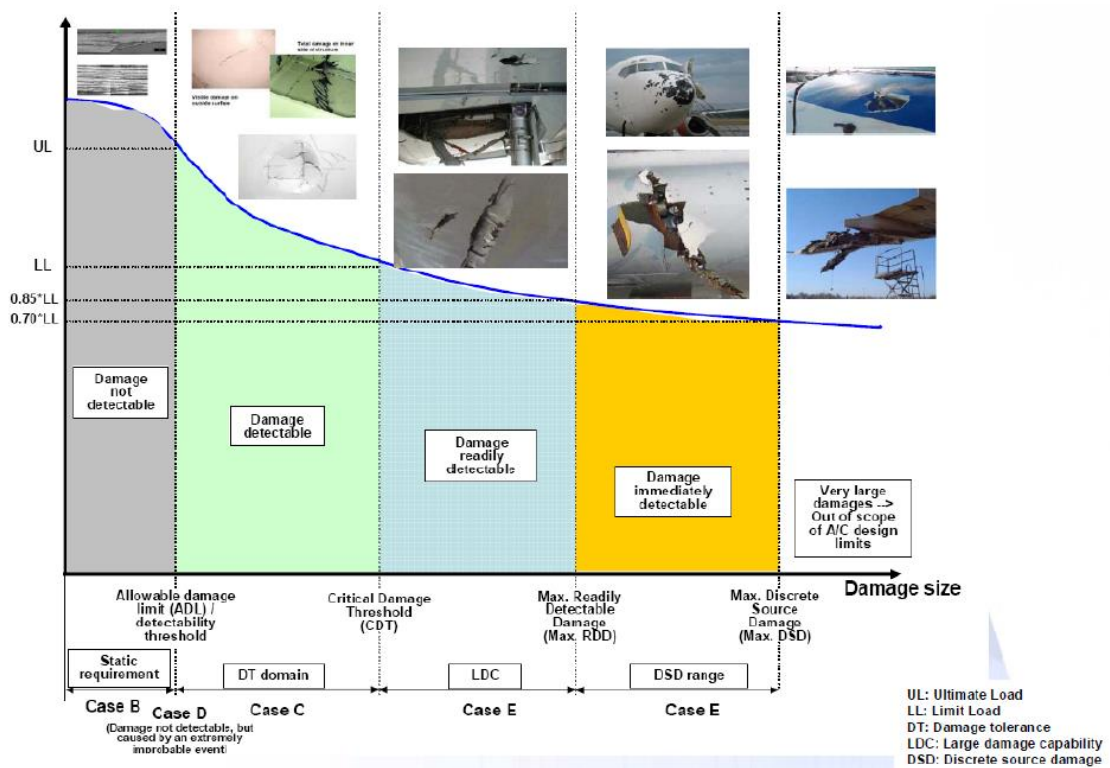
Figure 5: Different kinds of impact and structure residual strength

The most dangerous impact kind is the low energy impact: it could result in no damage evidence on the impacted surface, creating a wide damage inside the laminate. Therefore, there could be a reduction of structure characteristics, leading to a catastrophic failure before any evidence appears on external surface.

Hence, a better understanding on composite response to impact event and their after impact characteristics is necessary.

Principal aim of this PhD work was to develop a deeper comprehension of CFRP (Carbon Fibre Reinforced Plastic) behaviour under dynamic loads. Therefore, experimental and numerical results, of three years research, will be presented.

In particular:

Chapter 1 presents a brief introduction to Damage Tolerance design concept. This is the most advanced design criteria developed in aeronautic: it treasures all lessons learned from past airplane accidents and it is open to new raising concept, in order to create better structures. An example are guiding rules applied to composites; there is not a strict written path: beside safety requirements, industries are free to develop their internal methodologies and this is a good way to achieve a wider understanding of composites characteristics.

Chapter 2 concentrates on impact issues in aerospace fields, with particular attention to its interest development through aerospace and aeronautic history. Principal composite damages are described, focusing on low velocity impact damages.

Chapter 3 describes impact test method designed and realised at Hangar Laboratories of University of Bologna in Forlì. Charpy pendulum concept has been studied and modified to achieve low velocity impact tests and, therefore, Barely Visible Impact Damage (BVID).

Chapter 4 describes all Compression After Impact (CAI) and composite compression tests fixtures, with particular attention to Combined Loading Compression test Fixture that was used for all experimental campaigns performed in this PhD research.

Chapter 5 shows results from two experimental campaigns, regarding low energies impacts and BVID on carbon/epoxy composite laminate. First campaign involves 2.6 mm thick specimens while the second one is related to 5.5 mm thick specimens, giving opportunity to compare thickness influence of impact damages on residual compressive strength.

Chapters 6 and 7 focus on research work done during stay at TU Delft University. Trying to find an improvement for composite impact resistance, research led to Fibre Metal Laminate study. Therefore, taking the chance to be at the University which developed this kind of material, a deeper study related to aluminium layers position inside a stacking sequence was carried out. Quasi Static Indentation tests were performed and results are presented.

Chapter 8 is a brief introduction to Finite Element Theory, in particular to cohesive element theory, while Chapter 9 illustrates FE Model and results regarding simulations of impacts on carbon/epoxy and FML coupons that have been developed.

1

Damage Tolerance:

Aeronautics requirements

In this first chapter, after a brief history related to aeronautic requirements evolution, an introduction to Damage Tolerance philosophy is presented; in particular, composites regulations and application of No-Growth concept are described.

1.1   Hystory of airplane design development

Building airplanes has always been a difficult issue for who wanted to achieve fly. Many difficulties were faced by researchers but it was an interesting challenge: the first important proof of flying machines can be found during Renascence, in particular in 1485 when Leonardo da Vinci studied one of the first ornithopters and the first example of helicopter (Figure 1.1).
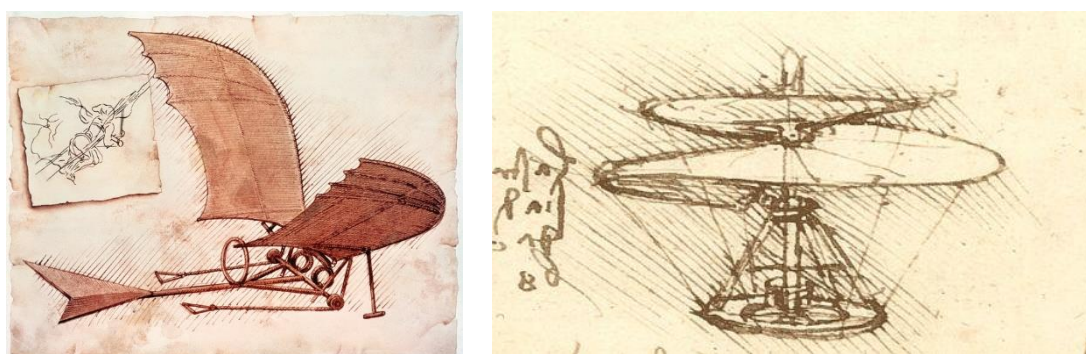
Figure 1.1: Leonardo da Vinci's ornithopter and helicopter

Other attempts were made but no one could really achieve this goal before Wright brothers. They tried many times before the day that is still considered the first flight of a motorized airplane controlled by a pilot: 17th December 1903. The Wright Flyer (Figure

1.2) is still considered the first airplane and it marks the beginning of modern airplanes history, even for what is related to resistance, reliability and endurance tests.
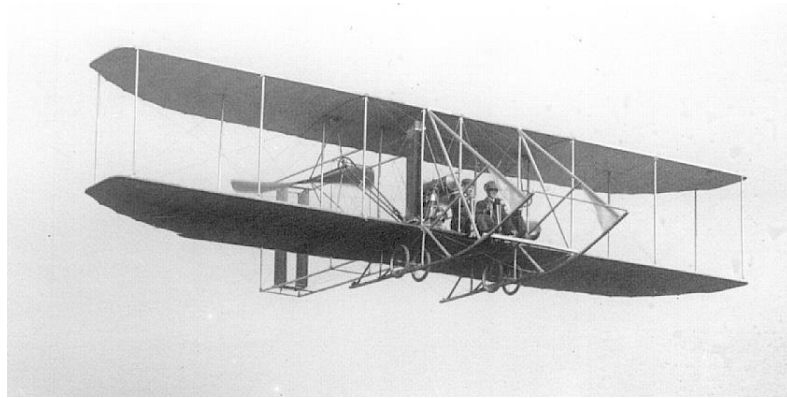
Figure 2.2: Wright Flyer

Those first airplanes were made with wood and canvas but only static tests were performed. Operative life or fatigue damages were not taken into account. An example is given by Fokker airplanes used during First World War (Fokker E.III, Fokker Dr.I, Fokker D.VII). For Fokker industry founder, Dutch pioneer and industrialist Antony Fokker, fatigue does not occur in seasoned wood. Nowadays it is well known that this is not true, and that fatigue is a structural phenomenon. But back in twenties, when airplanes were a new concept, seen as new weapon, and therefore used only during war, there was not any chance to actually develop fatigue damages.

During thirties, metal materials were introduced together with Safe-Life design concept. Structure Safe-life represents the number of events (such as flights, landings, or flight hours) during which probability to have a reduction of strength, under its design ultimate value, due to fatigue cracking, is very low.

Hence, it is assumed that fatigue failure is not going to occur during structure life and after this period the element is completely replaced by a new one (Safety-by-retirement). In that era, this approach still worked due to quite short airplanes operative life (caused by external factors); but when for economic reasons there was need for longer design lives, materials used where substituted with stronger alloys and, for a lower fuel consumption, higher altitudes were preferred. Hence, fatigue problems started and, with them, the necessity to change regulations.

The main event that made this necessity evident was the double accident of two Comet planes in 1954: those two airplanes were designed with Safe-Life concept and they crushed after 1286 and 903 flights due to a crack started from a window corner and propagated really fast, resulting in a fuselage explosion at cruise altitude. During design, full scale tests were performed and fatigue cracks were found after 16000 flights, so

accidents were totally unexpected after so lower number of flights; this was caused by an un-conservative way of testing: for fatigue tests was used the same airplane used before for static tests. Therefore, during static testing local plasticity was reached and this created a barrier for fatigue cracks growth under cyclic loads, resulting in a longer fatigue life than that of a really new airplane.

Hence, Fail-Safe methodology was therefore introduced: Fail-Safe is the attribute of the structure permitting to bear required residual strength for a period of un-repaired use even after failure or partial failure of a principal structural element. This means that, even with a fatigue or other cause damages, airplane has to safely bear flights loads: this kind of concept is also called Safety-by-design and it is achieved with 'multiple structural member concept' that consists of having redundancy of principal structures. But unfortunately, even this design method was not enough to prevent other accidents: first of all, a proper inspection plan is not defined and moreover there is not any concept of pre-existed flaws. Finally, due to economic reasons, airplanes later started to be used for very long time (longer than their design retirement period) and with Fail-Safe there was not any reference to aged planes.

In 1973 a F111 crashed due to the failure of one of its wings caused by growth of an initial flaw. This event demonstrated that assuming structures perfect when new, is completely un-real. Lately, in 1977 in Lusaka an airliner lost its entire horizontal stabilizer after it being redesigned for a higher take-off weight (from a passenger airliner it became a cargo one). This accident was caused by a fatigue crack in upper spar cap at bolt hole that was not detected due to not proper inspections and warnings for high bolt loads not taken into account. Other aged airplanes lately showed the same kind of cracks and they were also reproduced by full scale tests, that were not performed before releasing airplane.

These two accidents demonstrated which weak points were in Fail-Safe concept and led to a new design method: Damage Tolerance. With this term, it is called the ability of the structure to sustain anticipated loads in the presence of damage (due to fatigue, corrosion or external events) until it is detected through inspections or malfunctions and it is repaired.

Hence, with this methodology imperfections are assumed to be present even in new pieces, inspectability needs to be assured, inspections plans are defined and structures have to bear load until fatigue, corrosion or impact damages are detected and repaired (Safety-by-inspections). It is worth to notice that with Damage Tolerance introduction, the other concepts are not replaced: there still are structures that cannot be designed following DT requirements and therefore are designed under Safe-Life or Fail-Safe methods (Figure 1.3).

CGL = Crack growth Life
LP = Load path
a_{det} = detectable crack length
a_{cr} = critical crack length

(1) LP_1 crack growth, not affected by LP_2
(2) LP_2 crack growth, without failure of LP_1
(3) LP_2 crack growth, after failure of LP_1
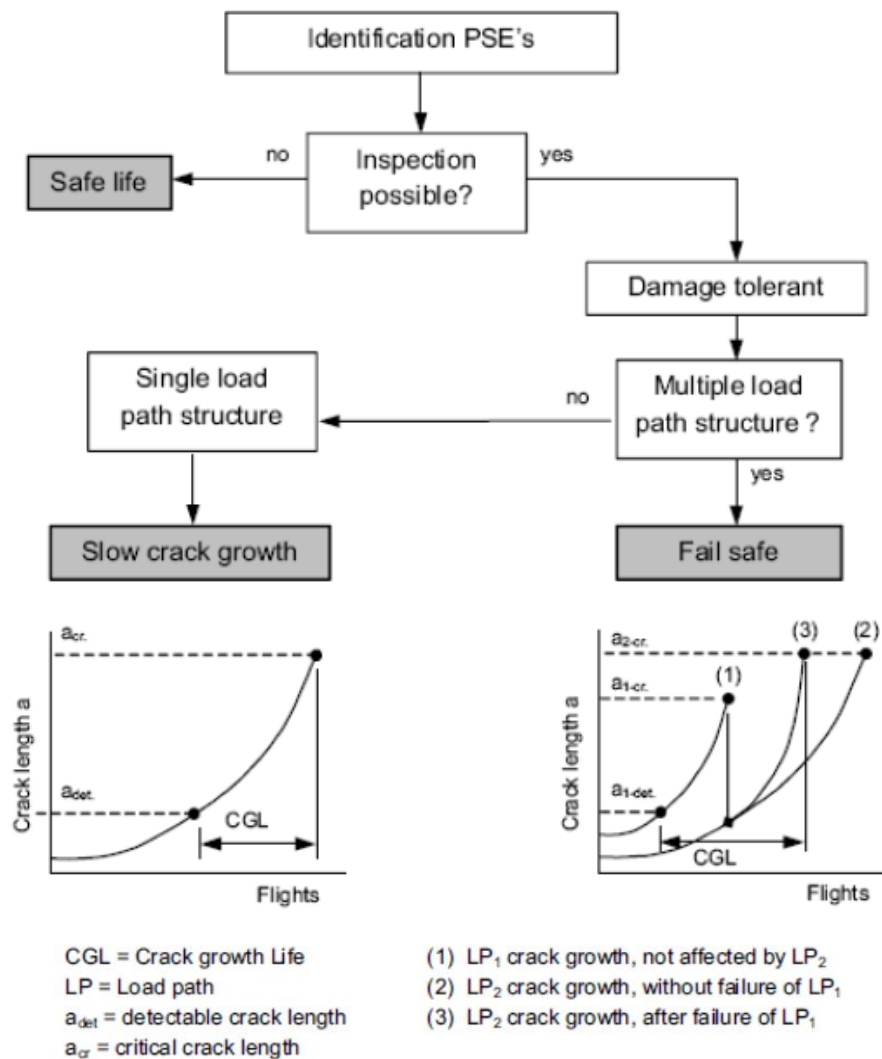
Figure 1.3: Airplane design methodology

Unfortunately, there was need to another accident to learn another aspect that DT did not take into account until 1988. That year a Boing 737 of Aloha airline succeeded in landing with a large part of upper fuselage missing. This was caused by 'Multiple Site Damage', i.e. many different cracks nucleated in different locations (in this case around riveted joints) grew and got connected all together resulting in a huge damage and in catastrophic failure. The cause of this was placed in insufficient inspections in relation with the operative environment where that airplane was flying: Hawaii islands with a flight period of 45 min per flight, so short ground-air-ground cycles in a warm, humid and salty environment. That kind of conditions accelerated MSD growth in cold bond/riveted lap joints: bond was damaged and it could not bear load anymore, transferring all of that to rivets creating stress concentrations and hence multiple fatigue damages.

After this accident, Widespread Fatigue Damage concept was introduced in regulation; in particular, they were acknowledged two different concepts: Multiple Site Damage, when there are many cracks in the same structural element, and Multiple Element Damage, when cracks are present within similar adjacent elements. The importance of these two new concepts introduction is very clear analysing Delta Boing 727 MSD discovery: during pre-flight walk around, pilots noticed two cracks growing under a lap joint; disassembly the joint, a 500mm long crack was discovered. This was a lucky case that prevented a probable catastrophic failure and many fatalities to occur.

1.2   Damage Tolerance phylosophy

Aeronautical design laws take into account many different perspectives:

- undamaged structure static resistance: structure must bear ultimate load (UL) for 3 sec, without any failure;
- undamaged structure deformation: there must not be any everlasting deformation if structure is loaded under Limit Load (LL) and, if there is any at LL, this must not affect flight safeness;
- fatigue crack nucleation in an undamaged structure: Damage Tolerance parts must satisfy durability requests while Safe Life parts must be pristine until the end of their operative lives;
- fatigue crack growth in damage structure: for DT parts inspection plans and NDI techniques must be well set up to reduce catastrophic failures;
- damaged structure static residual strength: damage structures must bear LL without any catastrophic failure.

Here a deeper description of Damage Tolerance philosophy, related to the last three points and more affecting design costs and airplanes safeness.

As already said, aeronautic structures face hard operative conditions and are subjected to complex load cycles. These affect considerably their durability and mechanical characteristics: cyclic loads could create new cracks or accelerate already existing damages (due to flaws in the material or caused by accidental impacts) growth. It is, hence, necessary to know static resistance of a damaged structure. This is defined as Residual Strength (RS) and it takes into account actual damage evolution during operative life. During structure operative life, in fact, due to loads or external parameters, cracks tend to growth with different rates decreasing Residual Strength.

The DT philosophy is presented, in short, in Figure 1.4:

- an initial damage is considered already present in the structure, even if NDI (Non Destructive Inspection) has not find any out; it is considered equal to the smallest NDI sensitivity, i.e. the smallest damage detectable (a_0);

- minimum detectable damage size (during inspections) is indicated with a_{det};
- structure Residual Strength decreases with damage growth: it is necessary, therefore, to detect damage before its size is equal to a_{cr} (critical damage size), where RS reaches LL values; detecting and repairing damage before reaching a_{cr}, it is possible to bring RS back to higher values and, hence, far from catastrophic failure chances.
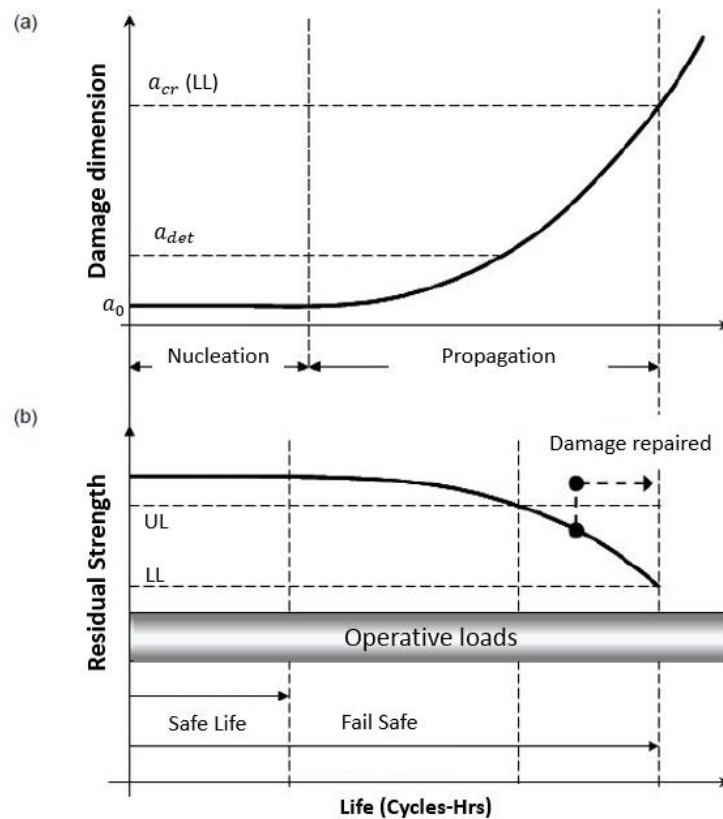
Figure 1.4: Damage Tolerance design graphs: (a) crack growth,
(b) residual strength, both referring to fatigue loads cycles

1.2.1 Damage Tolerance design

Fatigue and Damage Tolerance requirements are listed into part 25 of Section 571 of European Joint Airworthiness Requirements (JAR) and of American Federal Aviation Regulation (FAR) [1.1].

It is required that, each Principal Structural Element (PSE) must be identified and designed following DT philosophy due to their contribution to load bearing and airplane safety. An Inspection plan must be developed per each PSE in order to detect damages and repair them as soon as possible, before critical dimensions are reached.

As already said, if inspections are not possible (due to part position or inspections frequency is too high), it is necessary to follow Safe Life design approach. Hence, it is defined part operative life (Design Service Goal), in which no damages should nucleate.

At the end of this DSG, that part is substituted. This design concept is more expensive than DT due to higher safety factors applied and high rate of waste (when a piece is substituted, is cannot be used again) (Figure 1.5).
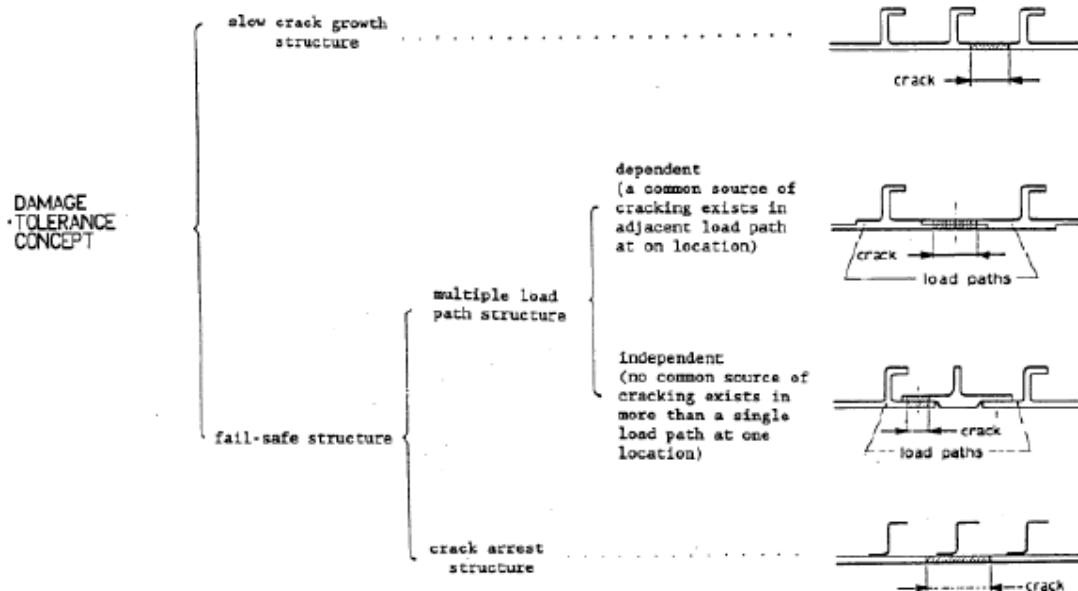
Figure 1.5: Damage Tolerance Design [1.3]

Ergo, as showed in Figure 1.1, if it is not possible to have inspection on an airplane part, this must be designed as Safe Life. If inspection is possible, Slow Crack Growth needs to be proved.

Slow Crack Growth concept is applied on those structure were load has to follow a single path, i.e. there is no other way to share that load and, therefore, any damage tends to growth only on that part. This philosophy says that, during airplane design, all precautions, related to geometry and materials, must be applied in order to obtain a crack growth as slow as possible. This leads to a longer time for damage detection without safe issues. In this way, supposing a pre-existent flaw, inspection plan is obtained dividing structure Crack Growth Life, i.e. number of cycles or flight hours for a damage to growth from a_{det} to a_{cr}, by a Safety Factor. The latter is function of many factors but usually it is around 2÷3.

When Slow Crack Growth cannot be demonstrated, other aeronautic concept is needed: Fail Safe. This philosophy is based on three principles:

- Redundancy: even if a structure fails, there is another one carrying out the same aim;
- Multi Load Path structures: loads are spread out between more ways in order to, if one of them is stopped due to a damage, others can keep carrying out loads;
- Crack Arrest structures: thanks to materials or geometry they oppose against damage growth.

Therefore, a Fail-Safe structure is able to bear loads even if badly damaged, until inspections (that, hence, can be more relaxed). In fact, in the Advisory Circular 25.571, it is referred as: "Fail-Safe is the attribute of the structure that permits it to retain its required residual strength for a period of unrepaired use after the failure or partial failure of a principal structural element".

1.2.2   Ageing structures

It is worth to notice that the described design criteria count for new airplanes: as already said, in fact, airplanes are designed for satisfy their Design Service Goal, i.e. a certain operative life span, but due to economical requests and aged airplane still good conditions, it was request to make them flight in safety a little longer. Hence, development of new line guides for aging airplanes [1.1].

Main issue is Widespread Fatigue Damage (WFD), i.e. contemporaneous presence of many damages. This could be Multiple Site Damage (MSD) or Multiple Element Damage (MED) (Figure 1.6).
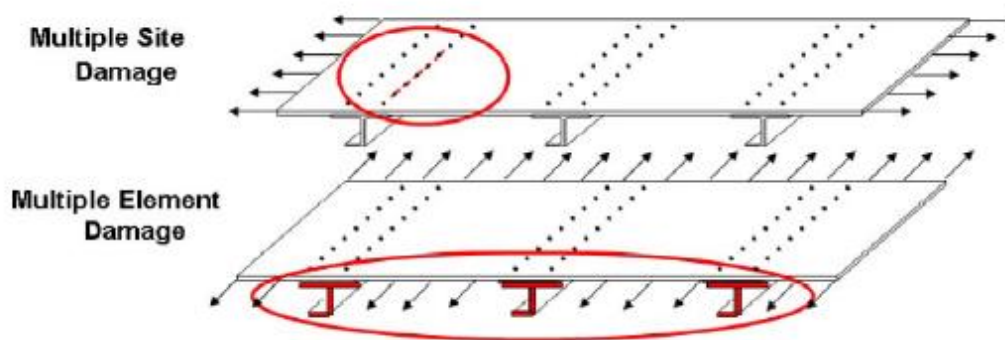
Figure 1.6: Multi Site Damage and Multiple Element Damage [4]

Multiple Site Damage happens when damages are on the same part and are geometrically similar carrying quite similar loads, e.g. riveting holes. Due to same driving force, fatigue cracks could nucleate and grow contemporary and, if cracks are close to each other, they could connect themselves and create a long crack, leading to a catastrophic failure way faster than a new structure (Figure1.7-1.8). Moreover, due to MSD, Crack Growth life is also shortened and more frequent inspections need to be performed. This could be not enough [1.5]; the only expedient to avoid dangerous situations is to design every airplane for avoiding WFD in all its operative life (Advisory Circular (AC) AC25.571-1C [1.1]), reducing load intensity in those areas where WFD could take place ('Damage Tolerance was not intended as a safety management tool for structures operating beyond their initial design life goals or beyond the point where WFD is likely to occur', [1.2].
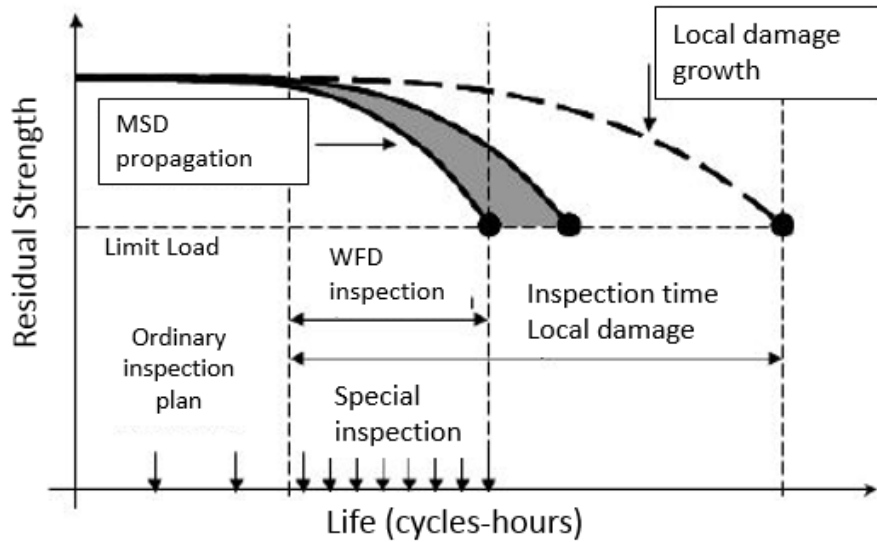
Figure 1.7: Residual strength with MSD
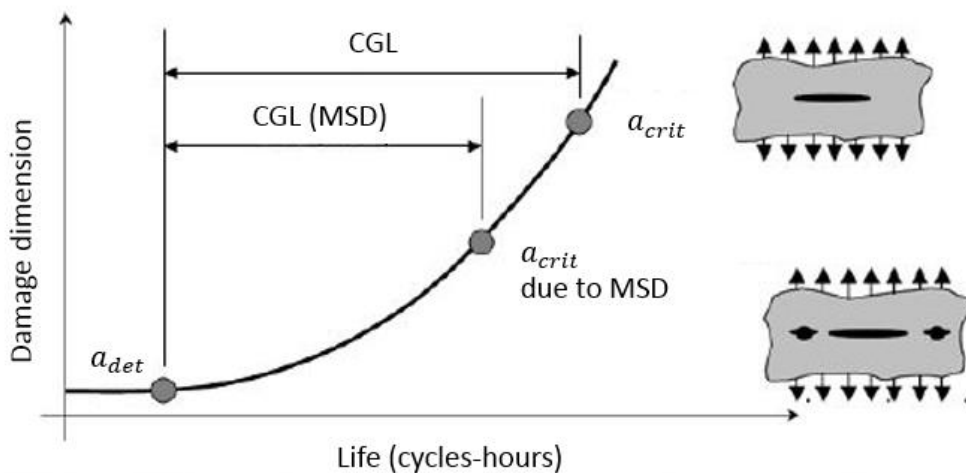
Figure 1.8: Smaller inspection gap due to smaller critical damage with MSD

In conclusion, nowadays, Damage Tolerance concept is obviously the most important and developed criteria that could be applied in airplane design. On the other hand, many things need to be sharpened a little more to obtain even safer requirements with a better usage of structures and materials.

It is worth to say that Damage Tolerance requirements do not put any limits on how to achieve them. Therefore, each industry can develop its own methods to build up safe and long lasting airplanes, even developing new and higher thresholds.

1.3 Composite Aeronautics regulations

Previously presented regulations are principally related to metallic materials. Advanced composite materials were introduced in the last thirty years and, due to their complexity and unpredictability, many operative behaviours are still unknown. Therefore, Airworthiness Regulations related to this kind of materials leaves more freedom to industries, pointing attention mostly on safety and damage 'no-growth' concept. In particular, peculiar wariness is granted to accidental damage during service life. In the following sections requirements are reported from original regulation documentations [8].

1.3.1 Airworthiness Regulations

> Static requirements (EASA certification Basis [1.8] Sec. 25.305)

Sec 25.305 (a): "The structure must be able to support limit loads without detrimental permanent deformation. At any load up to limit loads, the deformation may not interfere with safe operation."

Sec 25.305 (b): "The structure must be able to support ultimate loads without failure for at least 3 seconds. However, when proof of strength is shown by dynamic tests simulating actual load conditions, the 3-second limit does not apply."

> Damage Tolerance and Fatigue requirements (EASA certification Basis [1.8] Sec. 25.571)

Sec 25.571 (a): General "An evaluation of the strength, detail design, and fabrication just show that catastrophic failure due to fatigue, corrosion or accidental damage will be avoided throughout the operational life of the aeroplane. (…) Inspections or other procedures must be established as necessary to prevent catastrophic failure (…)"
Sec 25.571(b): Damage Tolerance (Fail-Safe) evaluation "The evaluation must include a determination of the probable locations and failure modes due to fatigue, corrosion, or accidental damage." (…) "The extent of damage for residual strength evaluation at any time within the operational life must be consistent with the initial detectability and subsequent growth under repeated loads. The residual strength evaluation must show that the remaining structure is able to withstand loads (considered as ultimate static loads) corresponding to the following conditions (…)".

> Acceptable Means of Compliance (AMC, non-inding guides used to transpose regulations into really applicable characteristics)

Sec 25.603 - 5: Proof of structure – Static

§ 5.3: "Static strength structural substantiation tests should be conducted on new structure unless the critical load conditions are associated with structure that has been subjected to repeated loading and environmental exposure. In this case either:

a) the static test should be conducted on structure with prior repeated loading and environmental exposure, or

b) Coupon/Element/Subcomponent test data should be provided to assess the possible degradation of static strength after application of repeated loading and environmental exposure and this degradation accounted for in the static test or in the analysis of the results of the static test of the new structure."

§ 5.8: "It should be shown that impact damage that can be realistically expected from manufacturing and service, but not more than the established threshold of detectability for the selected inspection procedure, will not reduce the structural strength below ultimate load capability."

Sec 25.603 – 6: Proof of structure – Fatigue/Damage Tolerance

§ 6.1: "(…) the following considerations are unique to the use of composite material systems and should be observed for the method of substantiation selected by the applicant. When selecting the damage tolerance or safe life approach, attention should be given to geometry, inspectability, good design practice, and the type of damage/degradation of the structure under consideration."

§ 6.2 Damage Tolerance (Fail-Safe) Evaluation

§ 6.2.1: "Structural details, elements, and subcomponents of critical structural areas should be tested under repeated loads to define the sensitivity of the structure to damage growth. This testing can form the basis for validating a no-growth approach to the damage tolerance requirements. (…)"

§ 6.2.2: "The extent of initially detectable damages should be established and be consistent with the inspection techniques employed during manufacturing and in service. (…)"

§ 6.2.3: "(…) the evaluation should demonstrate that the residual strength of the structure is equal to or greater than the strength required for the specified design loads (…). For the no-growth concept, residual strength testing should be performed after repeated load cycling."

§ 6.2.4: "An inspection program should be developed (…). For the case of no-growth design concept, inspection intervals should be established (…). In selecting such intervals the residual strength level associated with the assumed damage should be considered."

§ 6.2.6: "The effects of temperature, humidity, and other environmental factors (…) should be addressed in the damage tolerance evaluation."

1.3.2 Regulation applications

Due to difficulty in real application of previously reported regulations, they need to be interpreted.

In particular, for static requirements, paragraph 25.603-§5.8 defines two thresholds: the first is 'threshold detectability for in service inspection procedures' and it is called BVID (Barely Visible Impact Damage), while the second refers to the highest impact energy that could occur during production or service operations. A damage structure must be able to bear Ultimate Load under these thresholds.

In Damage Tolerance perspective, a damage that is outside static requirements must not lead to a catastrophic failure. Two different threshold are defined to describe DT domain: first corresponds to easily detectable damages, i.e. Large Visible Impact Damage (LVID), while energy threshold is linked to a probability of occurrence, usually around 10^{-9} per fight hours (fh). Within these limits, structure must maintain at least Limit Load (LL). Just below them, a damaged structure must carry out a load that is equal to $k * LL$, where $1 < k < 1.5$.

Probability value is calculated by means of a statistical analysis of in service damages had those have occurred. This led to an empirical formula that links energy level with its probability of occurrence:

$$(1.1) \qquad p_i\,(E \geq E_i) = \; 10^{-x\frac{E_i}{15}}$$

With x equal to 3.

Impact probability is, therefore:

$$(1.2) \qquad p_i\,(E \geq 30J) = 10^{-5}/fh$$

$$(1.3) \quad p_i\,(E \geq 90J) = 10^{-9}/fh$$

These equations have a general meaning: they need to be adapted for each aircraft location. In fact, as it will be presented in the following Chapter, different location on an aircraft has different impact probability with different energy level.
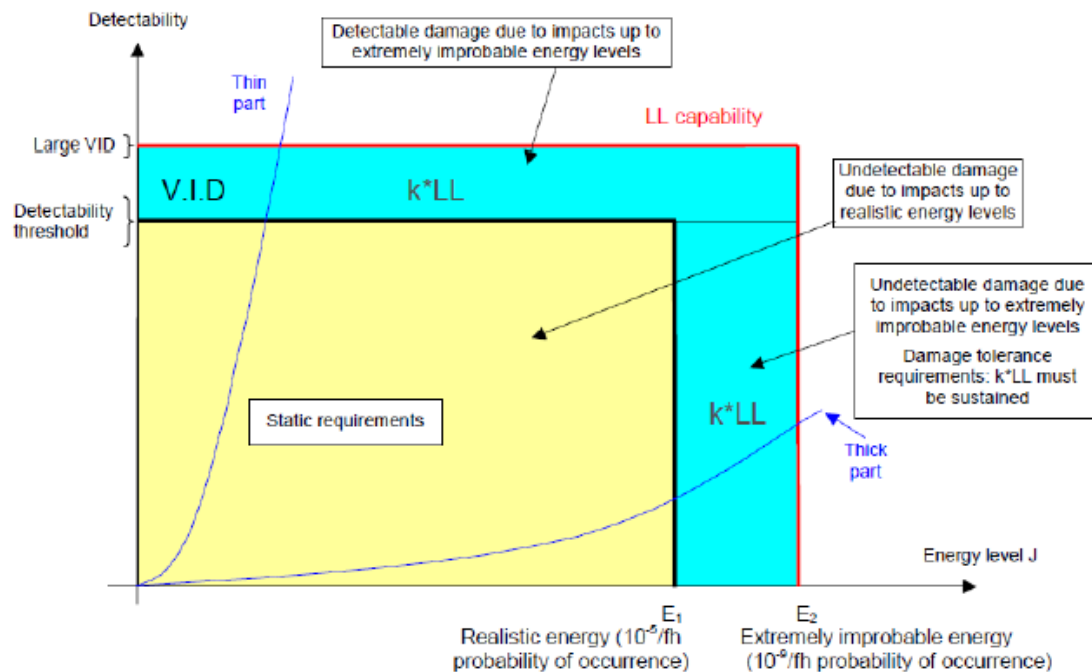
Figure 1.9: DT thresholds requirements

Hence, composite DT philosophy could be represented in Figure 1.9. For thick composite structures a cut-off energy criterion takes place (high impact energies that could heavily damage the structure) while for thin composite there is the detectability threshold. In the latter case, inspection plans are calculated by means of probabilistic study and intervals are usually small in order to avoid possible criticalities. This threshold does not refer to visible damages (low energy impacted do not produce visible damage but it can result in an internal failure). Therefore, it is important that structures are able to support effortlessly Limit Load.

1.3.3 No-Growth Concept

For composite structures, damage No-Growth theory is really important. It says that in a composite structure, under static or fatigue loads, there should be not any damage propagation and, even if the structure is damaged, it must be able to carry out loads. Moreover, new damages are not allowed to be created and structure strength must stay constant.

An airframer, wanting to certificate aircrafts with composite parts, must demonstrate composite structures no-growth satisfaction (at specimens level and with full scale tests). In particular, it needs to be demonstrated that: undetectable damaged do not grow before one Design Service Goal, detectable damages do not grow before one third of the Design Service Goal or during one inspection interval.

The reason of this lays on composite materials behaviour that is completely different from that of metallic materials. While for metals, residual strength tends to decrease progressively under cyclic loads once there is a damage, in composite materials higher loads and more load cycles are needed for damage nucleation; but once it starts, the damage growth could be really fast. Moreover, if an accidental event happens, structure strength could drop suddenly, even under Ultimate Load (Figure 1.10), staying at this level completely undetected. Therefore, without a proper design, there could be a safety issues. Hence, necessity of application of No-Growth requirement in aeronautic field.
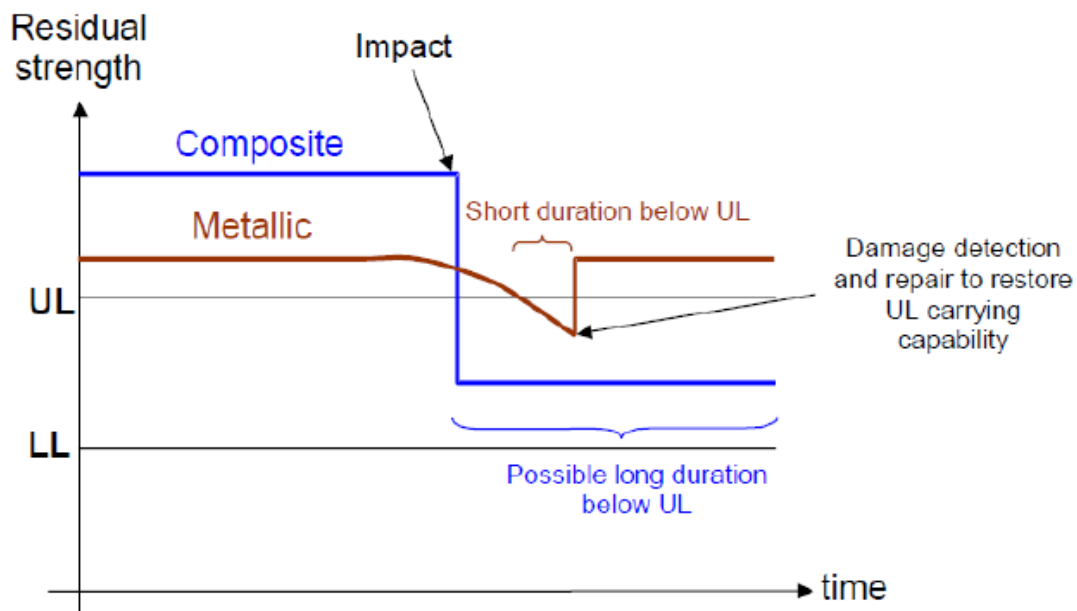
Figure 1.10: Residual Strength comparison between composites and metallic materials

References

[1.1] N.N., Damage Tolerance and Fatigue evaluation of structures, FAA Advisor Circular AC25.571-1C

[1.2] Swift T., Fail-Safe design requirements and features, regulatory requirements

[1.3] Chen D., Bulging of Fatigue Cracks in a pressurized aircraft fuselage, Tech. Report LR-647, Delft University of Technology, Delft, Netherlands, Oct. (1990)

[1.4] Schmidt H.-J., Damage Tolerance technology for current and future aircraft structure, Proceedings ICAF 2005, 23rd Symposium of the International Committee on Aeronautical Fatigue, Hamburg, Germany, June 6-10 (2005)

[1.5] Goranson U.G., Damage Tolerance - Fact and Fiction, Proceedings of the 17th Symposium of the International Committee on Aeronautical Fatigue (ICAF), A.F. Blom (ed.), Engineering Materials Advisory Services (1993)

[1.6] Broek D., Elementary engineering fracture mechanics, Martinus Nijhoff Publishers, The Hague, Netherlands, (1984)

[1.7] Broek D., The practical use of fracture mechanics, Kluwer Academic Publishers, Dordrecht, Netherlands, (1988)

[1.8] EASA regulations, http://www.easa.europa.eu

2

Impact on aerospace structures

Impacts on aerospace structures have not been considered an important issue for a long period. Short airplane life was not really affected by impact damages, but when it came to longer operative lives, due to better materials properties and constructive techniques, it had spotlights on it. Therefore, aerospace industries started to evaluate this issue and to study different kinds of impact effects on different materials, till their influence on composites.

2.1 Impact on airframes

Impact resistance was not considered an important feature for composite materials until '60. Due to short operating life, airplanes never faced impact effects issue until that period. The main reason can be found in the principal aim for which airplanes were used, i.e. wars. During First World War, it was discovered that air-force could be an important 'weapon' that could even be decisive of war resolution. Archaic engineering and need of fast production led to immature structures which, due to constructive issues or shooting down by enemies, had short lives; therefore, any fatigue, impact or aging damages could not rose.

Only lately, in peace times and after experience in construction was acquired, airplanes started to provide civil transportation; longer airplane lives were needed, entailing endurance and aging issues.

Moreover, with the introduction of advanced composite materials in aerospace structures, as long as only glass reinforced plastics were used, impact damages were not an issue thanks to glass-fibre high resistance to out of plane loads. With the introduction of aramid and carbon fibres, impact resistance had to be taken into account and specific studies started to be performed.

In particular 'Foreign object damage to composite' symposium [2.1] was an important step forward in the right direction. After this date, many studies have been done to understand in which way an impact can develop as damage and how the latter could grow in different loading and environmental conditions. Moreover, there was the necessity to investigate how many impact damages an airplane can incur in its operative life and where they are more probable, for a better design and optimization. It has been discovered that impact damage is a very probable event and it is usually located in quite sensitive areas. Cut-out surroundings and leading and trailing edges are one of the most 'impacted' areas.

Three different investigation results are summarized in the following to understand which kind of probability values it is about.

In 1988 a study regarding necessary repairs on 71 Aircraft Boing 747, operating in 17 different countries, and with an average life of 29500 flight hours, was conducted. 688 fatigue, corrosion and impact damages, were detected during maintenance inspections and repaired (Figure 2.2-2.3). Analysing only primary structures (scratches and lightning strike damages were not included), there were 396 fatigue cracks (57.6%), 202 corrosion defects (29.4%) and 90 impact damages (13.0%). Moreover, impact damages could have been in higher number because not all impact damages had been detected or repaired.

In figures 2.1 to 2.3 it is possible to see were these kinds of damages are mostly located [2.10]:

- fatigue cracks are more present in the bulkhead of nose wheel well, the splice at the canted bulkhead, around entrance doors and in APU section;
- corrosion is mostly present in the bottom part of the fuselage, especially around doors and at the canted pressure panel;
- impact damages are mainly located around doors, on the nose of aircraft, in the cargo compartments and at the tail.

More recently in Airbus, a similar study was conducted regarding A320 family: it has been shown that impacts cannot be neglected and they are highly located near cut-outs (Figure 2.1) [2.2,2.11].
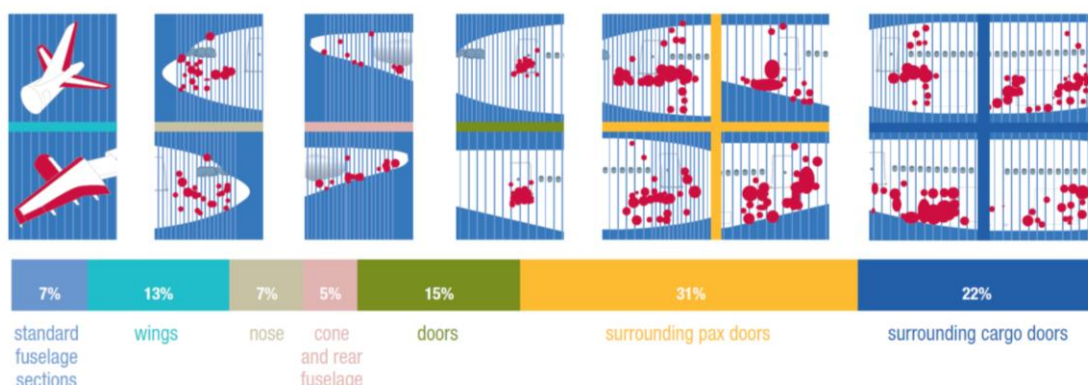
Figure 2.1: Airbus A320 impact damages probability study [2.2]

Therefore, the understanding of impact location influence on material response and damage nucleation is an important matter.
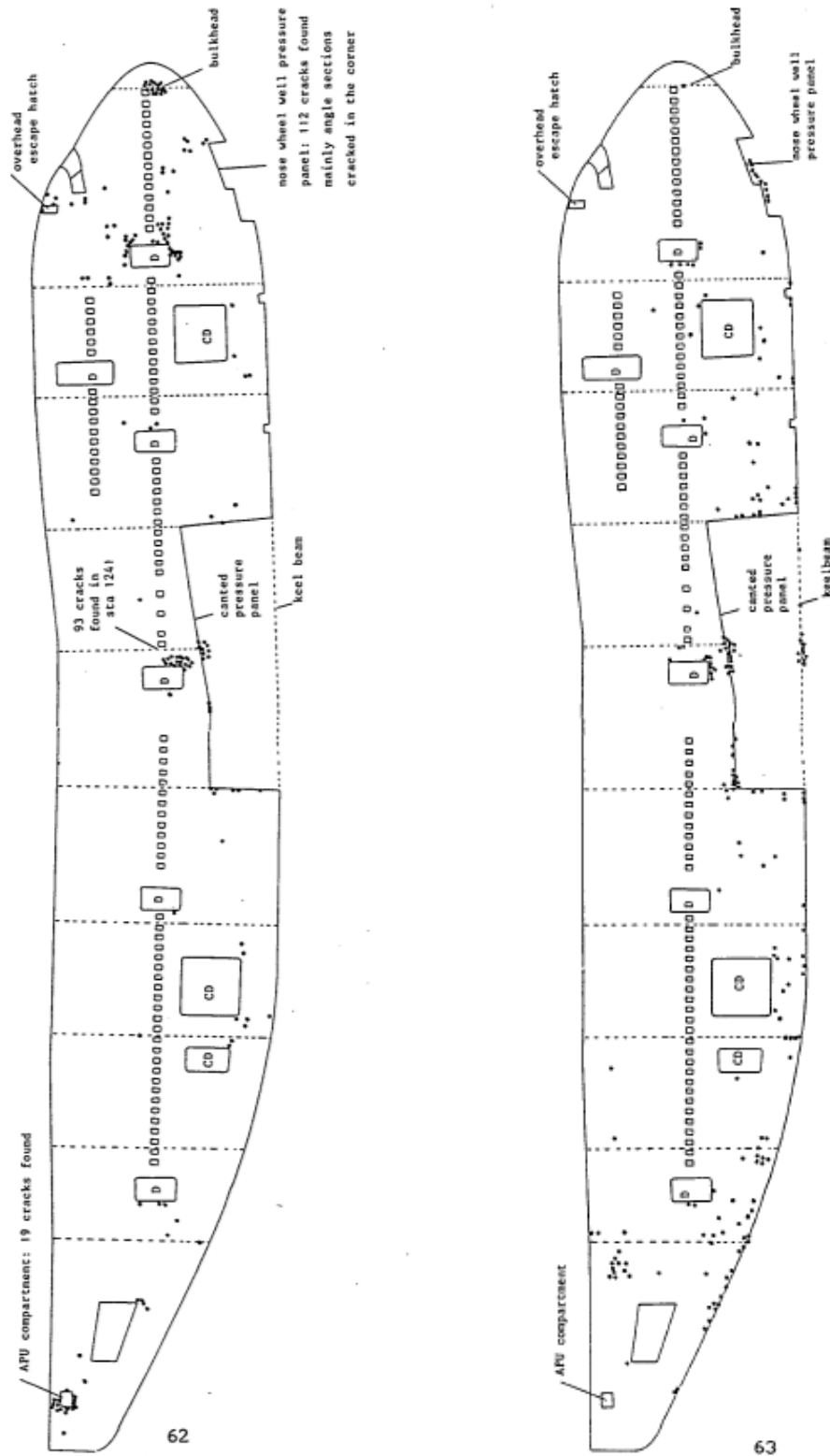
Figure 1.2: location of repaired fatigue cracks (on the left) and corrosion damages (on the right) in 71 B747 aircrafts [2.10]

64
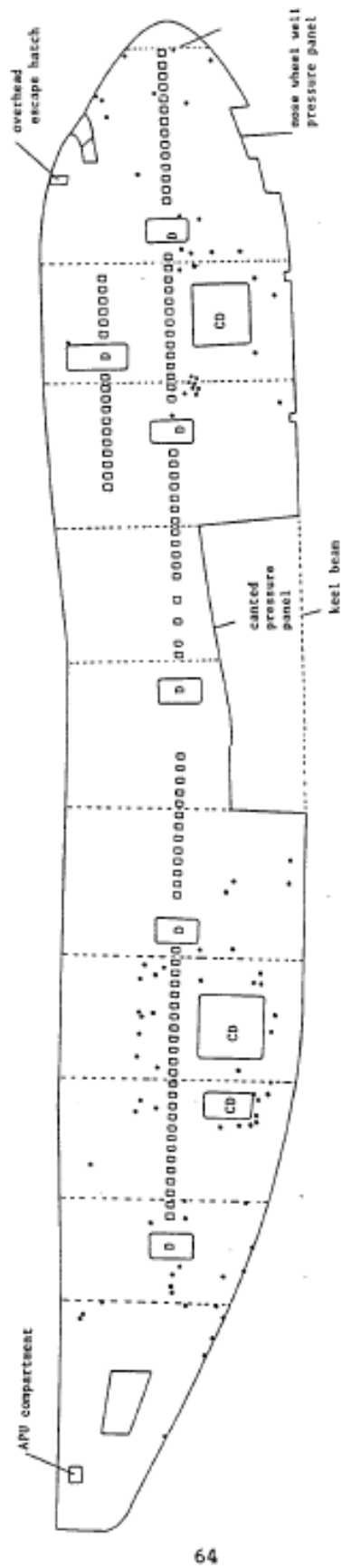
Figure 2.4: location of repaired impact damages in 71 B747 aircrafts [2.10]

2.2 Impact on space structures

For a long time being, impact issue on composite structures was underestimated even in space industry. A catastrophic event highlighted the issue: the 1st February 2003 Columbia Space Shuttle disaster. During the STS 107 mission take-off, 16 days before the accident, a piece of foam shed from the structure connecting the external tank to the orbiter (bipod ramp), and stroke against Columbia's left wing (Figure 2.6), creating a 150 to 250 mm diameter hole. This event was underestimated and, when the shuttle entered back into the atmosphere, high temperature plasma bled into the main structure, causing its explosion.
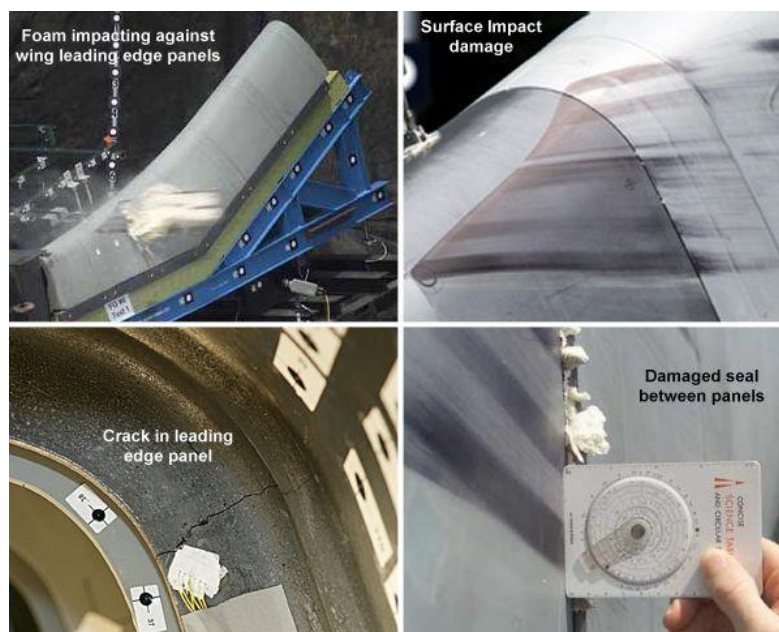
Figure 2.5: Laboratory reconstruction of foam impact on Columbia Space Shuttle left wing
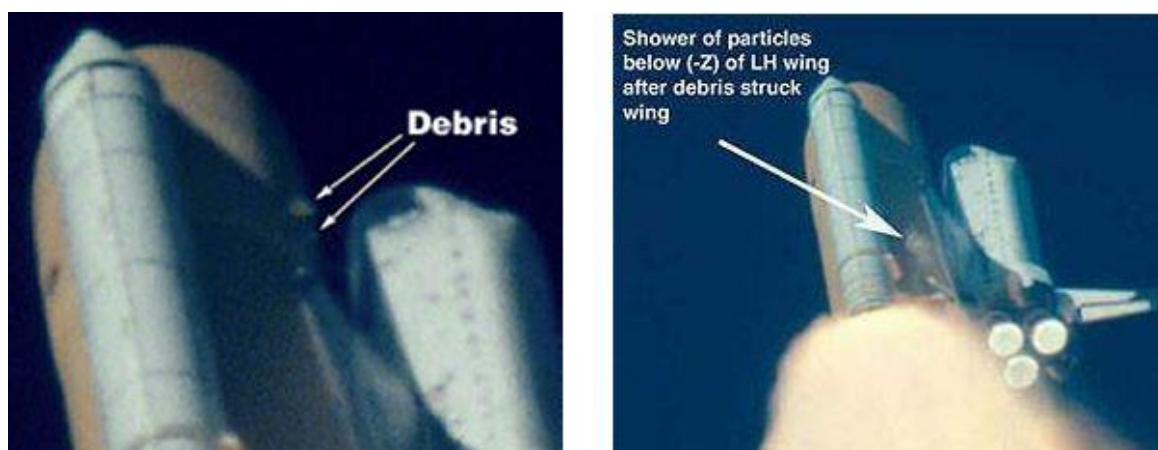
Figure 2.6: Columbia Space Shuttle launch video screenshots at impact moment

This was not the first time a piece of foam detached. It had happened in 4 previous shuttle missions (STS-7 in 1983, STS-32 in 1990, STS-50 in 1992 and STS-112 just two launches before STS-107) but always without consequences. Therefore, it was considered just a

collateral effect and named as 'foam shedding'. Here, like for airplane industry, improvements come from accidents ('learning by accidents' concept).

2.3 Impact causes

Impact damages on an aircraft have many causes. Three categories, based on when they could happen, can be defined: production/maintenance, boarding operation, flight.

The first group includes damages as dents and delaminations caused by tools drops or saw cuts, for structure modification. But also walk on no-step areas, which are usually the most critical and sensible areas (Figure 2.7).

Figure 2.7: Detail of no-walk area on airplane wing (out of black stripes)

During boarding operation, many different events can produce an impact damage: aircraft structure can be hit by cargo or service cars (Figure 2.8), passengers or employee could hit doors surroundings with luggage during loading operations.

Figure 2.8: Detail of an impact damage on airplane fuselage caused by a service car

During flights, from take off until landing, there are multiple possible causes of damages: runway debris can strike against lower structures and wing panel, as well as against flap or movable control surfaces; hail or ice, separating from engines or wings, can hit airplane creating quite big damages; bird strike, can result in wide damages, that structure must bear safely until landing.

There are moreover other kinds of impact that have to be taken into account depending on what kind of airplane is designed: e.g. bullet impacts for military aircraft.

Therefore, many parameters have to be taken into account designing a composite aerospace structure:

- Damage resistance: materials and structures should be able to absorb as much impact energy as possible, resulting in a small damage, if structure does not have a peculiar crashworthiness function.
- Damage tolerance: residual strength has to be higher than a threshold, even in presence of damage.
- Inspectability: this is a real issue with composite because internal delaminations are difficult to be detected during maintenance inspections, compared with dents on metallic surfaces. Different methods have been.
- Reparability.

2.4 Impact damages

Impact on composites has different consequences compared to impact on metals. For metals, impact damages are easily detectable on structure surface and they depends on energy: if it is low, there would be an elastic behaviour that does not influence material characteristics; at higher energies, plastic deformation occurs. In this case, damage would be seen and repaired.

For composite [2.12, 2.16], on the other hand, impact damages depend on many factors: thickness, stacking sequence, matrix and fibre kinds, impact energy and velocity, etc. Moreover, due to composites fragile behaviour, failure mechanisms is not related to plastic deformation but on elastic deformation and fragile failures. This means that there could be different kind of damages in an impacted composite structure [2.3-2.4]:

- Matrix cracks: it is the most common defect and the first one to happen. Matrix cracks can propagate through different layers or in the same fibre direction. They are clearly evident after an impact transversal to load direction. Principal effect is composite rigidity reduction.
- Delaminations: it is separation between two plies. Small delaminations could reduce laminate compressive resistance of about 50%, due to fibre stability reduction under load application. They are mostly common around rivets holes or cut-outs.
- Fibre cracking: could be caused by impact in transversal to load direction or compression loads that can create local instability conditions. This damage is the

most dangerous for tensile loaded structures, and it is even worse because fibre failure is difficult to detect.

- Detachment at fibre/matrix interface: it could happen if at fibre/matrix interface stresses exceed locally limit loads. It could be microscopic and difficult to detect. A way to avoid this problem is a fibres surface treatment. It does not represent a dangerous damage but it could result in an easier way for water to enter inside a laminate, decreasing compressive resistance.

Impacts can be divided, according to impact velocity, in: iper-velocity (more than 2km/s), high-velocity (from 50 m/s up to 1000 m/s), intermediate-velocity (from 10 m/s to 50 m/s) and low-velocity (up to 10 m/s) impacts [2.3].

An impact produces pressure waves in the laminate: comparing time necessary to waves to go through laminate and contact time between impactator and laminate, it is possible to catalogue impact into the previously described kinds. For example, in low-velocity impacts, pressure waves can go through laminate many times before contact ends.

This influences also damages: with high-velocity impacts there could be perforation and micro-delamination around event location, while with low-velocity ones result in barely visible damages on surface but with wide inner delamination.
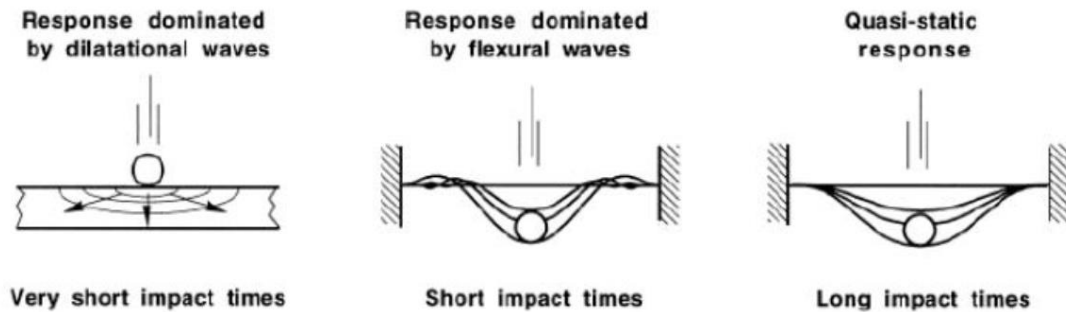
Figure 2.9: Material response under different velocity impacts [2.17]

2.5 Low-velocity impacts

Low-velocity impacts [2.6-2.9] are dangerous events on a composite structure. They could happen due to tool drops during maintenance, luggage hitting cut-outs, etc. This kind of impact can result in quite wide inner or on back surface damages but with no evidence on the external impacted surface.

This lack of evidence could lead to an unexpected sudden failure. It has been already shown (Fig. 1.8, Chapter 1) that, due to an impact, bearing load structure capacity could suddenly go under ultimate load and, therefore, result in an unexpected damage growth and then failure.

Low-velocity impacts could be compared with quasi-static events because the load-deformation behaviour is the same. This means that time of contact between impactator and structure is sufficiently long to assure entire structure reaction, and, therefore, an elastic energy absorption. This happens up to a threshold energy value, over which matrix or interface separation happen. Threshold and damage kind depend on many factors, first of all laminate thickness: thick laminate presents transversal cracks close to impact location; on the contrary thin laminate usually react as a membrane and, therefore, damages could be found on back surface, where flexural loads are the highest. These are called 'pine tree' and 'reversed pine tree' shapes (Figure 2.10) [2.3].
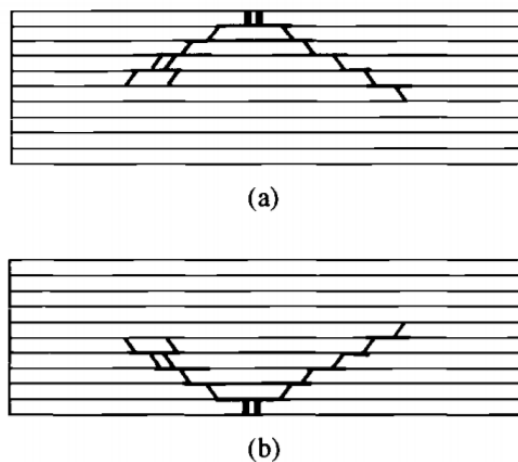
Figure 2.10: (a) pine tree and (b) reversed pine tree impact damage shapes [2.3]

One consequence of these transversal cracks are delaminations: depending on impact force and contact surface, they occur only over a certain threshold and when there is a previous matrix crack. Delaminations can propagate in different modes: mode I or 'opening', mode II or 'by shear', mode III or 'by tear'.
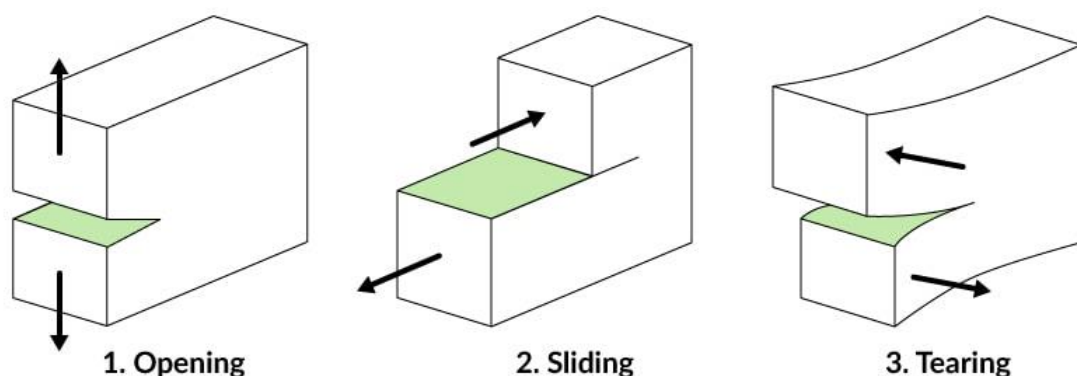
Figure 2.11: Material failure modes

Usually, mode I is related to delamination nucleation, while mode II or mixed mode to its growth.

Another evolution of transverse cracks is failure under contact location: by naked eyes, the only evidence of the impact is an imprint. This indentation could have different depth (creating different amount of damage), related to the involved energy and, therefore, the damage can be more or less visible.

Similarly, impactor material and dimensions can influence damage size: for a wide contact area, higher energy is needed to penetrate laminate, while for smaller areas the penetration is easier, with resulting smaller delaminations [2.13-2.15].

It is also worth to notice that stacking sequence influences delamination nucleation and growth: in fact, delamination happens commonly between layers with different fibre orientation. Therefore, an UD laminate is less prone to interlaminar interface separation.

References

[2.1] ASTM Symposium, Foreign Object Impact Damage to Composites, 1975

[2.2] FAST #48 Airbus, 2011

[2.3] S.Abrate, 'Impact on composites structures', Cambridge University Press, 2005

[2.4] Joshua M. Duell, 'Impact Testing of Advanced Composites'

[2.5] M. Siliotto, 'Valutazione analitica delle aree di delaminazione in materiali composite avanzati soggetti ad impatti a bassa velocità', tesi di laurea magistrale, Università di Bologna, Scuola di ingegneria e architettura, Corso di laurea in ingegneria aerospaziale, a.a. 2012- riguardare la vera reference

[2.6] M.O.W. Richardson, M.J. Whisheart, 'Review of low-velocity impact properties of composite materials', Composites Part A, pp. 1123-1131, 1996

[2.7] A. Malhorta, F.J. Guild, 'Impact damage to composite laminates: effect of impact location', Applied Composite Material, 2014

[2.8] A. Malhorta, F.J. Guild, M.J. Pavier, 'Edge impact composite laminates: experiments and simulations', J Mater Sci, pp. 6661-6667, 2008

[2.9] M. Quaresimin, M. Ricotta, 'Assorbimento energetico durante impatto in laminati in materiale composito', Associazione Italiana per l'analisi delle sollecitazioni, XXXIV National congress, 2005

[2.10] Ad Vlot, 'Low-velocity impact loading on fibre reinforced aluminium laminates (ARALL and GLARE) and other aircraft sheet materials', TU Delft repository, 1993

[2.11] Guy Hellard, 'Composites in Airbus A long story of innovations and experiences'

[2.12] MIL-HDBK-17 – 'Composite Materials Handbook', 2002

[2.13] Mitrevski T., Marshall I.H., Thomson R., Jones R., 'Low-velocity impacts on preloaded GFRP specimens with various impactor shapes', Composite Structures 2006

[2.14] Woodward R. L., Egglestone G. T., Baxter B. J., Challis K., 'Resistance to penetration and compression of fibre-reinforced composite materials', Composites Engineering 1994

[2.15] A. Katunin, M. Zuba, 'Influence of the impactor geometry on the damage character in composite structures'

[2.16] W.J. Cantwell, J. Morton, 'The impact resistance of composite materials---a review', 1991

[2.17] R. Olsson, 'Mass criterion for wave controlled impact response of composite plates', Composites Part A: Applied Science and Manufacturing, 2000

- 28 -

3

Experimental Impact tests

Different impact tests can be performed to study many kinds of damages. After a brief introduction to all of them, the 'modified Charpy pendulum' available in the MasterLab workshop, together with a description of its setup and usage, is shown.

3.1   Impact tests

There are many different ways to perform impact tests on composite materials, in order to study their behaviour. Each one has a specific velocity range of application, with different settings and issues:

- Quasi-static loading [3.1]: really slow indentation tests that can be performed by means of a hydraulic testing machine;
- Low-velocity impact [3.2]: velocity under 10 m/s, by drop weight testing (different weights, different heights to obtain different impact energies); it will deepened in the following section.
- High-velocity impact: with velocity up to 100 m/s, can be performed with gas guns (Figure 3.1); impact are fast and, therefore, damaged area is smaller. This means that geometrical considerations do not have any meaning in this contest.
  This system work by means of compressed gas that pushes against sabot; its pin is released and this entire part is pushed inside a tube. When sabot reaches the end of the tube, it is stopped properly while pellet is launched out of it; it hits specimen with a constant velocity. Pellet are usually made by hardened steel or zirconium; specimen deformation can be measured by means of specific strain-gauges.
- Ballistic impact: velocity up to 500m/s, made with powder guns;
- Hypervelocity impact: really high velocities obtained by means of electromagnetic guns [3.3].
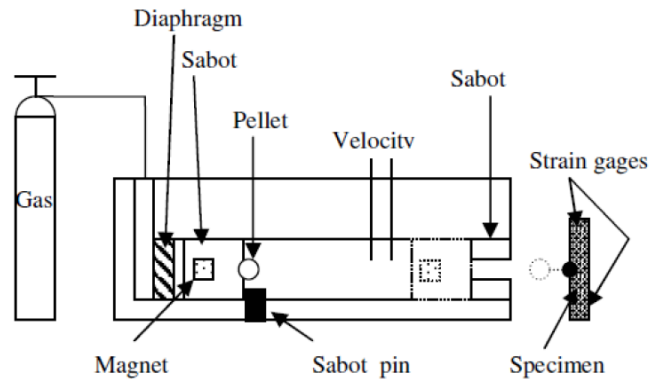
Figure 3.1: Gas gun impact system

Many variables are implied in an impact and can change its result on the structure [3.4-3.8]:

- Indenter shape: a sharper indenter results in an easier indentation but in smaller internal damage;
- Indenter mass;
- Impactor velocity;
- Impactor/clamps materials: usually indenter are in steel to better comparison, but there could still be influence due to this variable, as well;
- Target material and dimensions;
- Impact direction: relative impact direction (perpendicular, parallel or oblique to target medium plane) influences the internal damage;
- Impact location: near-edge impact can result in a wider damage due to lower materials local stiffness;
- Boundary conditions: a clamped specimen shows a wider damage compared to a simply supported one due to the lack of membrane behaviour.

In literature, many papers describing experimental campaigns on composite impact behaviour were found; most of them were related on central impacts (as described in [3.2]). Unfortunately, impacts rarely occur in such a situation, since they are more probable near cut-outs and corners as shown in 2.1 paragraph. Hence, it was worth of interest to deepen the knowledge of location influence.

Impacts are catalogued in two groups (Figure 3.2): normal and on-edge impacts. In the first, impact direction is orthogonal to material middle plane while, in the second, impacts take place on structure edges. Normal impacts could take place centrally (Central Impact, CI) or near specimen edge (Near-Edge impact, NE), while on-edges could be directed along specimen plane (In-line) or create a sharp angle with it (Oblique impact).
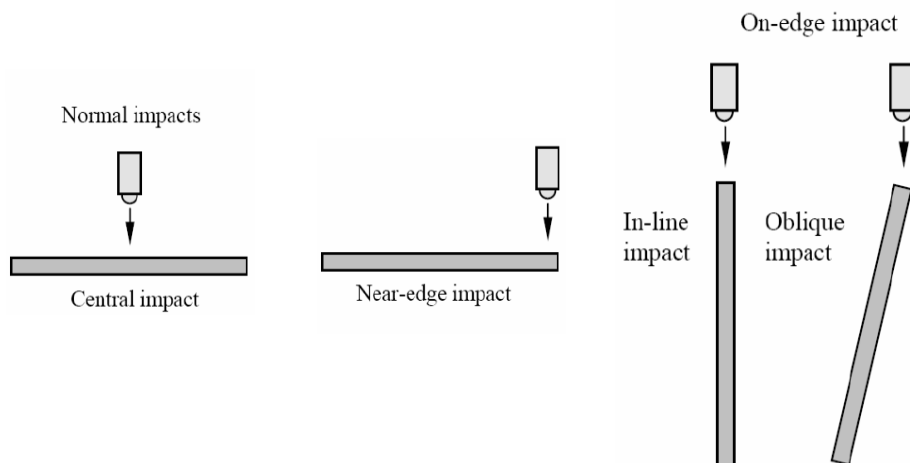
Figure 3.2: Impact locations

Throughout literature research, few papers related to normal and transversal impacts were found [3.8-3.9]. In these works, an experimental campaign on glass/epoxy laminates, impacted with different energies, was described. The impacts are located near specimen edges or directly on its edge. Using glass/epoxy it is possible to see, by naked eyes, damages created through the thickness and correlate these to compression after impact test results. It was demonstrated that composites are quite sensitive to impacts and that location is a fundamental parameter.

No studies were found related to impact location influence on impact resistance of a carbon/epoxy laminate. Hence, it was decided to deepen this material behaviour under impact loads, starting with normal impacts.

3.2 Low Velocity Impact tests

As previously said, many different methods exist for impact performance. Choosing one of them is related to which kind of velocity is under investigation. In the case of this PhD research, it was chosen to perform low-velocity impact tests, in order to obtain BVID (Barely Visible Impact Damages). The most common equipment used for this aim is a Drop weight tower (Figure 3.3) [3.2].
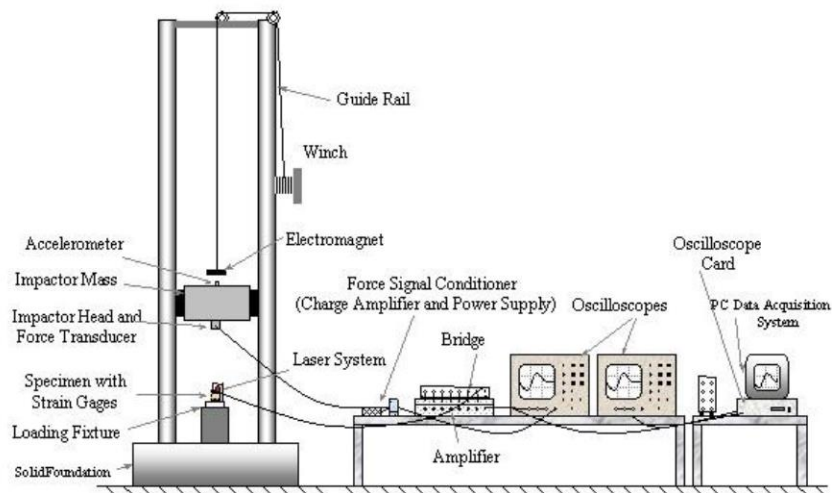
2

Figure 3.3: Drop Tower Impact test system

It consists of a weight fixed under a cart, free to glide on two or more vertical tracks. It can be fixed in a specific height and then release to obtain a certain energy impact. Specimen is fixed in a proper fixture, circular or rectangular, positioned between rails.
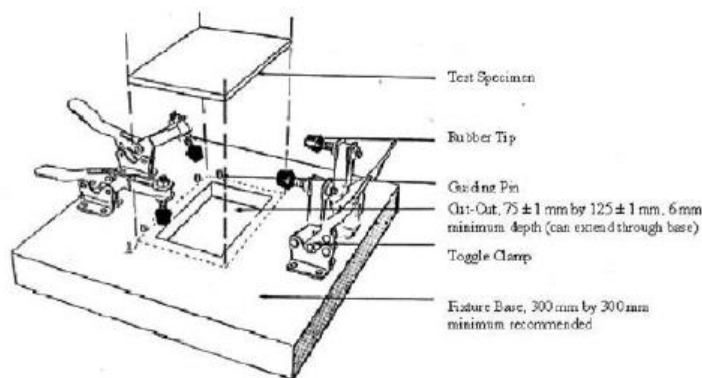
Figure 3.4: Drop tower fixture for specimens [3.2]

After impact takes place, weight bounce could be stop or let it go to obtain a multiple impacts tests.

After a literature and technological review of impact test procedures and facilities, it was found out that Charpy pendulum is usually used to perform impacts, as well.

Originally, it was developed for testing materials impact resistance [3.5], with a maul hitting in the middle and breaking long specimens (Figure 3.5). It is, therefore, possible to calculate absorbed and residual energy just looking at final maul position after breaking the specimen. Hence, this kind of test is a destructive test where only property of impact energy absorption is acquired.
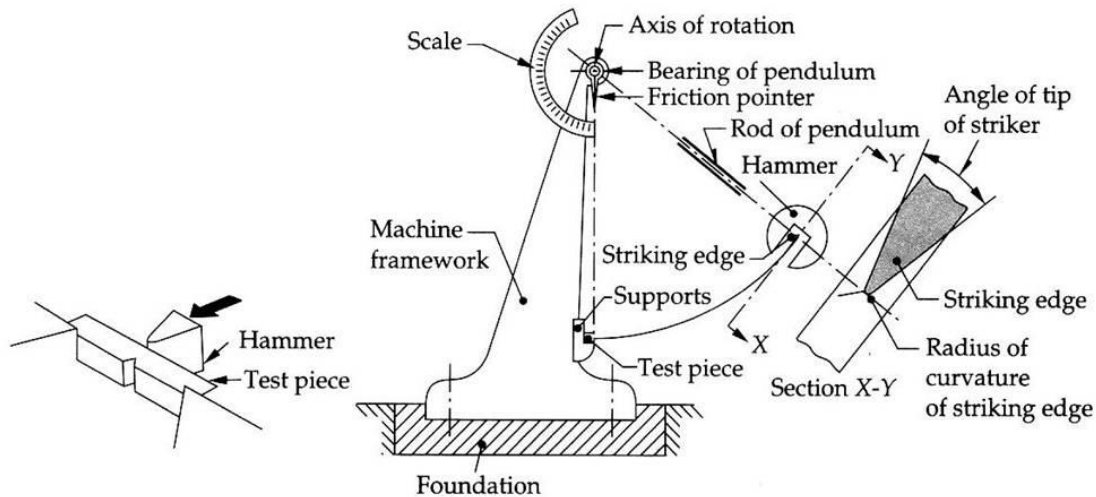
Figure 3.5: Charpy pendulum tests system

In this way, it is impossible to use Charpy pendulum to obtain BVID and be able to test specimens in compression after impact. This is also the main reason of whom refer to Charpy (or Izod) pendulum as not suitable for aeronautical impact test performance: it is not representative of real impact condition on airplanes, due to different boundary conditions. [3.11-3.12].

Therefore, it was necessary to modify pendulum original set up in order to achieve the main goal. Kind of test under investigations and possible boundary conditions were taken into account to create a modified Charpy pendulum. It was design and built up in the MasterLab facilities of University of Bologna, in Forlì.

3.2.1 Charpy pendulum

The realized pendulum has been obtained modifying a structure already present: it is an L shaped 1 m tall structure with a steel bar hinged in the middle with a bearing that let bar revolve around it (with low friction). At the end of the bar, there is a cylindrical impactator with a hemispherical end. Bar is hinged in the middle to avoid any contribution of it to impact energy. In this way, impact energy is only based on impactator weight and beginning height from where weight is released.

Two versions of this pendulum were realised.

- First one, used in the first experimental campaign (described in chapter 4), had a 630 mm long steel bar hinged with a one-line bearing. On the other bar end, the impactator was attached: it was a steel cylinder with a hemispherical 7 mm diameter end, and its weight was 1.81 kg. Bar was tighten to a counterweight (Figure 3.6) in order to balance bar weight. In this way impact energy is only based on impactator weight and beginning height from where weight is released.
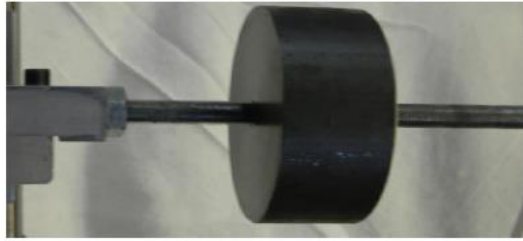
Figure 3.6: Counterweight

- Second version, differs from first only for steel bar that was in this case 1226 mm long and hinged in the middle (Figure 3.7). In this way it was already balanced, without need for the counterweight. Bearing in this case was a double line in order to have a more stable movement of the bar in the transversal direction.

Figure 3.7: Modified Charpy pendulum (second version)

Energies were calculated measuring bar angles by means of a goniometer located at the hinge. It is, in fact, possible to correlate energy level to bar angle due to trigonometric laws:
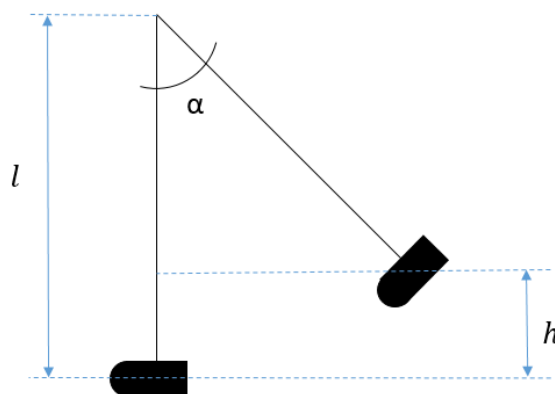
Figure 3.8: Charpy pendulum concept

(3.1) $E = mgh$

where E is the energy, m is the impactator mass, g gravitational acceleration and h height at which impactator should be released to obtain that energy (Figure 3.8). Therefore, the unknown, in this case, is h. To calculate h it is possible to use trigonometry: knowing the distance, l, of the impactator centre of gravity from hinge centre, it is possible to calculate:

(3.2) $\overline{AB} = l \cos \alpha$

where α is the angle that bar forms with its initial position.

It is hence easy to see that h is equal to:

(3.3) $h = l - l \cos \alpha$

and therefore, substituting in (3.1)

(3.4) $E = mg(l - l \cos \alpha)$

Equation (3.4) can be used for calculating all energies involved, it would be necessary only to change the angle involved: for actual energy, initial angle is required; for residual energy, bounce angle is used:

(3.5) $E_{initial} = mg(l - l \cos \alpha_{initial})$

(3.6) $E_{residual} = mg(l - l \cos \alpha_{bounce})$

Calculation of absorbed energy could be done after knowing both initial and residual energies, by means of:

(3.7) $E_{absorbed} = E_{initial} - E_{residual}$

where $E_{absorbed}$ is the energy absorbed by specimen due to elastic response and damage formation, $E_{initial}$ is given by (3.5), $E_{residual}$ is given by (3.6).

3.2.2 How to use 'modified pendulum' at Unibo (MasterLab) laboratories

This modified pendulum is easy to use:

-   adjustable feet are under main plate (Figure 3.8-3.9) to level the pedestal inclination;

Figure 3.8: level used to avoid longitudinal ground inclination
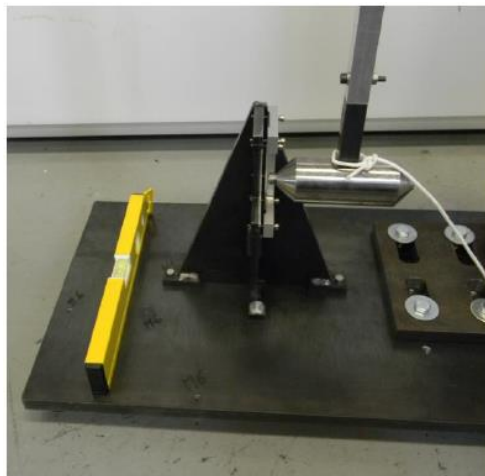
Figure 3.9: level used to avoid transversal ground inclination

- specimen is put in the fixture (Figure 3.10), where it is fixed in position during test by means of six screws;
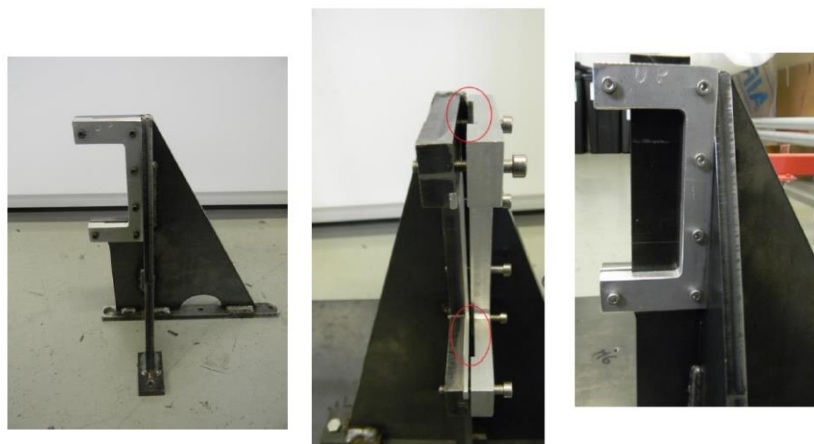
Figure 3.10: specimen holding fixture

- pendulum structure is moved transversally till impactator is in the right position to obtain impact on previously decided location on specimen; it is then fixed with 4 screws to steel pedestal (Figure 3.11);

Figure 3.11: screws to connect pendulum to the basement

- bar pivot is moved back or forward and then fixed in position to have bar orthogonal to the floor. It results, therefore, an impact normal to specimen middle plane (Figure 3.12);

Figure 3.12: Level used to check bar impact position

- goniometer is set and fixed and test can start.

3.2.3 Accelerometer acquisitions

In the first version of this pendulum (where the only difference was bar shape and balancing method), an accelerometer had been located at rear impactator surface (Figure 3.13). Multiple impact tests were performed on a carbon/epoxy laminate.

This was made to obtain information regarding pendulum dynamics.

The accelerometer was a PCB Mod 356B21. It has nominal sensitivity of 10 mV/g on acquisition channels with a frequency range of 2-7000 Hz; full scale of 10 V equal to 500g. Acquiring system is LSM SCADASCM 05; sampling frequency used was 6400 Hz.
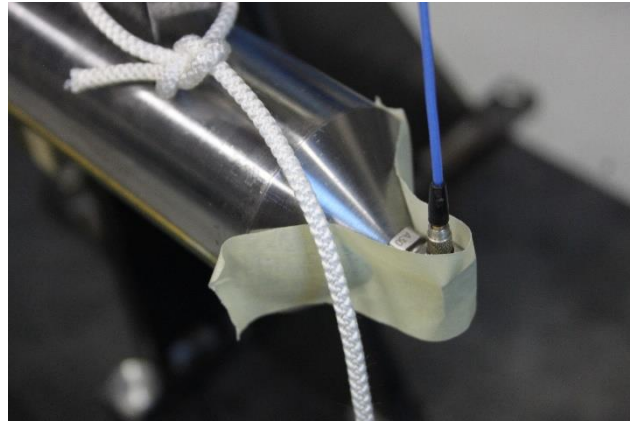
Figure 3.13: Accelorometer at the impactor end

Data acquired are shown in following pictures (Figure 3.14-3.18); in those tests acquisition time was set as 5 sec and data from main impact and 5/6 rebounds were recorded. For the work presented in this thesis, only the first impact is however taken into account.
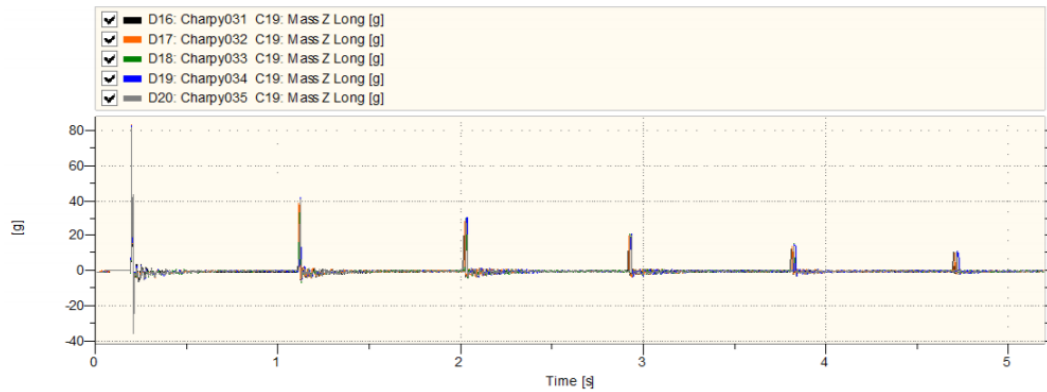
Figure 3.14: Acceleration through the thickness direction

- **4 JOULE**
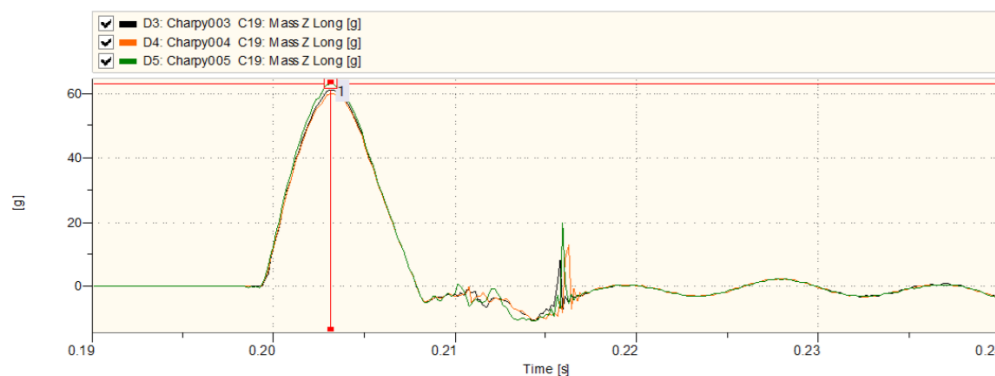
Figure 3.15: Acceleration acquired during 4 J impact test (max value 63.28 g)

- 5 JOULE
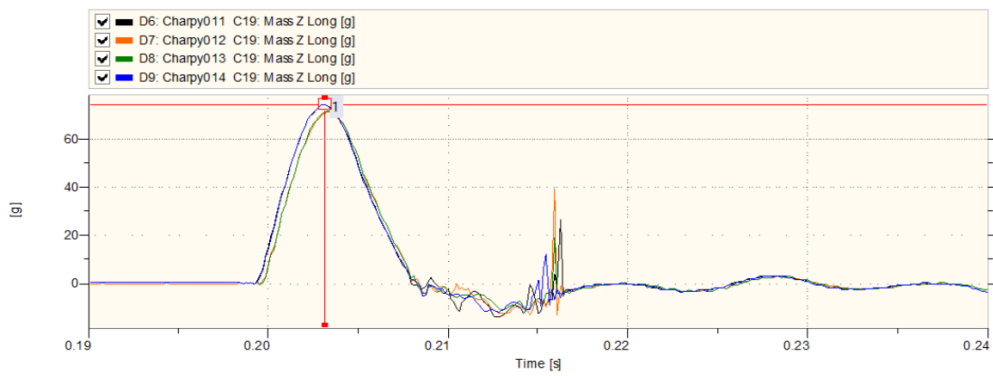
Figure 3.16: Acceleration acquired during 5 J impact test (max value 74.66 g)

- 6 JOULE
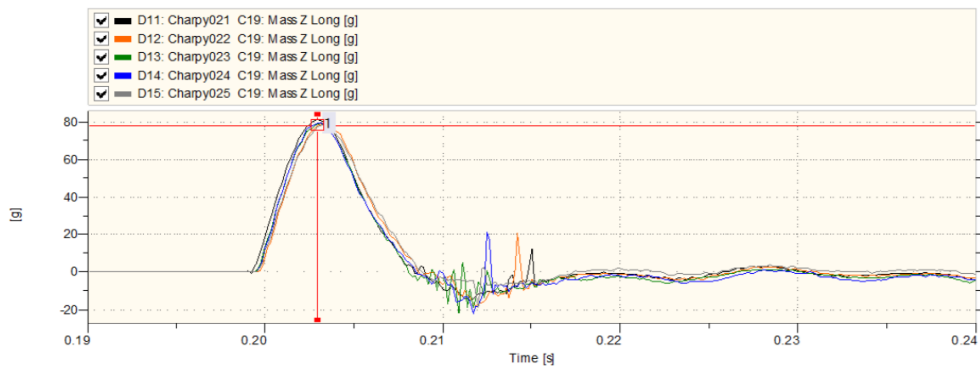
Figure 3.17: Acceleration acquired during 6 J impact test (max value 81.54 g)

- 7 JOULE
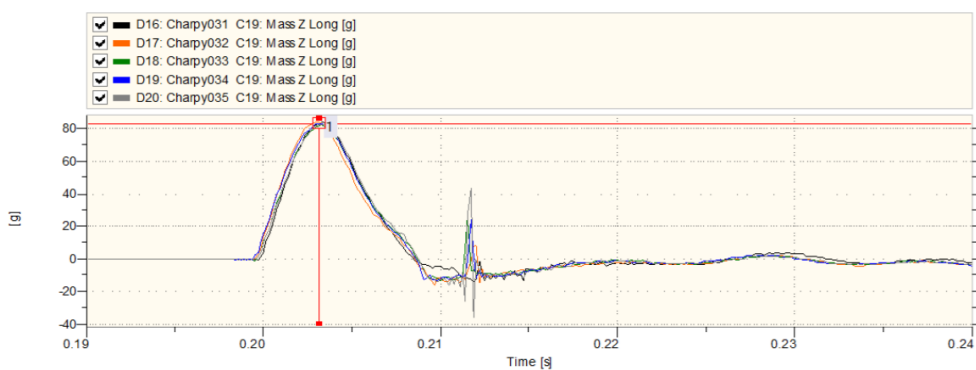
Figure 3.18: Acceleration acquired during 7 J impact test (max value 83.35 g)

Maximum acceleration values acquired in x direction are shown in Figure3.19.
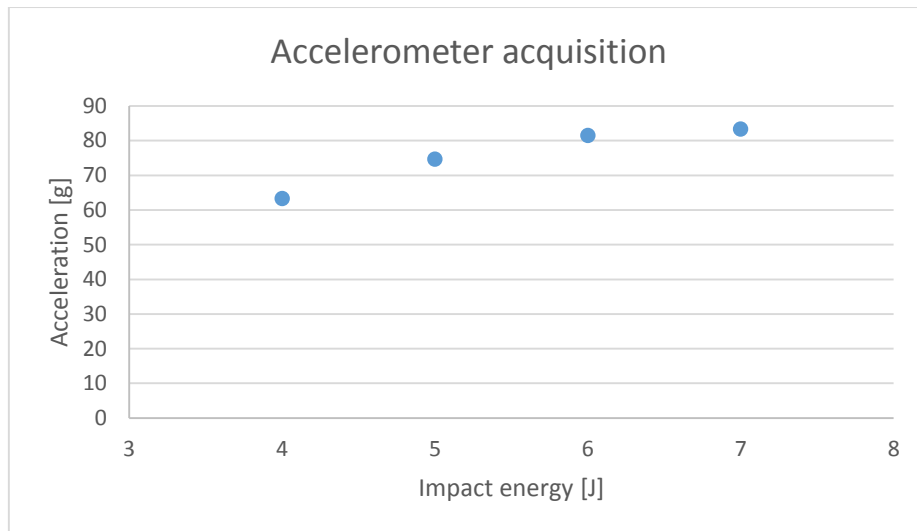
Figure 3.19: Max acceleration values

The x-direction acceleration grows with impact energy reaching an asymptote from 7 J energy impact on.

The modifications in pendulum structure do not influence x-direction dynamics; therefore, values of acceleration are supposed to be the same.

For every energy level, almost the same acceleration peak value is achieved in all performed tests; therefore, this shows the reliability and repeatability of impact tests with this 'modified pendulum'.

References

[3.1] ASTM D6264/D6264M – 12, Standard Test Method for Measuring the Damage Resistance of a Fiber-Reinforced Polymer-Matrix Composite to a Concentrated Quasi-Static Indentation Force.

[3.2] ASTM D7136/D7136M – 15, Standard Test Method for Measuring the Damage Resistance of a Fiber-Reinforced Polymer Matrix Composite to a Drop-Weight Impact Event.

[3.3] S. Abrate, Impact on Composite Structures, Cambridge University Press, New York, 1998.

[3.4] M. Sadighi, et al., Impact resistance of fiber-metal laminates: A review, International Journal of Impact Engineering, 2012.

[3.5] S. Agrawal, et al., Impact damage on fibre-reinforced polymer matrix composite - A review, Journal of Composite Materials, 2013.

[3.6] W. J. Cantwell et al., The Impact Resistance of Composite Materials-A Review, Composites, 1991.

[3.7] G.B. Chai, et al., Low velocity impact response of fibre-metal laminates – A review, Composite Structures, 2014.

[3.8] A. Malhotra, F.J. Guild, 'Impact damage to composite laminates: effect of impact location', Applied Composite Material, 2014.

[3.9] Malhotra, A., Guild, F.J. & Pavier, Edge impact to composite laminates: experiments and simulations, M.J. J Mater Sci (2008).

[3.10] ASTM D6110-10 Standard Test Method for Determining the Charpy Impact Resistance of Notched Specimens of Plastics

[3.11] W. Hufenbach et al., Charpy impact test on composite structures – An experimental and numerical investigation, Composites Science and Technology, 2008.

[3.12] A. C. N. Singleton, On the mechanical properties, deformation and fracture of a natural fibre/recycled polymer composite, Composites: Part B, 2003.

<div style="text-align: right; font-size: 3em;">4</div>

Compression After Impact (CAI) tests

In this chapter, a brief description of all compression and CAI test fixtures on composites is given. In particular, CLC line guides are described.

4.1 Compression tests on composite materials

Compressive resistance of composite materials is not as high as tensile resistance due to their intrinsic nature. In fact, compression loads act on matrix properties and matrix/fibre adhesion. Therefore, testing this characteristic of composites is an important experimental field.

This is even more important when related to impacted materials: due to inner damages, close plies adhesion could be compromised and a not uniform load distribution could take place (Figure 4.1).
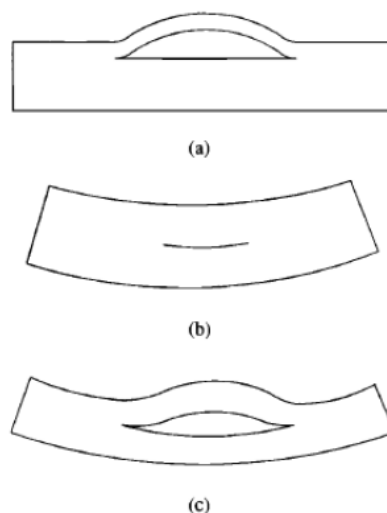
Figure 4.1: Buckling modes for a damages composite material under compressive load

Many different kind of fixture have been developed to be used with advanced reinforced plastics. These can be divided into 3 main groups: Shear loaded, Sandwich-beam compression, End loaded. In the following section, fixtures are described together with their advantages and disadvantages.

4.1.1 Shear loaded

There are two main fixtures:

- Celanese [4.1-4.4] (Figure 4.2)

  Developed in 1971 by I.K.Park of Celanese Corporation, it transfers shear load by means of conical grip surfaces. Main issue is related to a not perfectly uniform load transfer, a common problem for this kind of compression tests.

  Moreover, there could be possibility of bending that could give rise to flectional instability, due to peculiar surfaces structure. Geometrical tolerances, of both specimens and fixture, are strict (±0,002''), due to need to have a proper coupling at grip surfaces.
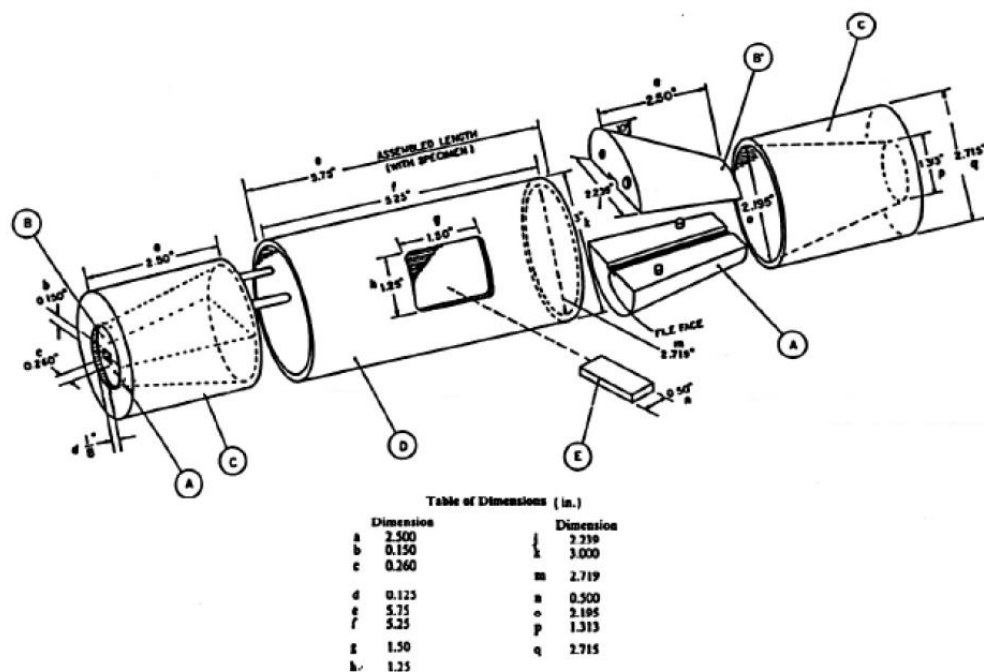
Figure 4.2: Celanese test fixture [4.3]

- IITRI ('B method 'ASTM D 3410, 1987') [4.1-4.4] (Figure 4.3-4.4)

  Developed in 1977 by Hofer and Rao at Illinois Institute of Technology Research Institute (IITRI), trying to solve issues related to Celanese. It is made of flat wedges which can solve load alignment and specimen buckling. It is characterised of a high

results reliability and, therefore, data acquired by mean of this fixture are usually used as a term of comparison. Main drawback is its weight: it is a massive structure of about 40 kg with a moving part of 16 kg; moreover, costs are high due to geometrical tolerances for cavities which house wedges.
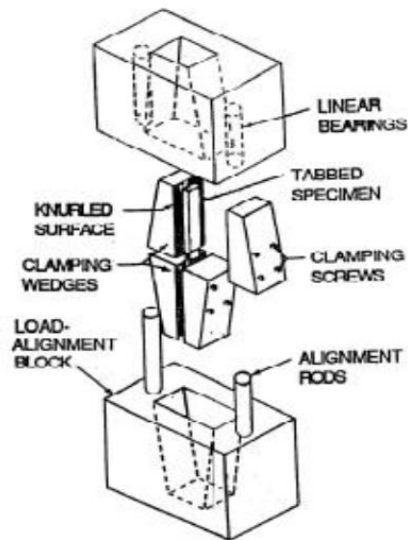
Figure 4.3: IITRI test fixture scheme
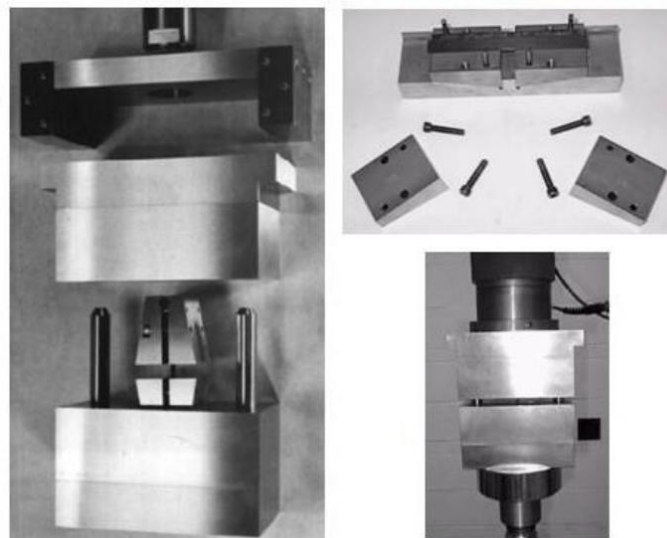
Figure 4.4: IITRI test Fixture [4.3]

4.1.2 Sandwich-Beam Compression Test Method

This kind of test is described in ASTM D 5467-93 [4.5], even if it was already addressed as 'method C' in ASTM D 3410 [4.1]. It consists of a four points bending test on sandwich-beam specimens (two layers of composite pre-preg with a honeycomb core in the middle). Hence, the upper surface is in compression. Load is supposed to be uniform

due to low thickness of the tested surface in comparison with specimen thickness (Figure 4.5-4.6).
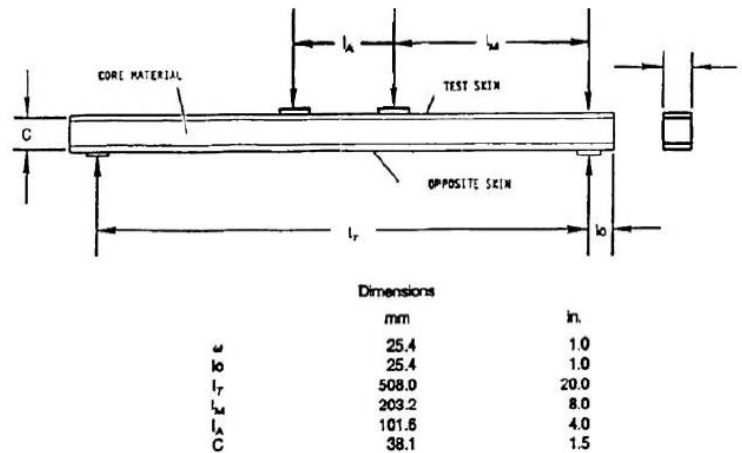
Figure 4.5: Sandwich-beam Compression test method scheme [4.5]
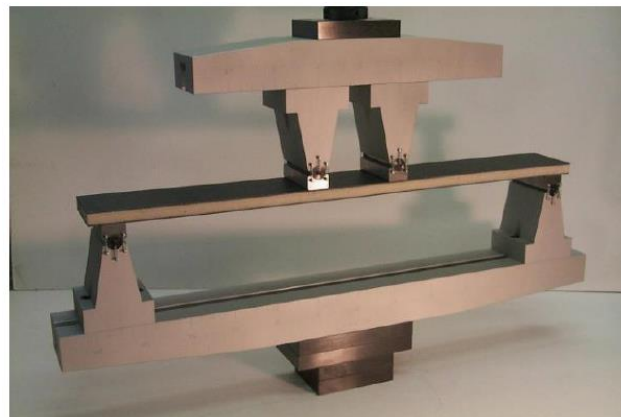
Figure 4.6: Sandwich-beam Compression test fixture [4.3]

This method gives high compressive resistance that it is not representative of real material behaviour; this is caused by honeycomb stabilising composite compression buckling. At the same time, however, results could be influenced by honeycomb failure or interface separation. Therefore, specimens preparation needs time, skills and it costs a lot, due to many factors that should be checked to respect requirements, and to avoid effects on tests result.

4.1.3 End-loaded Test Method

There are two methods in this category:

- Modified ASTM D695 [4.1][4.3-4.6] (Figure 4.7)

    Derived from ASTM D695, fixture for un-reinforced plastics. Specimens are rectangular and not dog-bone shaped as in the original version. Load is transferred

only at the specimen ends and, therefore, there could be an unwanted failure. Tabs could solve this issue but, at the same time, could rise an issue related to their preparation (glue kind and cure, that could be a weakening point for the test).

It was realised in 1988 by Suppliers of Advanced Composite Materials Association (SACMA) and it is made of two lateral supports, T shaped, and four bolts. These are used to tie supports to specimen surfaces that are going to be under compression.

Moreover, gage section is small and therefore it is not possible to put a strain gauge on specimens. This fixture is not often used due to some friction that could occur between specimen and lateral surfaces and that could influence results, leading to stress concentrations.
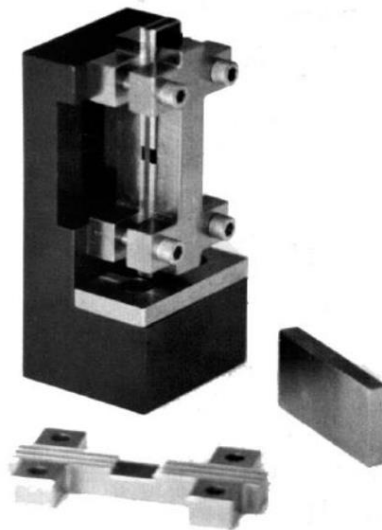
Figure 4.7: ASTM D695 fixture [4.3]

- End-Loaded Side-Supported (ELSS) Compression Test Fixture

Developed in '80s at University of Wyoming, it can be used with untabbed specimens, solving problems related to tab during tests that could invalidate results. In this fixture (Figure 4.8) load is transferred at the specimen ends and, therefore, fixture internal superficies are flat and smooth with only aim to be an anti-buckling structure. Issues can raise, however, from how load is transferred: it could cause ends failure and therefore results are not representative of real material characteristics.

Figure 4.8: ELSS test fixture [4.3]

4.1.4 Shear and end-loading Test Method [4.3,4.7-4.8]

Due to issues rising from all previous compressive test methods (especially stress concentrations at grip surfaces for shear methods and ends failure for end loading tests), a new concept was developed at University of Wyoming by D.F. Adams (Figure 4.9-4.10).

This new fixture has the same geometry of ELSS (of which, it represents an improvement) but with rough inner surfaces that allow load transfer partially by shear. Changing tightening torque it is possible to change percentages of load transfer by shear and at specimens ends in order to obtain the best combination possible. With this expedient, it is possible to avoid problems risen from other methods and, therefore, it is a reliable method to test high strength materials.

Moreover, this fixture is small and light; hence, easy to move and use.
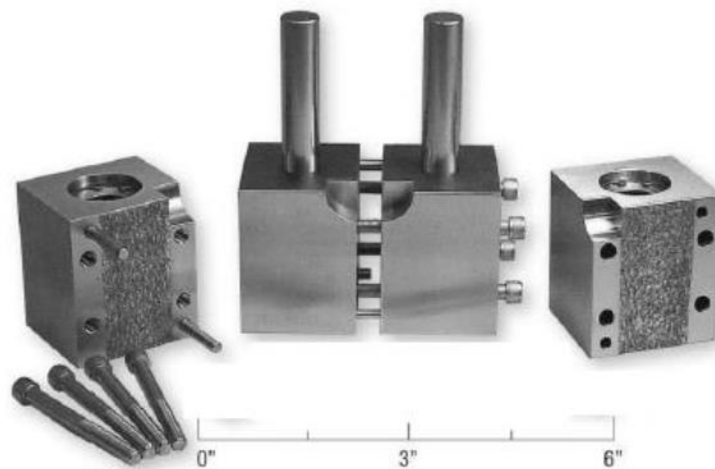
Figure 4.9: CLC test fixture
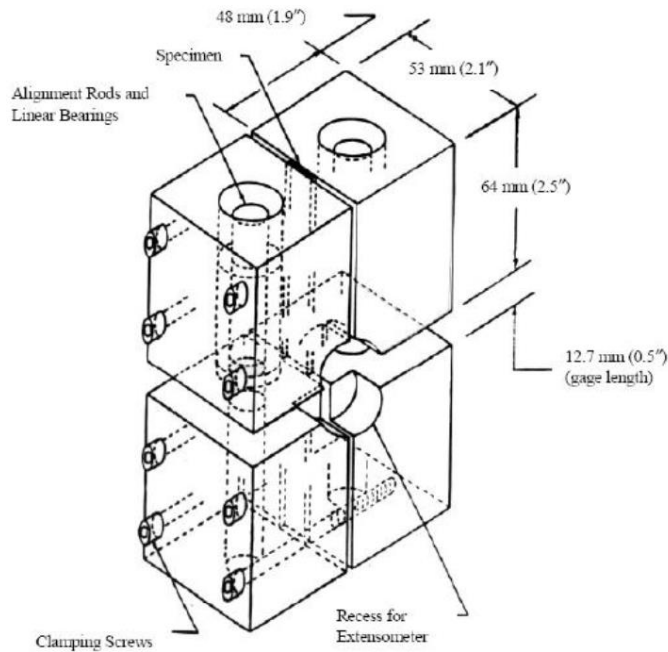
Figure 4.10: CLC test fixture characteristics

4.2 CAI test

Previously described fixtures are usually used for pristine composite materials testing but they could also be employed to study compressive residual strength of damaged composites. Other fixtures were specifically developed to achieve this aim. They are called Compression After Impact (CAI) fixtures.

In the following sections, the most important CAI fixtures are described.

4.2.1 NASA CAI Fixture

NASA fixture (Figure 4.11) consist of four separate parts which, when assembled, create a simple support for the specimen at every edge and, therefore, an anti-buckling guide.

The specimen height could vary from 254 to 318 mm and width from 127 to 178 mm. In NASA test directive [4.9], impact test is also described.
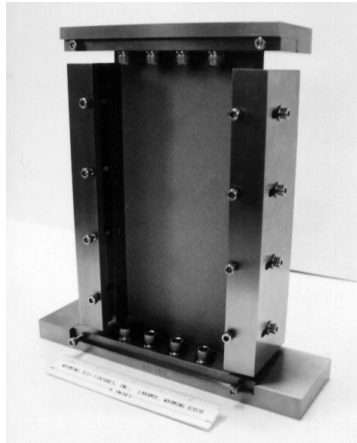
Figure 4.11: NASA Compression After Impact fixture [4.9]

4.2.2 Boeing CAI Fixture

In this case, specimen is clamped at all edges by means of a steel frame. Only a 5mm long gauge section is left unsupported, in the middle of specimen height. This allows specimen failure at that section, in correspondence of impact location. Vertical fixture sides are knife-edge shaped [4.10].

Boeing CAI Fixture (Figure 4.12) is versatile and can be used with different specimens dimensions.

This fixture has been standardised by ASTM [4.11].
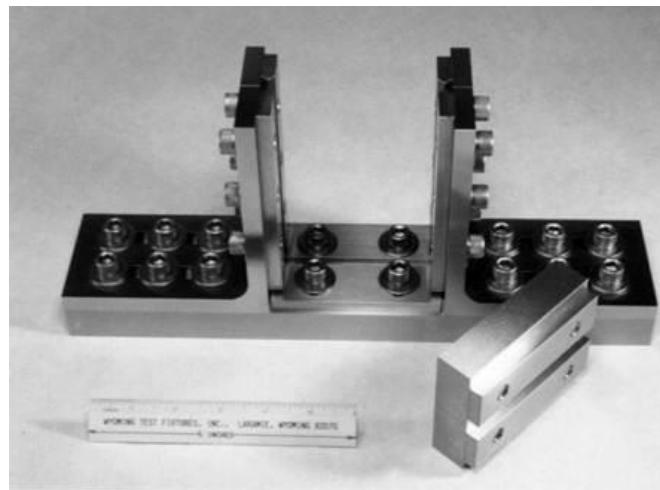
Figure 4.12: Boing CAI Fixture

4.2.3 BAE Systems CAI Fixture

BAE Systems CAI Fixture allows testing large dimension specimens and panels (Figure 4.13).
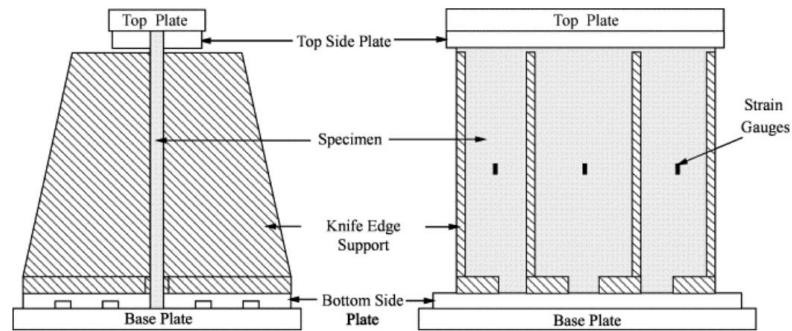
Figure 4.13: BAE CAI Fixture

In this fixture, top and bottom specimen edge are clamped and there are not side supports. Front and back support can be moved as specimens dimensions require. Top part does not have any vertical rails, therefore, there could be early buckling.

4.2.4 Airbus CAI Fixture

Airbus CAI test Fixture is quite similar to Boeing CAI fixture (Figure 4.14). Specimen is supported on its four edges by a steel frame; top clamping part is smaller than specimen width and vertical support are all along specimen height.

Figure 4.14: Airbus CAI Fixture

After a deep study of all previously described fixtures and a critical analysis of present experimental campaign conditions, it was decided to use CLC test fixture. In fact, due to the necessity of testing specimens with near-edge impacts, compression fixture should not support specimens longer edges, at least at the impact location. Moreover, this fixture would have avoided improper specimen failures, caused by stress concentrations and end loading.

4.3 CLC tests at ENEA Laboratory of Materials Technologies Faenza

Thanks to a collaboration with ENEA SSPT-PROMAS-TEMAF (Sustainability Department of Production and Territorial systems - Division of technologies and materials processes for sustainability – The Laboratory of Materials Technologies Faenza), in particular with Eng. Matteo Scafé, it was possible to use CLC fixture at this Laboratory. In present section, therefore, main step followed during Compression After Impact tests are described.

Combined Loading Compression test fixture was used to test in compression all specimens of the experimental campaigns presented in this thesis. It was used with a universal testing machine (Figure 4.15), equipped with an MTS 100 kN load cell and an LVDT with scale ±100mm.

Figure 4.15: MTS universal testing machine at ENEA laboratories

ASTM D6641/D6641-M15 [4.8] describes specimens dimensions and tolerances. For experimental campaign described in this thesis, it was chosen a width of 30 mm, in order to be able to perform central and near edge impact on the same geometry (Figure 4.16).
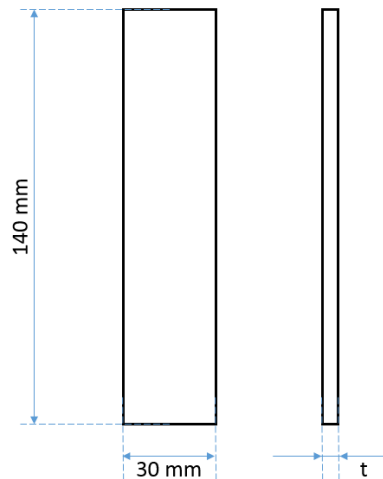
Figure 4.16: specimens dimensions (t indicates thickness that is different depending on experimental campaign)

To use CLC test fixture there are some steps that need to be properly done in order to achieve a reliable test:

- Specimen is housed, vertically, in the bottom part of CLC test fixture, using a flat table as reference surface (Figure 4.17). Bottom specimen surface has to be in contact with the table, while lateral edges should be vertical and in the middle of fixture (vertical rails could be used as reference for this step).
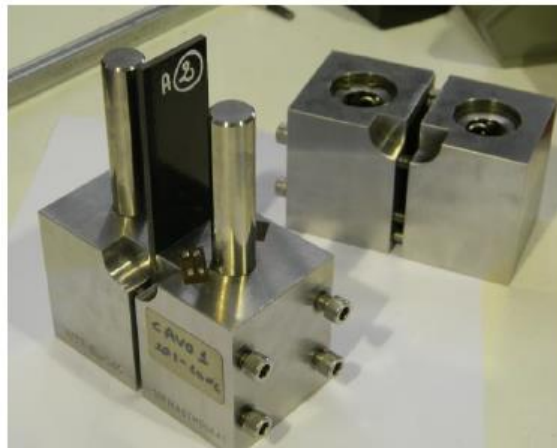
Figure 4.17: Specimen housed in the bottom of CLC fixture

- Screws are tied by means of a hex key, following an X path in order to tie them uniformly. Tightening torque, in this step, is low: hex key is used manually (Figure 4.18) and only lately screws would be tied with a torque wrench.

Figure 4.18: screws tightening by means of a hex key

- If specimen has strain-gauges on it, sensors terminals and acquiring system terminals have to be tinplate on sideburns already present on CLC fixture (Figure 4.19). Acquisition terminals are also connected to a 'dummy' strain-gauge: this is a sensor glued on a specimen made of same kind of material and stacking sequence, not exposed to any load (Figure 4.20). This sensor there will only acquire temperature and humidity effect on the material strain and give the chance of get rid of them for post-processing test data. Strain data are then acquired by an acquisition system (Figure 4.21).

Figure 4.19: Strain-gauges terminals connected to sideburns

Figure 4.20: Dummy Strain-gauge and Strain acquisition connections

Figure 4.21: Strain Acquisition sistem

- Fixture top part is then put on the table and assembly is completed. Screws of this part are tied by means of a hex key. Then, the fixture is laid down on the table and a torque wrench is used (Figure 4.22), with a proper tightening torque previously decided. This tightening torque was decided by means of some tests performed on spare specimen, before every experimental campaign; main aim of this set up is to get a good load partition between shear and end loading.

  In fact, tightening torque is the only factor that can change this distribution: it has to be a fixed value individuated in order to obtain reliable test results and specimen failure.
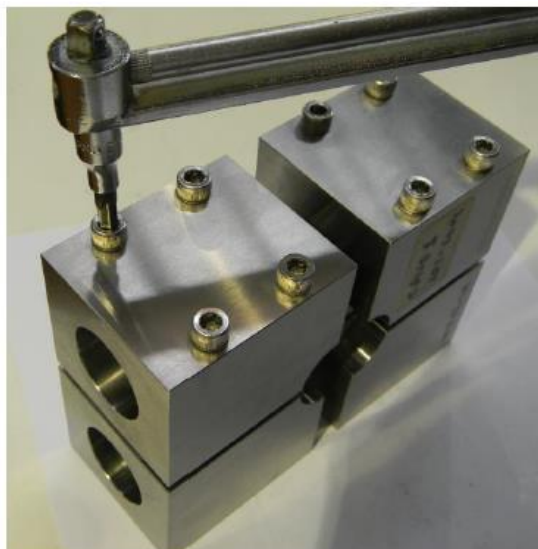
Figure 4.22: Screws tightening by means of a tightening torque

- Assembly is, then, put on the loading plate of universal testing machine, exactly at its centre, in order to align the loading chain (Figure 4.23).
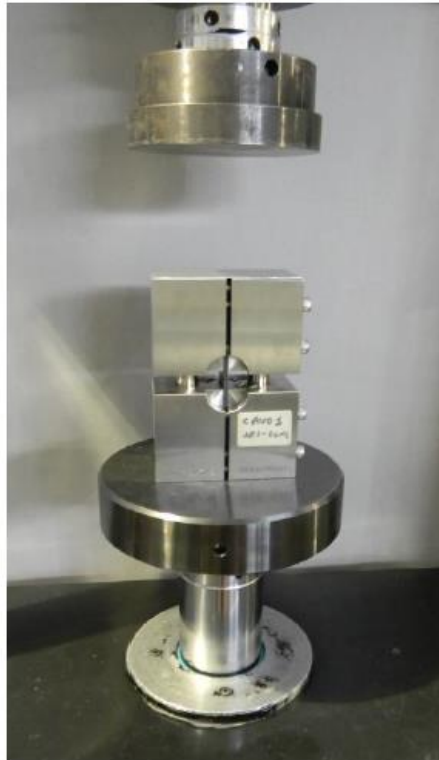
Figure 4.23: Test fixture placed on testing machine plate

- Test is then started in displacement control with a rate of 1.3 mm/min as described in ASTM. Test end is at the specimen failure, commonly when load bearing capacity decreases of around 80% of maximum force (Figure 4.24-4.25).
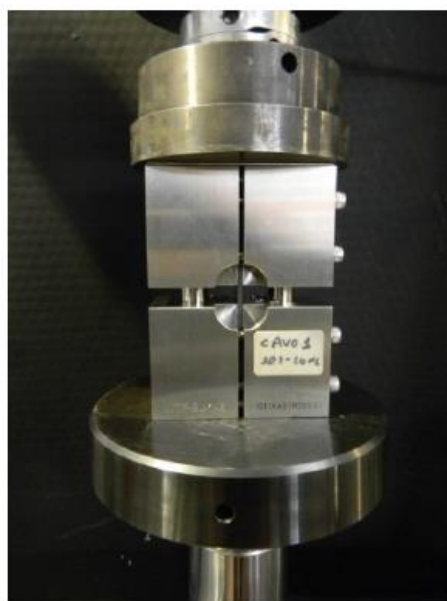
Figure 4.24: Test Fixture under a compressive test
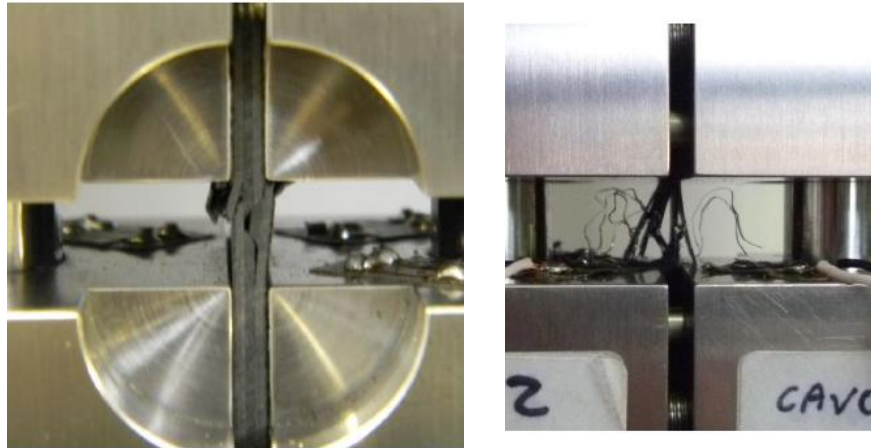
Figure 4.25: detail of a failed specimen

- Failed specimen is removed (Figure 4.25), after disconnecting electric connections, if present. Failure mode are then classyfied following ASTM instructions.

Figure 4.25: Detail of a failed specimen after removing it from CLC test fixture

'Brooming' failure mode (Figure 4.26) is usually common in this kind of test; this is to be ascribed, according to Adams [4.3], to a post failure phenomenon: short delay, after failure, in the removal of compression load, causes this kind of shape.

Figure 4.26: Detail of a brooming failure mode

4.4 Post-processing data

Data acquired by load cell and strain-gauges are recorded in a '.txt' file, that has to be processed by means of analysing software like Microsoft Excel or Matlab.

Every test is analysed: stresses and strains are calculated. For stress, calculation is given by:

(4.1) $\qquad \sigma = \frac{L}{A}$

where σ is stress, L is load and A specimen section area.

Strains are calculated starting from voltage data acquired from strain-gauges. Relation between voltage and strains is given by:

(4.2) $\qquad \varepsilon\,[\mu\varepsilon] = \frac{V * SG * 2}{K_{SG}} * 10^{-6}$

where ε is strains in $[\mu\varepsilon]$, V is voltage acquired from sensor $[V]$, SG is the slope of calibration curve acquired during acquisition system set up, K_{SG} is k factor of specific strain-gauge used.

Usually two strain-gauges per specimen are used in configuration 'back-to-back'. Therefore, there is a sensor on both specimen surfaces (through the thickness direction is not considered) in order to check if compressive test data are reliable, i.e. failure in the middle section of the specimen (called gauge-section) occurred with no instability (buckling). Having two sensors monitoring specimen movements, it is easy to check if flexural instability occurs:

(4.3) $\qquad \% \, Bending = \frac{\varepsilon_1 - \varepsilon_2}{\varepsilon_1 + \varepsilon_2} * 100$

where $\% \, Bending$ is percentage value that gives flexural instability reference, ε_1 is displacement of strain-gauge put on one surface while ε_2 is strain coming from the opposite surface.

References

[4.1] DOT/FAA/CT-93/17 II, Test 'Methods for Composites a Status report', Volume II. Compression Test Methods, 1993.

[4.2] ASTM D3410/D3410M-03 Standard Test Method for Compressive Properties of Polymer Matrix Composite Materials with Unsupported Gage Section by Shear Loading.

[4.3] P. M. Wegner and D. F. Adams, 'Verification of the Combined Load Compression (CLC) Test Method', DOT/FAA/AR-00/26, August 2000

[4.4] Andrew E. Pearson, 'Capabilities of compression test method for evaluating unidirectional carbon fiber reinforced composites', San Jose State University, 1990.

[4.5] ASTM D5467 / D5467M - 97(2010): Standard Test Method for Compressive Properties of Unidirectional Polymer Matrix Composites Using a Sandwich Beam.

[4.6] ASTM D695 – 10: Standard Test Method for Compressive Properties of Rigid Plastics.

[4.7] Donald F. Adams, Leif A. Carlsson, R.Byron Pipes, 'Experimental Characterization of Advanced Composite Materials', third edition, CRC PRESS 2003.

[4.8] ASTM D6641 / D6641M – 15: Standard Test Method for Compressive Properties of Polymer Matrix Composite Materials Using a Combined Loading Compression (CLC) Test Fixture.

[4.9] NASA Reference Publication 1092, Standard Tests for Toughened Resin Composites, NASA-Langley Research Centre, Hampton, Virginia, Revised Edition, July 1983

[4.10] Boeing Specification Support Standard BSS 7260, "Advanced Composite Compression Tests," The Boeing Company, Seattle, Washington, 1988.

[4.11] ASTM D7137/D7137M-12 Standard Test Method for Compressive Residual Strength Properties of Damaged Polymer Matrix Composite Plates

5

Experimental campaigns on carbon/epoxy coupons

Two experimental campaign have been made to understand carbon/epoxy laminate behaviour under impact circumstances. First campaign involved thin specimens and was intended to be the first attempt for proving impact location influence. After having this proved, using the same material, thicker coupons were made, impacted and tested to understand thickness influence on impact resistance.

5.1 Carbon/epoxy coupon experimental campaigns

In order to understand carbon/epoxy (CFRP) composite behaviour under low energy impact events and how these could influence material compressive strength, two experimental campaign were performed.

In the first campaign impact location effect was studied on 2.6 mm thick CFRP specimens: two energy levels (3 and 5 J) and two impact location (central and near-edge) were chosen. The second campaign aimed to individuate thickness influence on impact resistance and damage creation. Therefore, while first group of specimen had an average thickness of 2.6 mm, the latter involved 5.5 mm thick (av.) coupons. Thicker material was tested under 5 and 7 J impact energy while locations were kept the same as previous campaign.

A unidirectional carbon/epoxy pre-preg was used to make both specimens series. Hand-layup was used to build stacking sequences up. After building up, laminates were cured in an autoclave, under pre-decided pressure and temperature, following material datasheet information.

UD lamina properties are not reported, due to industrial importance of material; furthermore, due to specific campaign aims, i.e. a comparison between different impact locations and energy influence within the same kind of material, they are not fundamental for results understanding.

5.1.1 Manufactoring of specimens

For both campaigns, specimens were cut from a 490x420mm laminate obtain by means of hand-layup. Main passages of this process are:

- Pre-preg roll is removed from freezer 8/10 hours before it would be used, and it is left at room temperature. It is put on a rack, trying to avoid any wrinkle formation on pre-preg surface.
- Specimens stacking sequences were, in both cases, chosen to have a cross-ply, symmetric and balanced laminate. Only plies number was different: for the first experimental campaign, specimens had 9 plies $[90/0_2/90/\overline{90}]_s$, while thicker laminate was obtained heaping 17 layers in $[(90/0_2/90)_2/\overline{90}]_s$ sequence. (Figure 5.1)

Figure 5.1: Carbon Epoxy prepreg cutting (by means of a cutter and a ruler)

- An Aluminium mould (Figure 5.2) was used: it was cleaned very carefully from old resin remains; three layers of release fluid are applied by means of a brush; bars are fasten on it to obtain laminate dimensions and to prevent a substantial resin outflow; a release film is put on the mould, in order to obtain an easier removing after curing.

Figure 5.2: Aluminium mould with edge bars (on the left); aluminium mould with a release film (on the right)

- After cutting all layers, those were put in the mould paying attention to fibres direction in order to obtain correct stacking sequence. Every ply has two plastic/paper foil, necessary to protect pre-preg from humidity and to prevent that, when rolled, layers would paste all together; these foils need to be removed before adding a new pre-preg layer. It is, also, fundamental to remove, with a Teflon spatula, all air bubbles that could result from an incorrect deposition (Figure 5.3).
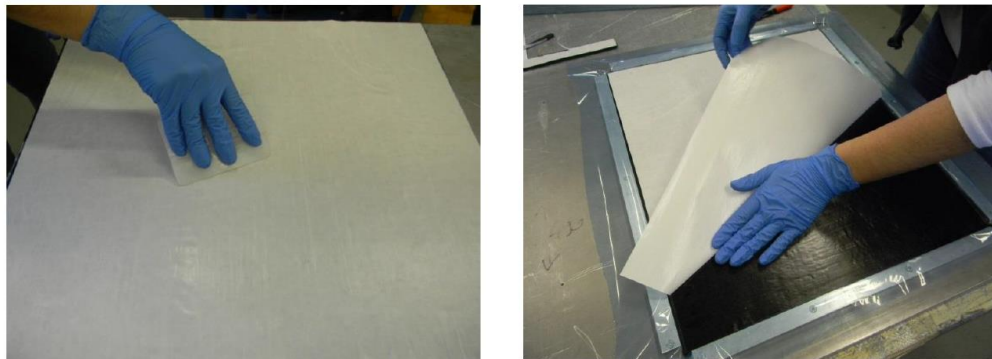
Figure 5.3: Pre-preg laying up: use of teflon spatula for removing air bubbles (on the left), removing of protection films from pre-preg layer (on the right)

- An Aluminium top is wrapped with release film and then eased down on the final stack (Figure 5.4).
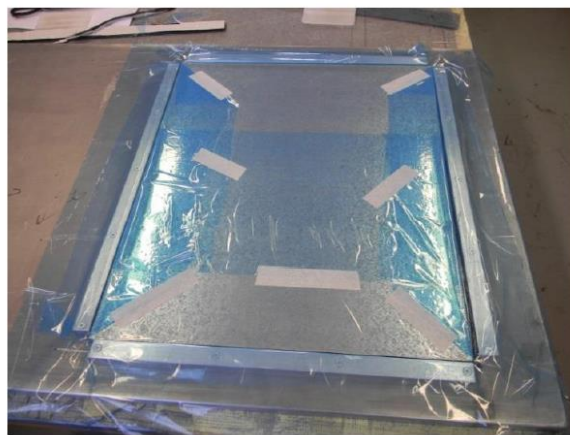
Figure 5.4: Complete stacking sequence with top plate (wrapped in releasing foil)

- By means of scrap pre-preg, coming from cutting phase, a small sample of laminate is made (Figure 5.5). It is necessary to have a better monitoring of cure cycle: same amount of layers are used and a thermocouple is put in the middle of stacking sequence. This sensor is then connected to the autoclave. In this way it is possible to know laminate inner temperature and to control cure cycle in order to obtain the best cure for laminate involved.

Figure 5.5: material sample with a thermocouple in the middle of its stacking sequence

- Everything is wrapped within breather/bleeder, a vacuum valve is positioned and a vacuum bag is realized with proper foil. Internal vacuum bag atmosphere isolation, from external one, is assured by means of a sealant tape (Figure 5.6).

Figure 5.6: (on the top) positioning a vacuum bag foil; (on the left) sealant tape to close vacuum bag; (on the right) vacuum pump is connected to vacuum valve to remove air

- Vacuum valve is then connected to a vacuum pump until air inside bag is removed. Pump is disconnected and sealant tape grip is tested: if bag is still well compacted after two hours, it is put inside autoclave (Figure 5.7). Valve and thermocouple are connected properly to autoclave system: with the first one, vacuum is assured for entire cure cycle duration; thermocouple would make thermal cycle fit for real needs.

Figure 5.7: vacuum bag connected to autoclave vacuum pump and thermocople acquisition system

- Autoclave is hermetically closed and cure cycle started. This is decided in accordance with resin datasheet provided by the pre-preg producer.
- When cycle is done and everything is back to room temperature and pressure, autoclave is opened and everything is removed. Then all unneeded layers are taken away and cured laminate is extracted from mould (Figure 5.8).
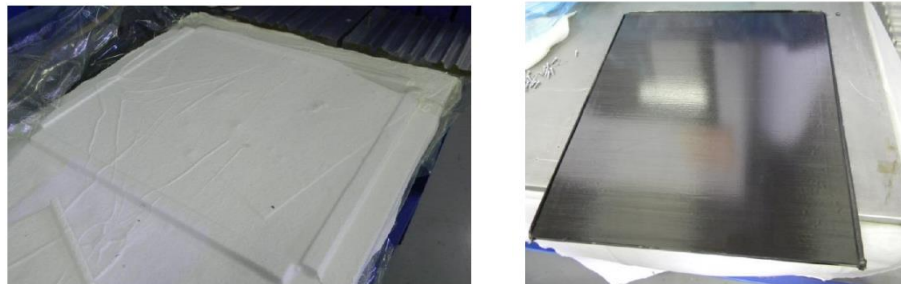
Figure 5.8: mould after cure cycle, removed from autoclave and without vacuum bag (on the left); cured laminate (on the right)

Laminates cured with previously described process, were cut with a band saw to obtain 25 specimens. Dimensions were chosen taking into account requirements for using CLC as a CAI fixture. CLC characteristics are discussed in chapter 4.

There was not, in fact, any ASTM standard related to this kind of tests: low velocity impact tests are regulated only with drop weight tower [5.1] and for central impacts. There still is no standard for near-edge impacts.

Furthermore, the CAI standard [5.2] is only related to central impacts and set-up tests results were not really reliable. Therefore, CLC standard was chosen [5.3].

Hence, coupons 140x30 mm have been cut, in order to get the maximum possible width not interfering with screws in CLC blocks. At the same time, central and near edge impact, with same specimen geometry (Figure 5.9), have been carried out.
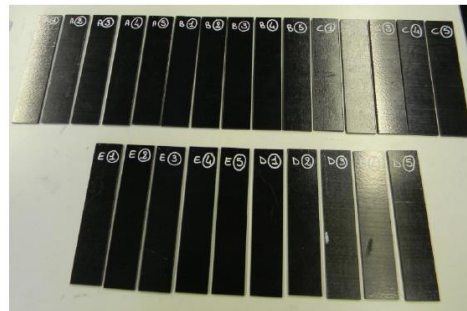
Figure 5.9: example of cut specimen

There is not in [5.3] a specific limit for specimen thickness; therefore, stacking sequences were freely chosen. Thinner laminate average thickness was 2.6 mm while thicker one was 5.5 mm.

Both specimens dimensions can be found in Appendix A.

5.2 Impact tests

Impact tests have been performed by means of 'modified Charpy pendulum' described in chapter 3. Settings steps there described, are narrowly followed. Different energies are arranged with different starting position of the maul, and, therefore, of bar angle.

Each test is filmed to evaluate also residual energy, thanks to record of bounce angle.

After impact tests each specimen is inspected, visually, and in the case of thicker coupons, also with Ultrasonic signals. By bare eye, impact damage was checked to verify its shape and external dimensions. By means of UT NDI, moreover, it was possible to acquire damage extension and depth.

5.3 CAI tests

Damaged specimens were tested in compression with a CLC test fixture, using a MTS electro-hydraulic universal testing machine, equipped with a MTS 100kN load cell. All tests were conducted in displacement control with a 1.3mm/min rate. Data were acquired with a 10 samples/s rate.

During tests, compressive force was acquired until a load bearing capacity drop of 80%. Compressive strength was calculated by means of:

(5.1) $\qquad \sigma_{max} = \dfrac{L_{max}}{A}$

where σ_{max} is maximum compressive strength, L_{max} is maximum force reached, A is specimen sectional area.

Some specimens per each group were also instrumented with strain-gauges: some of them with two longitudinal strain-gauges while few with a bi-directional strain-gauge and a longitudinal one. All strain-gauges are in a 'back-to-back' configuration (one per each specimen surface) in order to acquire displacement on both surfaces and check if any buckling occurs. In that eventuality, data acquired are not reliable because failure would be affected by instability.

Bending [%] is calculated by means of:

(5.2) $\qquad \% \, Bending = \dfrac{\varepsilon_1 - \varepsilon_2}{\varepsilon_1 + \varepsilon_2} * 100$

where $\% \, Bending$ is the bending in percentage, ε_1 is the displacement of the first surface, ε_2 is the displacement acquired at the second surface.

Mean values, standard deviations and variation coefficients are reported, as well, for measured quantities:

(5.3) $\qquad \bar{x} = \dfrac{1}{n} \sum_{i=1}^{n} x_i$

(5.4) $\qquad y = \sqrt{\dfrac{\sum_{i=1}^{n}(x_i - \bar{x})^2}{n}}$

(5.5) $\qquad CV = \dfrac{y}{|\bar{x}|}$

where $\bar{x}$ is the mean value of a x quantity, n is the number of samples, y is the standard deviation, CV is the variation coefficient.

5.4 Thin specimens experimental campaign

5.4.1   Impact tests

Twenty-six specimens were tested. They were divided in 5 groups (5 specimens per each, beside group A with 6 specimens), characterised by different kind of impacts:

Table 5.1: Thin specimens groups (impact kinds)

Group	Impact
A	No-impact (pristine)
B	3J near-edge
C	5J near-edge
D	3J central
E	5J central

Average dimensions are reported in the following table:

Table 5.2: specimens average dimensions

	Quantity	Width [mm]	Thickness [mm]	Length [mm]	Mass [g]
A	**Mean value**	29.79	2.90	139.4	18.06
	St.Dev.	0.04	0.02	-	-
B	**Mean value**	29.87	2.77	139.6	17.70
	St.Dev.	0.05	0.02	-	-
C	**Mean value**	29.80	2.868	139.7	18.02
	St.Dev.	0.05	0.03	-	-
D	**Mean value**	29.71	2.53	139.0	15.94
	St.Dev.	0.10	0.03	-	-
E	**Mean value**	29.76	2.80	139.3	17.50
	St.Dev.	0.07	0.03	-	-

Impact tests were performed as already described. Video per each test was recorded and analysed. Actual energy, residual energy and absorbed energy were calculated with method described in chapter 3.

Table 5.3: Actual, residual and absorbed energies

Specimen	Actual energy [J]	Residual energy [J]	Absorbed energy [J]
B1	3.3	0.9	2.4
B2	3.1	0.8	2.2
B3	3.1	1.2	1.8
B4	3.3	1.2	2.1
B5	3.2	1.3	1.9
C1	4.7	0.9	3.8
C2	4.9	1.2	3.6
C3	4.9	1.1	3.8
C4	4.7	1	3.7
C5	4.5	0.8	3.7
D1	3.3	1.2	2.2
D2	3.3	1.1	2.3
D3	3.5	1.1	2.4
D4	3.2	1.1	2.1
D5	3.2	1	2.2
E1	5	1.4	3.6
E2	5.2	1.5	3.7
E3	4.9	1.3	3.5
E4	4.5	1.2	3.3
E5	4.9	1.4	3.4

All impacted specimens were visually inspected. Impacts resulted in difficultly detectable superficial damages and therefore they could surely be catalogued as BVID. Following pictures show some examples:
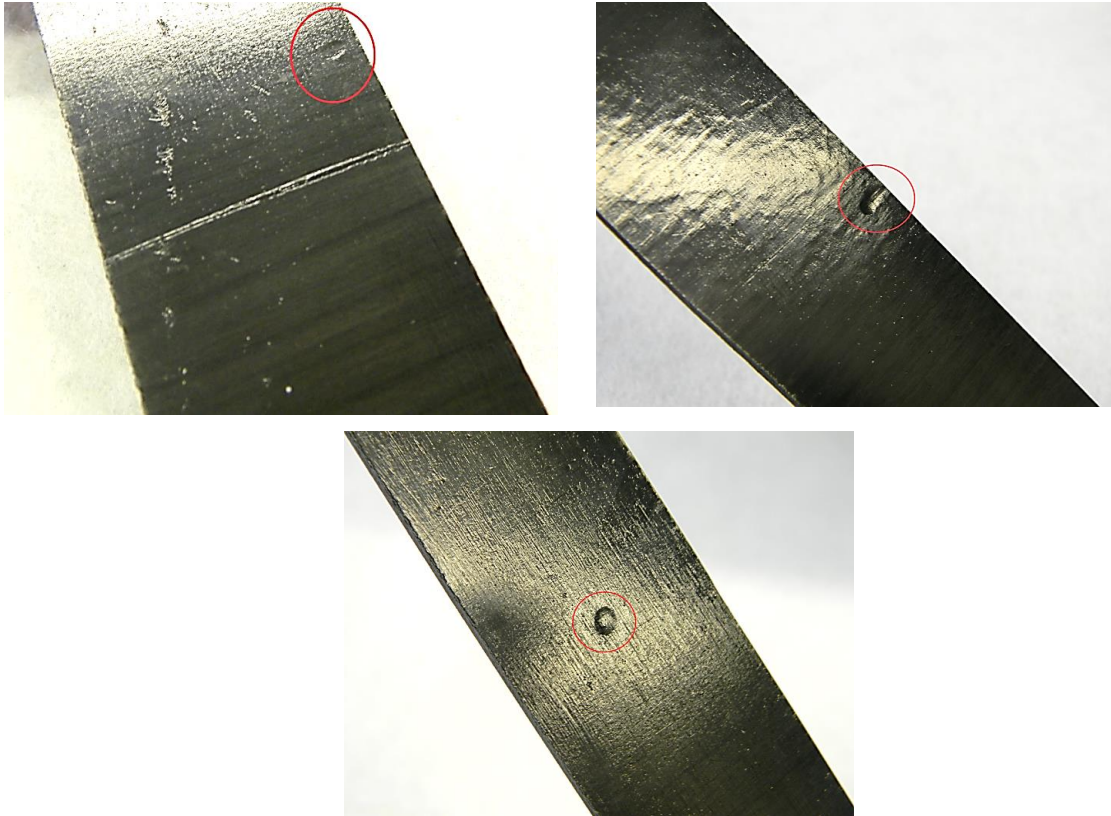
Figure 5.10: BVI Damages on 2.6mm thick specimens: 3J NE on the left, 5J NE on the right, 5J CI in the lower picture.

5.4.2 Compression After Impact

Specimens were tested in compression by means of CLC test fixture. Principal steps are described in chapter 4.

Compressive tests results are shown in the following table:

Table 5.4: Compressive residual strength

Group	Impact	$\sigma_{average}$ [MPa]	% DEV
A	No impact	386.34	-
B	3 J near-edge	342.46	-11.36%
C	5 J near-edge	265.36	-31.31%
D	3 J central	347.58	-10.03%
E	5 J central	331.22	-14.27%

Impact on a composite laminate can reduce its compressive resistance: even a very low energy can affect residual strength; furthermore, near-edge impact influences the residual strength more than central one. The higher energy (5 J) near-edge impacted specimens have a considerably lower compressive residual strength (-31.31 %).

For the lower impact energy a less clear correlation between central and near-edge location.

Therefore, it could be said that:

- low-energy impact can affect composite compressive residual strength;
- 5 J impact creates wide inner damages in a 2.6 mm thick carbon/epoxy specimen, that result in a lower compressive resistance compared to 3 J impact energy;
- 5 J impact can reduce of around 30% compressive residual strength in a carbon/epoxy and therefore it could be considered a dangerous event;
- Impact location is extremely important for impact resistance and therefore it was demonstrated that impact around an airplane cutout could be really dangerous for safety issues.

5.5 Thick specimens experimental campaign

5.5.1 Impact tests

Twenty-five specimens were tested, split in 5 groups (5 specimens each). Each group is impacted with a different energy or location, as described in the following table:

Table 5.5: Impact types for 5.5mm thick specimens

Group	Impact
A	No-impact (pristine)
B	5J near-edge
C	7J near-edge
D	5J central
E	7J central

Average dimensions are:

Table 5.6: 5.5mm thick specimens average dimensions

	Quantity	Width [mm]	Thickness [mm]	Length [mm]	Mass [g]
A	**Mean value**	30.05	5.42	139.96	33.60
	St. Dev.	0.02	0.01	-	-
B	**Mean value**	30.00	5.59	140.00	34.18
	St. Dev.	0.02	0.02	-	-
C	**Mean value**	30.04	5.57	140.01	34.14
	St. Dev.	0.01	0.02	-	-
D	**Mean value**	30.04	5.53	140.01	34.02
	St. Dev.	0.01	0.01	-	-
E	**Mean value**	30.04	5.41	139.96	33.76
	St. Dev.	0.01	0.01	-	-

Impact tests were performed as described in chapter 3. Recorded videos were watched to calculate actual energy, residual energy and absorbed energy (Table 5.7).

Table 5.7: Actual, residual and Absorbed energies for 5.5mm thick specimens

Specimen	Actual energy [J]	Residual energy [J]	Absorbed energy [J]
B1	5.3	2.2	3.1
B2	5.6	2.3	3.3
B3	5.3	2.2	3.1
B4	5.5	2.2	3.3
B5	5.7	2.2	3.5
C1	7.5	2.7	4.8
C2	7.5	2.8	4.7
C3	7.5	2.7	4.8
C4	7.3	2.7	4.6
C5	7.3	2.7	4.6
D2	5.6	1.2	4.4
D3	5.6	1.1	4.5
D4	5.7	1.2	4.5
D5	5.7	1.3	4.4
E1	7.6	1.6	6.0
E2	7.6	1.6	6.0
E3	7.3	1.6	5.7
E4	7.5	1.6	5.9
E5	7.4	1.6	5.8

All impacted specimens were visually inspected. All damages resulted to be BVID. An example of near-edge impact is showed in the following pictures:
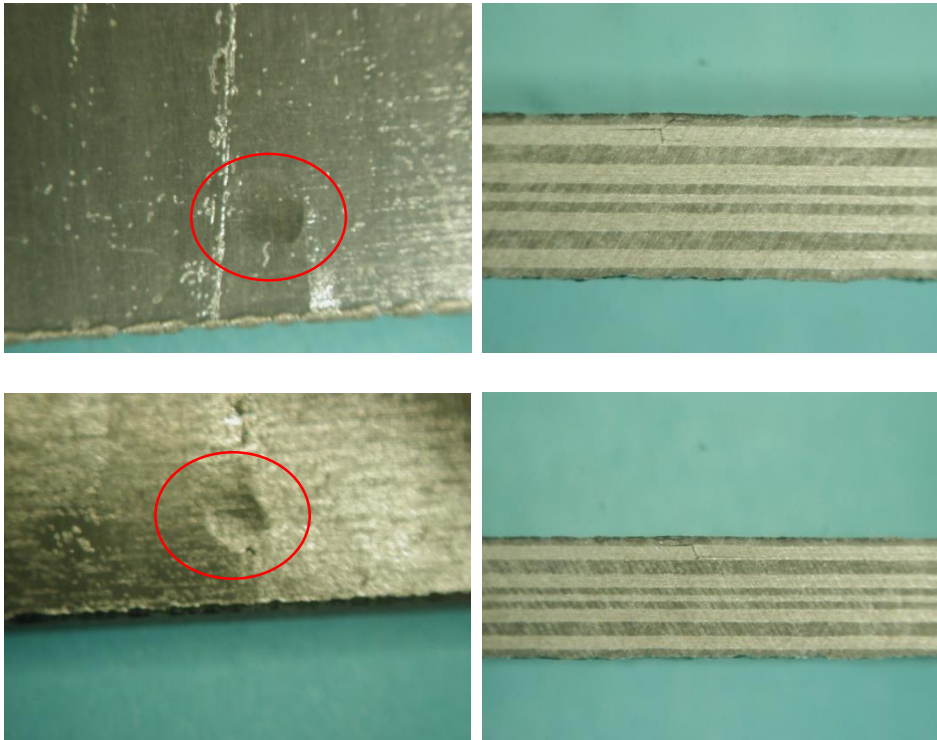
Figure 5.11: 5J and 7J near-edge impacts: impact dent and through ther thickness damage

Moreover, Non Destructive Inspections (NDI) were conducted on impacted and pristine materials in order to individuate internal damages.

Two laboratories were involved: ENEA SSPT-USER-SITEC (Sustainability Department of Production and Territorial systems - Efficient Resources use and Closing Cycles Division – The Laboratory of Technologies for Sustainable Innovation Casaccia) and Vetorix Engineering.

In the first laboratory, Ultrasonic tests were performed: 7 J impacted specimens showed clearly inner damages while 5 J impact created a well defined damage only for the near-edge location (Figure 5.12-5.13).
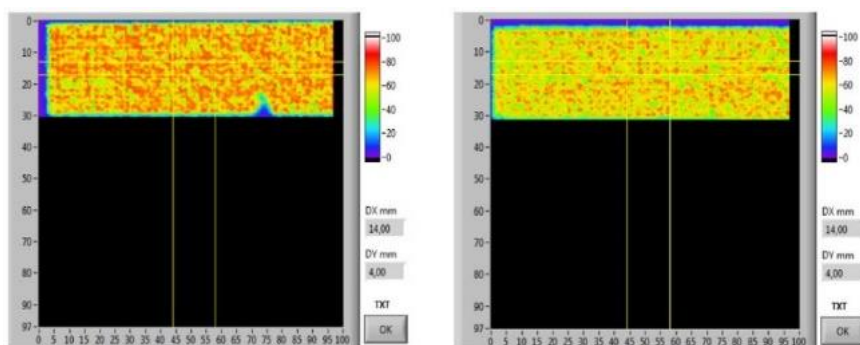
Figure 5.12: C-scan specimen C1 (7 J NE) on the left, specimen B5 (5 J NE) [5.7]
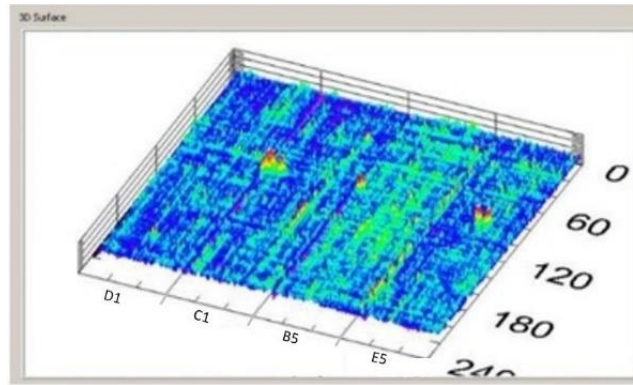
Figure 5.13: 3D scan impacted specimens (from the left D1, C1, B5, E5) [5.7]

Therefore, an additional inspection was performed by means of tomographic test at Vetorix Engineering (Marcon, VE). Two examples are showed in Figure 5.14-15, where impacted area is presented in red squares.
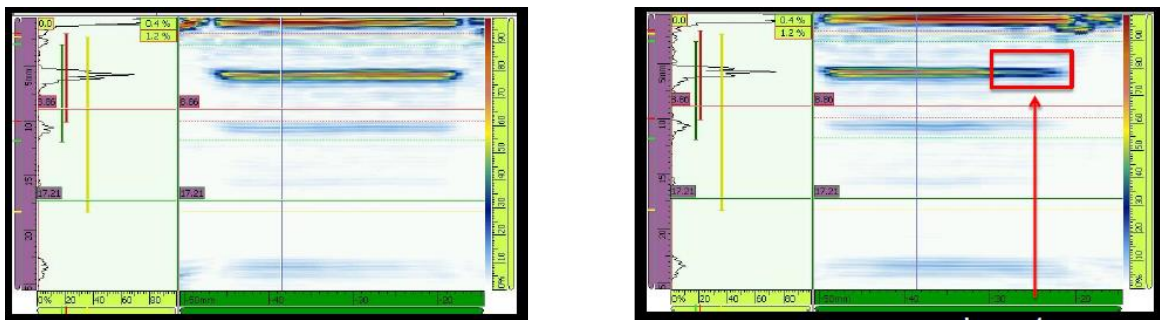
Figure 5.14: C2 7 J NE specimen tomography (impact zone in the red square)
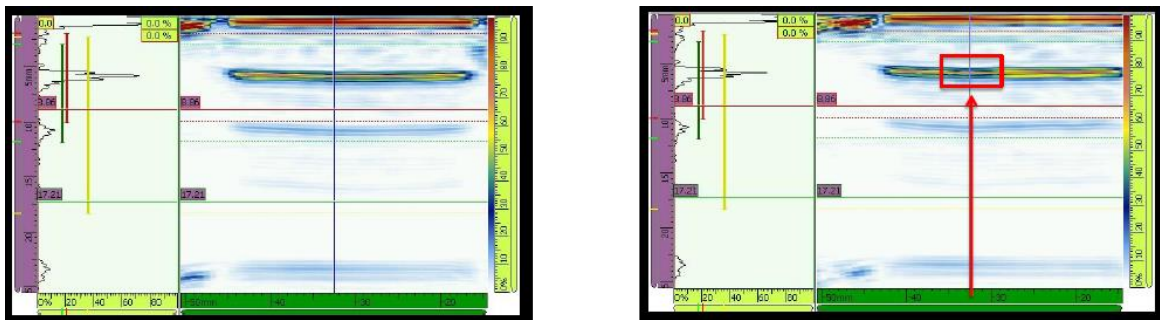
Figure 5.15: B4 5 J NE specimen tomography (impact zone in the red square)

5.5.2 Compression After Impact

Specimens were tested in compression by means of CLC test fixture following guide lines in chapter 3.

Results are in the following table:

Table 5.8: Compression After Impact results (comparison with pristine specimens)

Group	Impact	$\sigma_{average}$ [MPa]	% DEV
A	No impact	468.71	-
B	5 J near-edge	446.06	-4.83
C	7 J near-edge	457.55	-2.38
D	5 J central	510.63	8.94
E	7 J central	498.57	6.37

Looking at compression tests mean values, in 5.5 mm thick specimens there is not a clear evidence of impact location influence on residual strength. This is true, in particular, for central impacted specimens: their compressive strength is even higher than pristine coupons. In this case is strictly necessary to consider the dispersion of results: for composite materials data scatter is quite high, and percentages that were obtained are too low to overcome this dispersion.

Looking at near-edge impacted coupons, a lower compressive strength has been obtained; this decrease is quite small but still could be evaluated as an impact effect. Failure modes can be a proof of this effect: during compression tests, in fact, almost all near-edged impacted specimen resulted in an acceptable failure mode (at gauge sections), while pristine and central impacted specimen groups had more unreliable failures (edge failure or between grip surfaces). This shows that a near-edge impact creates a low resistance area that acts as a trigger for failure.

5.6 Overall conclusions

Comparing results from both campaigns, it was seen that, while for thin specimens impact location and energy are really effective on residual compressive strength, thick specimen tests did not show clearly this effect. A small drop in residual strength appeared only for near-edge impacted specimens while central impacted ones do not show any decrease.

These strength reductions (2.38% for 5 J NE and 4.8% for 7 J NE), however, could be ascribed, in addition to the impact location, to many factors, as: manual lay-up process, curing process, cutting process, etc.

Therefore, low energy impact location does not affect compressive residual strength of thick specimens (5.5 mm), as certainly as for thinner specimens (2.6 mm): for 5.5 mm thick specimens, a 5 J near-edge impact resulted in a 4.8% reduction of compressive residual strength, while for 2.6 mm thick specimens, it produced a 31.2% drop. This value is quite high and shows an objective influence of the low energy level of impact, on residual strength for the 2.6 mm thick laminate.

In the case of 5.5 mm specimens, it was undoubtedly demonstrated that even a low energy near-edge impact (without high effect on residual strength) can result in a trigger for damage growth, creating a weak spot in the structure and, therefore, a stress concentration point.

Hence, impact location and energy level are important parameter that could deeply influence composite structures characteristics.

References

[5.1] ASTM D7136 / D7136M – 15, Standard Test Method for Measuring the Damage Resistance of a Fiber-Reinforced Polymer Matrix Composite to a Drop-Weight Impact Event

[5.2] ASTM D7137/D7137M-12 Standard Test Method for Compressive Residual Strength Properties of Damaged Polymer Matrix Composite Plates

[5.3] ASTM D6641 / D6641M – 16, Standard Test Method for Compressive Properties of Polymer Matrix Composite Materials Using a Combined Loading Compression (CLC) Test Fixture.

[5.4] M.P. Falaschetti, M.Scafè, E.Troiani, V.Agostinelli, S.Sangiorgi, Experimental determination of compressive residual strength of a carbon/epoxy laminate after a near-edge impact, XXIII IGF, 2015.

[5.5] M.Scafè, M.Labanti, A.Coglitore, G.Raiteri, R.Dlacic, E.Troiani, E.Besseghini, M.P.Falaschetti, Experimental determination of compressive strength of an unidirectional composite lamina: indirect estimate by Using Back-out Factor (BF), XXII IGF, 2013.

[5.6] M.Scafè, G.Raiteri, A.Brentari, R.Dlacic, E.Troiani, M.P.Falaschetti, E.Besseghini, Estimate of compressive strength of an unidirectional composite lamina using cross-ply and angle-ply laminates, Frattura ed Integrità Strutturale 29, 2014.

[5.7] M.P. Falaschetti, M. Scafè, A. Tatì, E. Troiani, Experimental determination of thickness influence on compressive residual strength of impacted carbon/epoxy laminate, XXIV IGF, 2017.

6

History and development of Fibre Metal Laminate

Fibre Metal Laminate were firstly developed at University of Technology Delft. They showed, since the beginning, good impact resistance and, therefore, they were a good spark in the search of an improving for carbon/epoxy impact issues.

In this chapter, Fibre Metal Laminate development, since their birth, is summarised.

6.1 Introduction

As already said, composite materials have low impact resistance: when an object hits composite surface, it will create an internal damage (mainly matrix cracks and delaminations), and, if it does not exceed a threshold, remaining in elastic behaviour, no damage could be noticed on the external surface. Only if this threshold energy is exceeded, fibres start to fail and damage starts to be evident on surface as well. It has been demonstrated that, even with just internal damages, composite materials could face a substantial variation of their properties, in a reduction of compression resistance [6.1-6.2].

Therefore, a question raised: how is it possible to improve this composite drawback?

Many studies have been carried out to achieve this goal: nano-composites layers between pre-pregs plies, different kind of matrix, combination of pre-pregs with metal layers, etc.

Each of previous was taken into account trying to understand which parameter could be the most important to choose one over the others. Hence, it was decided to find something that could be implemented with a low increase of costs compared to pure composite components.

With this in mind, nano-fibres reinforced composites had to be discarded. This method, in fact, shows good results [6.3-6.7] but it is still in development and therefore prices are still high. Furthermore, nano-technologies could also rise topics for health safety discussions.

In the same way, matrix changes or improvements were not taken into account due to a more chemical nature of these solutions.

Therefore author's choice fell on adding metal layers in composite stacking sequence.

Bonding metal layers with composite is a technology that has been developed for a long time in aeronautical field. Therefore, it is a well-consolidated procedure that has reached quite low costs compared to other production methods [6.8-6.12].

Main research environment regarding this kind of hybrid composites is in the Netherland, at TU Delft Aerospace Engineering faculty. Since 80s' a new kind of material was developed in this university: Fibre Metal Laminate. Many different stacking sequence and studies were carried out proving material good properties.

Professor Calvin Rans, at Structure Integrity & Composites (SI&C) group, proposed author to spend an exchange period at TU Delft University to take advantage of Dutch experience in FML production. Therefore, author spent a period in Holland performing Quasi Static Indentation (QSI) tests, Three Point bending, and improving knowledge in optical sensors and micrographic inspections.

Before going through the Quasi Static Indentation experimental campaign, performed during author's stay at Aerospace Engineering Faculty at TU, it is worth to introduce a brief history of FML.

6.2 Fibre Metal Laminate (FML)

In aeronautical history, there have been three important materials changes: the first one in '30s, when aluminium was introduced instead of wood and canvas; another step took place with progressive introduction of composites in '80s and '90s. The last one can be individuated with hybrid materials development, and in particular of Glare, that is nowadays used for A380 fuselage sections [6.12-6.16].

Hybrid materials are a particular kind of composite materials that was developed trying to overtake metals and common composites issues. In fact, metals have good properties, mostly related with plasticity, but they are poor in fatigue and corrosion. On the other hand, composites show good resistance to fatigue and corrosion but fragile failure and mechanical characteristics mostly dependent on many factors.

Combining these two materials, it is possible to overtake their drawbacks and obtain a hybrid material that shows high mechanical characteristics and good fatigue properties thanks to fibre bridging.

This is due to the FML lay ups (Figure 6.1): they are obtain by hand-layup, alternating thin metal foils and composite pre-pregs plies. Therefore, when a fatigue crack nucleates in any metal layer, its growth is delayed thanks to fibres contained in close layers, that are

more resistant and transfer load from one side to the other of crack. In this way, metal layers are still carrying load, even in crack section, reducing stress concentration factors and, therefore, crack growth.

Figure 6.1: FML stacking sequence example

6.2.1 History

Metal Laminate were developed as an evolution of adhesives use in aeronautic. It started with bonding together wooden layers at DeHavilland industry: during First World War, DeHavilland Mosquito, completely made with wood, was one of the best fighting airplanes. Due to this good result, metal bonding started to be investigated. At the beginning of '40s a British researcher, Norman de Bruijne, at Cambridge University discovered a synthetic glue suitable for metal. He had already developed a synthetic glue for wood (called 'Aerodux') that was used by DeHavilland. He also developed the method used to bond together more layers: those needed to be press together and heated in order to ensure adhesive solidification and layers connection. This was made by means of a hot-press and represent the first example of what nowadays is known as 'curing process' and was discovered by accident: after one of De Bruijne tests, due to a mistake, glue had flowed in between wooden external layers and hot-press plates and, therefore, it had bonded metal layers as well. From this failed test, he developed a new idea: metal bonding.

De Bruijne could also be defined as 'father' of composite: in 1937, he proposed to embed natural fibres in a plastic (such as Bakelite). This was suggested by natural fibres properties: they have four times strength-to-weight ratio compared with aluminium one. But, obviously, they can not be used alone to build structures; therefore, the need to embed them into a matrix to ensure their location, protect them from external factors and to equally transfer load.

Metal bonding was, in those days, unfortunately, seen as an inappropriate technic in aeronautics. Adhesive suffered from its association with glue used for papers and reminded airplanes built through artisanship and not a real industrial process.

This problem is nowadays solved, with composites, but shows itself again when it comes to 'weak bonds': with this name are indicated all repairs where patches are bonded

together with the pre-treated structure by means of an adhesive. Legislation criteria established that, to ensure safety to the structure, this kind of repairs must be put side by side with riveted joints. Still, mechanical coupling is preferred to an adhesive one, even if other kinds of issues rise (especially related to stress concentration factors and fatigue.

Other steps forward were made to obtain industrial application and acknowledgement: good bonding between metal and adhesive needed to be not only physical but also chemical. Therefore, anodization and pre-treatment with a primer were developed to obtain the best adhesion possible. It was developed by Schliekelmann at Fokker industry which today is still one of the most important industries in aeronautic field.

In this research environment, mostly concentrated in collaborations between Fokker and Delft University of Technology, many other tools and ideas were developed: even ultrasonic devices for adhesion inspections were first used for this aim during this period.

First airplane that was realised with a combination of metals and composite (in particular glass fibre and plastic) was Fokker F-27, in the '50s. Later in those years also carbon fibre were studied extensively but, even if the combination of carbon fibre and plastic had showed since the beginning high strength and stiffness with low weight, they did not instantly spread amply. This was caused by their typical high costs and the necessity of a complete revolution in aircrafts design and construction. It was something really difficult to realise in an era where much knowledge, about metal properties and behaviour, was still in developing.

Therefore, a combination of metal and composite was even seen as a good compromise: at the beginning they were used as a reinforcement on metallic structure, showing good properties without being forced to face issues new materials could rise. Metal laminates had already showed better properties than monolithic metal sheets, but, with introduction of fibres inside adhesive, this improvement was even higher. Later, Fokker abandoned this project due to high costs for a whole new full-scale test to enrol an airplane made with a new material. Delft University of Technology fortunately continued research, until ARALL (Aramid Reinforced ALuminium Laminate, Figure 6.2) at the end of the '70s.
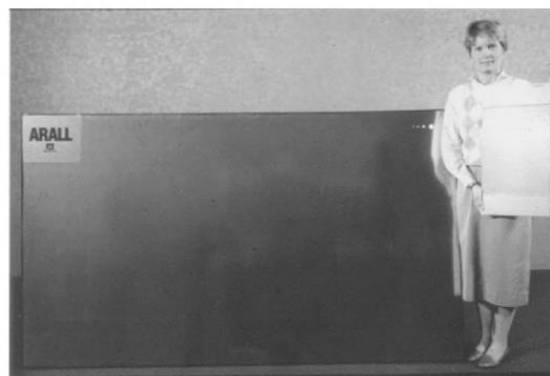

Figure 6.2: Arall panels produsec at ALCOA

Alternation of metal layers and adhesive reinforced with fibres in F-27 can not really been defined as a material; instead it was more similar to a bonded structure. Only with industries participation in ARALL development (in particular for pre-pregs development and less than 1mm thick aluminium foils), it was clear that a real new material was born.

ARALL was then presented at 1985 airshow and it obtained a lot of interest in it, but it took time to be applied on a flying aircraft. Costs were still quite high and they would be accepted only in the contest of developing of a completely new airplane, and not in a modification on an already existing one. Research did not fall down thanks to Delft University (Figure 6.3).

Figure 6.3: Strain survey on a bicycle made from Arall tubes, at TU Delft

Later, when Fokker decided to start a new aircraft project, ARALL development had a new sparkle. It was used principally for wing structures and this could be seen as its fortune in this phase, because when, later, it was studied under fuselage pressurization loads, its properties were found out to not suit that loading condition as expected.

This bonded laminate was also investigated against lightning strike. During thunderstorms, an airplane could be hit by a lightning and it has to have protection to avoid catastrophic failures. It was demonstrated that monolithic aluminium can melt if hit by a lightning while fibre reinforced plastics can even explode due to their low conductivity. ARALL, therefore, appeared to be superior because only the external aluminium layer melted while the first layer of aramid protected lower strata [6.17].

A new step forward, in FML development, was made when glass fibre were used instead of aramid ones. Glass showed good properties against fuselage pressurization loads and high impact resistance. This step represented the raise of a new material: GLARE.

Many studies (regarding fibre kinds or stacking sequence) have been carried out on these material to achieve extremely good properties that it shows nowadays. After all these researches and improvements, Glare is the most used Fibre Metal Laminate. It started to

be used on A320 and A330, up to A380 (Figure 6.4), where it is adopted in fuselage top panels.

Figure 6.4: Materials used on a A380

Other improvements are still in development regarding FML and GLARE in particular, e.g. out of autoclave Glare cure or the use of Vacuum Assisted Resin Transfer Moulding [6.18]. This last enhancement could lead to a cheaper and easier to produce material, opening more application opportunities.

References

[6.1] M.P. Falaschetti, M.Scafè, E.Troiani, V.Agostinelli, S.Sangiorgi, Experimental determination of compressive residual strength of a carbon/epoxy laminate after a near-edge impact, XXIII IGF, 2015.

[6.2] M.P. Falaschetti, M. Scafè, A. Tatì, E. Troiani, Experimental determination of thickness influence on compressive residual strength of impacted carbon/epoxy laminate, XXIV IGF, 2017.

[6.3] P. Akangah, S. Lingaiah, and K. Shivakumar. Effect of Nylon-66 nano-fiber interleaving on impact damage resistance of epoxy/carbon fiber composite laminates. Composite Structures, 92(6):1432–1439, May 2010.

[6.4] L. Liu, Z.M. Huang, G.Y. Xu, Y.M. Liang, and G.H. Dong, Mode II Interlaminar Delamination of Composite Laminates Incorporating With Polymer Ultrathin Fibers. Polymer Composites, 2008.

[6.5] L. Liu, M.Z. Huang, C. He, and X. Han, Mechanical performance of laminated composites incorporated with nanofibrous membranes. Materials Science and Engineering: A, 2006.

[6.6] L. Liu, Y.M. Liang, G.Y. Xu, H.S. Zhang, and Z.M. Huang, Mode I Interlaminar Fracture of Composite Laminates Incorporating with Ultrathin Fibrous Sheets. Journal of Reinforced Plastics and Composites, 2008

[6.7] R. Sadeghian, S. Gangireddy, B. Minaie, and K.T. Hsiao, Manufacturing carbon nanofibers toughened polyester/glass fiber composites using vacuum assisted resin transfer molding for enhancing the mode-I delamination resistance. Composites Part A: Applied Science and Manufacturing, 2006

[6.8] C. Vermeeren, An historic Overview of the development of Fibre Metal Laminates, Applied Composite, 2003

[6.9] Ad Vlot,Jan Willem Gunnink Fibre Metal Laminates: An Introduction, Springer-science+Businnes Media, B. V., 2001.

[6.10] Vlot A., Impact loading on fibre metal laminates, International Journal of Impact Engineering, 1996

[6.11] A. Vlot, M. Krull. Impact Damage Resistance of Various Fibre Metal Laminates. Journal de Physique IV Colloque, 1997.

[6.12] Ad Vlot, Low-velocity impact loading on fibre reinforced aluminium laminates (ARALL and GLARE) and other aircraft sheet materials, TU Delft repository, 1993

[6.13] Ad Vlot, Glare: History of the Development of a New Aircraft Material, Kluwer academic publishers, 2001

[6.14] L.B Vogelesang, A Vlot, Development of fibre metal laminates for advanced aerospace structures, Journal of Materials Processing Technology, 2001

[6.15] J. W. GunninkA. VlotT. J. de VriesW. van der Hoeven, Glare Technology Development 1997–2000, Applied Composite Materials, 2002

[6.16] Coen Vermeeren, Around Glare: A New Aircraft Material in Context, Kluwer academic publishers, 2004

[6.17] B. J. Jensen, R. J. Cano, S. J. Hales, B. W. Grimsley, and E. S. Weiser, Fiber Metal Laminates Made by the VARTM Process, Langley Research Center, Hampton, Virginia, 2015

[6.18] http://www.compositesworld.com/blog/post/the-resurgence-of-glare

- 84 -

Experimental campaign on Fibre Metal Laminate

The period spent at Structure Integrity and Composite research group at TU Delft was an interesting opportunity to start a new section of author's PhD research. Thanks to experience and features gained in years of research in Fibre Metal Laminate, Aerospace Engineering at TU Delft is one of the best environment to deeper composites and hybrids knowledge.

In this chapter, the experimental campaign performed on Fibre Metal Laminate is described.

7.1 FML experimental campaign

In the following section, experimental campaign performed at Aerospace Engineering faculty at TU Delft University on FML composites is described. As already explained in Chapter 6, the choice for an improvement of CFRP impact behaviour, fell on this material due to the necessity of a quite cheap and well-founded method.

7.1.1 Specimens

For this experimental campaign, a carbon/epoxy fabric was chosen. Many issues could raise from this choice: carbon fibres and aluminium is not one of the best combination due to galvanic corrosion issues and different thermal expansion factors.

It is worth to notice that author's aim was not the presumption to recommend material used in this experimental campaign as the most interesting one in aerospace field. Author knew issues related to these constituents mix before starting tests; but it was also known that those issues would not have influenced experimental results. In fact, galvanic corrosion happens if fibres and metal come into contact in peculiar thermal and humidity environment. These conditions were avoided and specimens production and

tests implementation were performed in a really short time, one after the other: therefore, any galvanic corrosion issues could be safely neglected.

On the other hand, it has to be taken into account that this experimental campaign had characterization of metal layers position influence on impact resistance as first aim. Therefore, comparison between specimens groups behaviour is the most important goal that author had in mind at the beginning of this campaign.

Pre-preg chosen was Hexcel M18/1 43% G939 Fabric.

Table 7.1: Pre-preg properties

Property	43% G939 Fabric
Fibre density	1.78 g/cm^3
Resin density	1.22 g/cm^3
Fibre areal weight	220 g/m^2
Nominal ply thickness	0.227 mm
Nominal fibre volume	55 %
Tensile strength	800 MPa
Compressive strength	800 MPa
Tensile modulus	65 GPa
Compressive modulus	64 GPa
In-Plane shear strength	100 MPa

Aluminium layers were of a 2024-T3 alloy 0.4 mm thick sheets were treated to obtain the best interaction with pre-preg layers: their surfaces are usually anodized and covered with a primer to protect metal itself and to make a better connection with the resin of pre-preg plies.

Table 7.2: Aluminium sheet properties

Property	Al 2024-T3
Ultimate Tensile Strength	483 MPa
Tensile Yield Strength	345 MPa
Elongation at Break	18 %
Modulus of Elasticity	73.1 GPa
Poisson's Ratio	0.33
Fatigue Strength	138 MPa
Shear Modulus	28 GPa
Shear Strength	283 MPa

An unsupported resin was also used to ensure adhesion between Aluminium layers when those are close to each other without any pre-preg layer in the between. Chosen resin was 3M Scotch Weld resin AF 191U.

Table 7.3: Resin properties

Property	AF 191U
Thickness	0.0625 mm
Foil Weight	73 ± 24.4 g/m^2
Cure temperature	177°C
Cure time	60'
Stress (at 23°C)	13 MPa
Strain (at 23°C)	2.11 %
Young Module (at 23°C)	0.71 GPa

Four different stacking sequence were made:

Table 7.4: laminates steacking sequences

Metal location	Stacking sequence	Bending Stiffness [Pa*m^3]
EXT	Al/(0/90)$_9$/Al	132
MID	(0/90)$_2$/Al/(0/90)$_4$/Al/(0/90)$_2$	98
INT	(0/90)$_4$/Al/resin/Al/(0/90)$_4$	107
No-Metal	(0/90)$_{12}$	108

Specimens stacking sequences were chosen having in mind that many parameters could change material characteristics: ply orientation, metal lamination direction, stacking sequence, thickness, etc. Hence, it was decided to erase as many parameters as possible, opting for a symmetrical balanced staking sequence that could result in similar bending stiffness for all specimen groups.

Bending stiffness was calculated by means of an Excel work cartel developed at TU Delft University. It was based on linear elastic fracture mechanics.

Specimens were obtained with hand layup and autoclave curing, all realized at Delft Aerospace Structures and Materials Laboratory (DASML) at TU Delft.

The procedure consists of following steps:

- The pre-preg roll is removed from freezer 8/12 hours before starting lamination. It is put on a support that permits to keep it lifted inside its plastic bag. This would assure that the material defrosts without forming wrinkles or moisture on it. These two factor could be prejudicial for mechanical characteristics of final product.

- Plies are cut in the right shape by means of an automatic cutting machine. This allows saving time in order to put again in the freezer the pre-preg roll.

- Aluminium layers are cut in proper dimensions by means of a cropper machine, paying attention to the lamination direction of the sheet.

Figure 7.1: Al sheet and cutting machine

- Hand layup of all plies realizing the four panels needed. This step takes place in lamination process consists in a hand layup performed in a 'clean room' where humidity, temperature and particles are controlled.
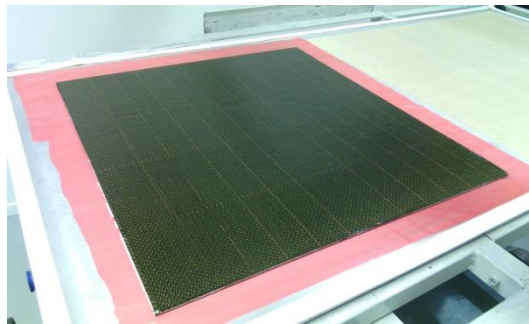
Figure 7.2: FML laminate

- These four panels are then put on an aluminium table, already sprinkled with releasing liquid and covered with a releasing film. All the edges are left free of release liquid and film in order to realize a good interaction with the sealant tape used to close the vacuum bag.

- For those panels that have pre-preg ply as outer layers, a counter mould is put on them. This is because we want to have the same roughness on both side and also for all panels.
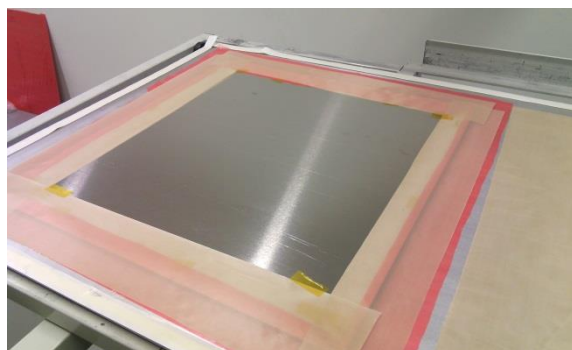
Figure 7.3: Al counter mould

- All is covered with a bleeder/breather layer and a vacuum bag.

Figure 7.4: Bleeder/Breather clot

- A vacuum valve is put in the vacuum bag.

Figure 7.5: Vacuum valve

- Sealant tape is used to seal vacuum bag on the aluminium table.

- The vacuum valve is connected to the vacuum pomp until the pressure inside is good enough, and then disconnected to test if the vacuum bag has been well done. If there is a vacuum leak, the vacuum bag need to be made again.

- Tables are placed in the autoclave and the vacuum bag is connected with the pomp inside the autoclave: this will assure a continuous conservation of the pressure difference between outside and inside the bag.
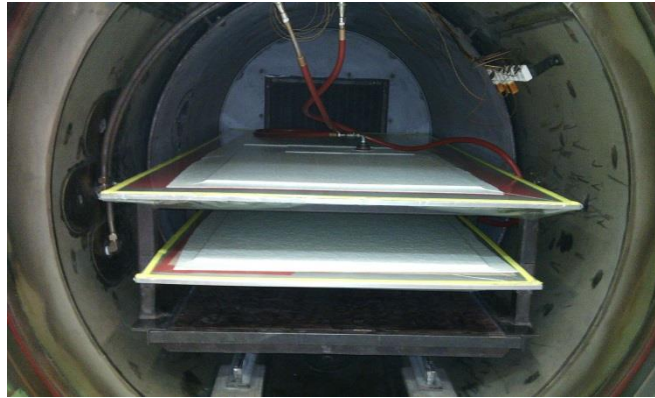
Figure 7.6: Laminates inside the autoclave
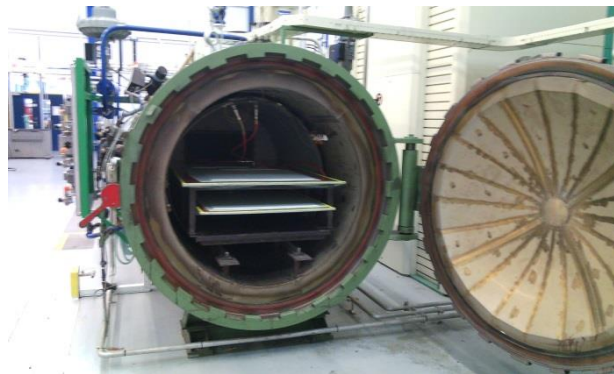
Figure 7.7: TU Delft autoclave

- The cure cycle is upload and the autoclave is turned on.

- After the cure cycle, panels are left to cool down to room temperature.

Figure 7.8: Laminate after curing

- Pieces are removed from autoclave and there is a visual inspection of them.

After a preliminary visual inspection, it has been clear that there had been a problem during cure cycle: panels showed many wrinkles and resin-poor spots on both faces. This kind of problem could be linked to pre-preg dryness or a pressure leak during cure cycle. The latter has been checked and it was noticed that a problem happened during cure

cycle and had resulted in a pressure leak. This led to a not good gas evacuation and material compaction.

For a better understanding of what this means for the material, a C-scan and a microscopic inspection have been performed.

Due to the homogeneity in bubbles distribution inside the panels, C-scan images do not show huge defects. Only INT material (where aluminium layers are in the inner part of the material, glued together with a thin layer of epoxy resin) shows a very huge delamination. This was caused by the absence of a proper pressure during the cure cycle: all gasses produced during curing had no possibility to evacuate.

Furthermore, edges are better consolidated than central part of panels. This is due to a higher pressure applied on the edges by vacuum bag and tops.
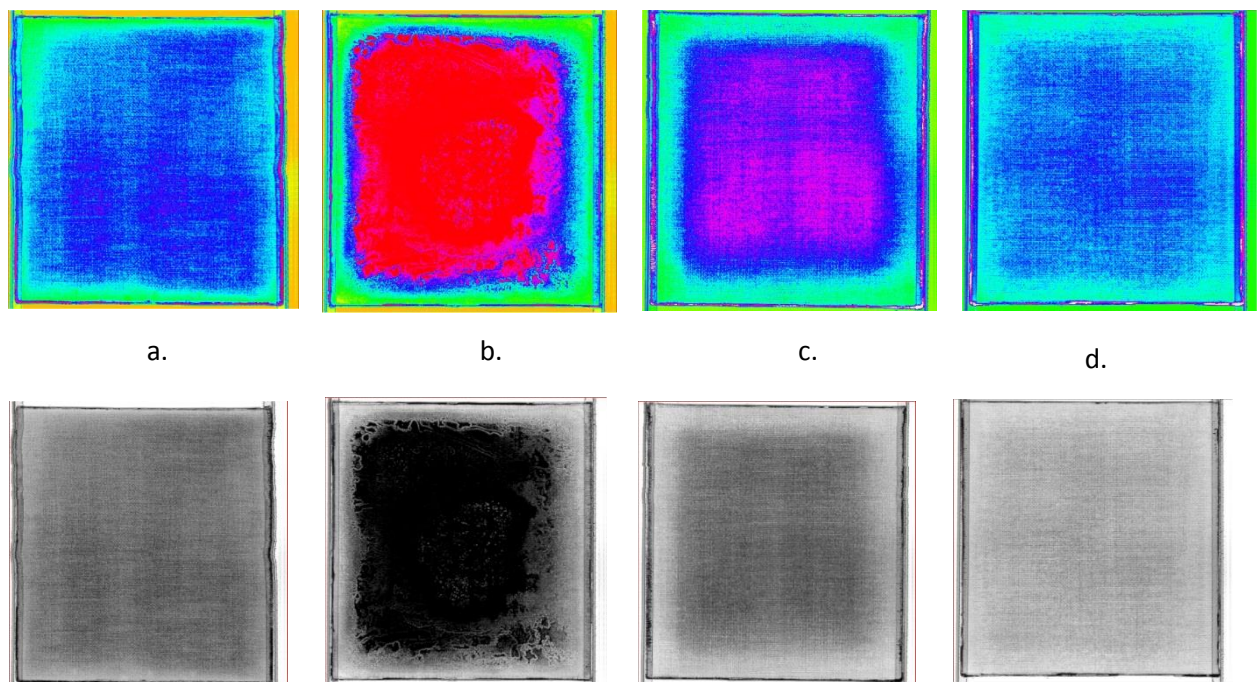
Figure 7.9: C-Scan images in greys scale (a. EXT, b. INT, c. MID, d. No-Metal)

With the microscopic inspection, the material condition through the thickness was analysed. In this way it was possible to see how many bubbles were inside the material.

The procedure regarding microscopic inspection consists in two steps: in the first one is necessary to embed specimens in resin to make them more manageable and the second is to polish, in the best way possible, their surface in order to have more detailed picture.

Figure 7.10: Vacuum impregnation system

A liquid resin with 24 hours for end curing has been chosen (Figure 7.11). This kind of resin gives better results if used with a Vacuum impregnation system.
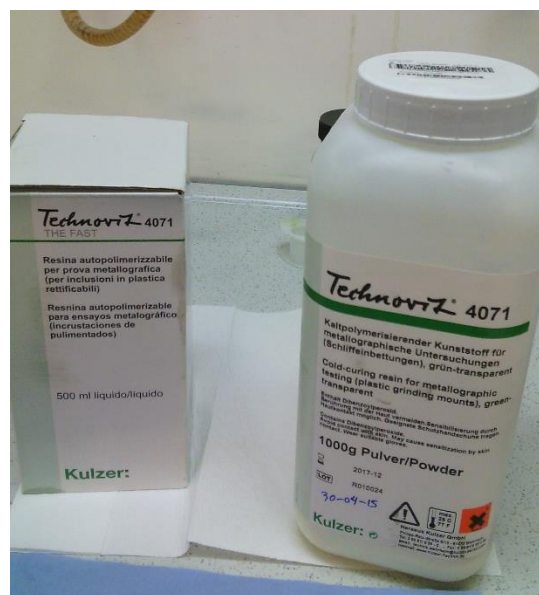
Figure 7.11: Resin and catalyst used for specimen embedding

The procedure to use this kind of method is described in the following:

- The resin is prepared: the one that is used in this work is an epoxy resin that needs a catalyst to cure. Two components are mixed together in proper quantities and slowly blended with a wood stick (to not create bubbles).

- A flexible tube is positioned in the right position: one end inside the vacuum chamber (it will be the tub) while the other in the jar where resin will be put. The tube is put through a structure that will work as a valve.

- All cups with specimens inside (small pieces of material, 10x15mm) are collocated in the vacuum chamber. Specimens are collocated with the face that we want to inspect facing the bottom part of the specimen.

- After checked that the valve is closed, mixed resin is put in the jar.

- The vacuum program is started and the top is pressed on the vacuum chamber until vacuum is enough to hold that against gasket.

- The valve is opened slowly to let resin flow in the tube due to pressure difference. Resin is poured slowly in every cup until they are all full.

- After all resin has been poured, a 30 minutes time is set during that the vacuum is hold.

- After 30 minutes, the top is removed. Every cup has to be checked if specimens has moved; in that case, it is possible to fix that with a needle. Everything is left in the same position until resin is completely cured (24 hours in this case).

- After this time, specimens are ready for being polished for microscopic inspection.

The polishing was done with a Struers Tegramin 20 machine (Figure 7.12): the procedure consists of different phases during which sandpapers with different roughness are used (from very rough one to smoother ones). In the last phase clothes saturated with a particular solution (diamond micro-particles in suspension) are used instead of sandpapers in order to obtain a better finishing surface. Then specimens are ready for microscopic inspection.

Figure 7.12: Struers polishing machine

Figure 7.13: Struers diamond saw cutting machine

The following pictures have been taken with a Leica DM LM Optical Microscope. They show voids present inside the material in a through the thickness view.

(a)   (b)
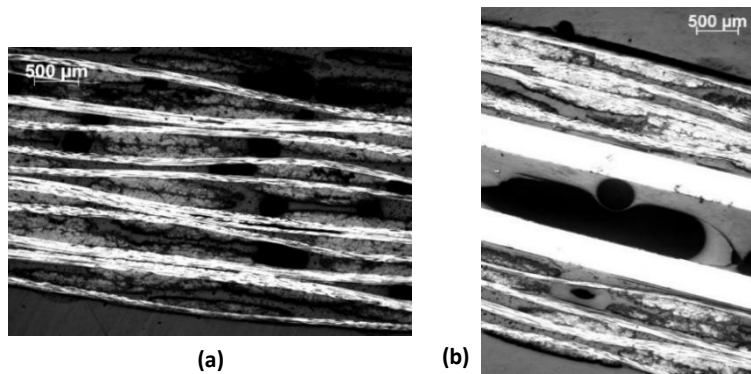
Figure 7.14: microscopic images of voids inside material (a. No-Metal, b. INT)

New laminates have been made with the same layout and procedure described above. This time there were no problems with the pressure settings and, therefore, panels resulted well compacted. C-scan and microscopic inspection have been done as well (Figure 7.15).

During cutting, it was possible to notice some issues regarding stresses caused by diamond saw: maybe due to a too high force applied by saw to the material, those specimens with aluminium layers present near edges delaminations. It was decided, hence, to perform another C-scan inspection on some coupons to establish the extension of these delaminations (Figure 7.16).
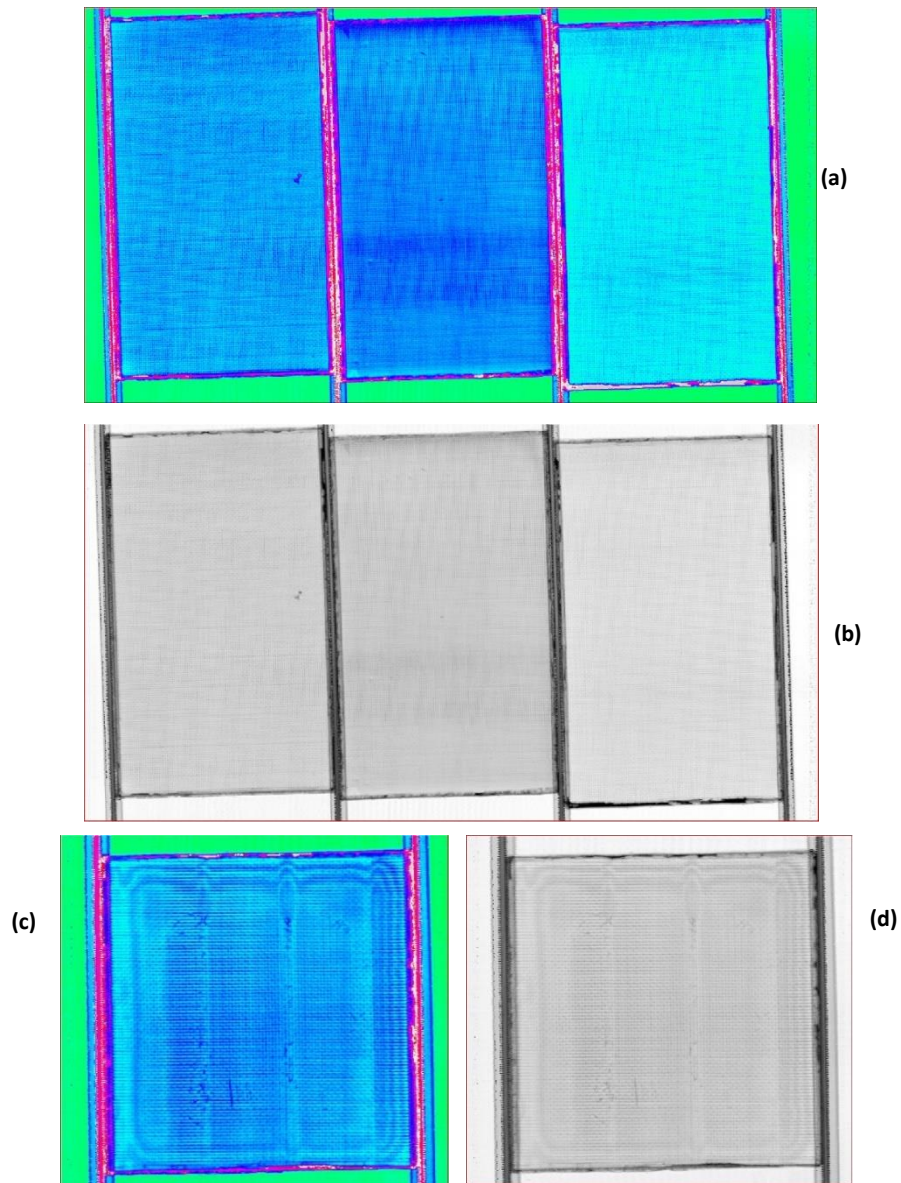
Figure 7.15: C-Scan images (a. MID, EXT, No-Metal in colour scale, b. MID, EXT, No-Metal in grey scale, c. INT colour scale, d. INT grey scale)
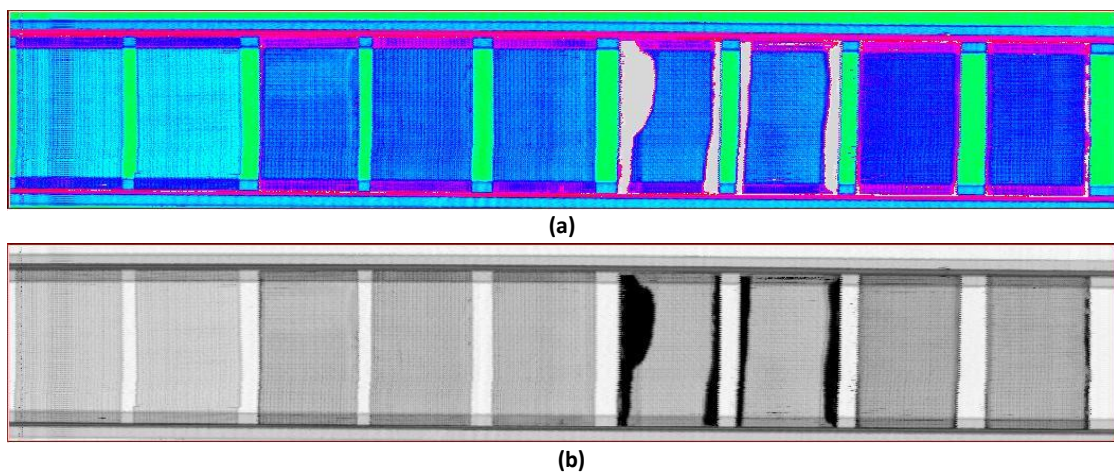
Figure 7.16: C-Scan images from the left to the right, two No-Metal, three INT, two MID and two EXT specimens (a. coloured scale, b. grey scale)

Delaminations are wider on long edges (cut with a big diamond saw) than on short ones (cut with a smaller precision saw). This means that, with a smaller saw, lower stresses are transferred to the material and it is preferable to the other one.

The same issue could be noticed in microscopic picture of EXT material (Figure 7.17): the first one shows the delamination due to higher stresses inducted by bigger diamond saw while the other picture shows the edge cut with the smaller saw.
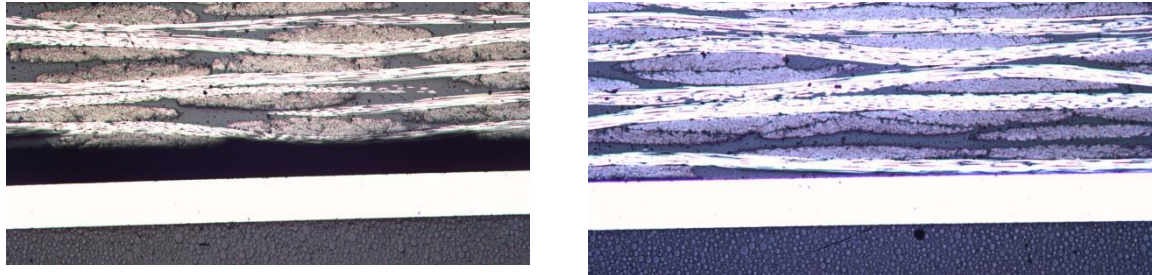
Figure 7.17: Microscopic pictures of EXT (left, big diamond saw; right, small saw)
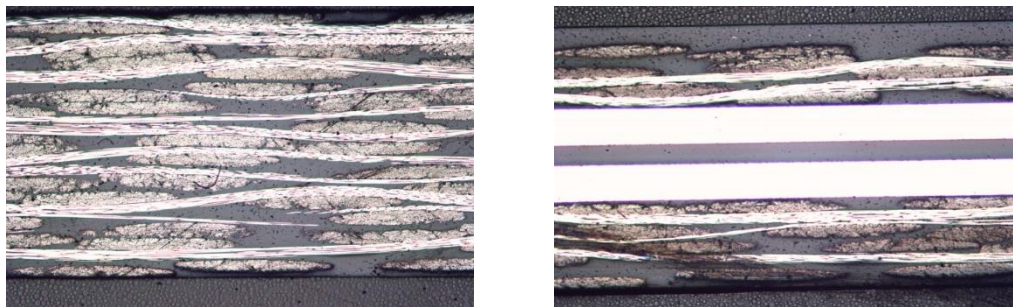
Figure 7.18: Microscopic pictures (left, No-Metal specimen; right, INT specimen)

Specimens were cut according to [7.1] (150x100 mm) and their dimensions have been measured: 7 measures for thickness, 5 measures for width and 3 for length (Figure 7.19). each specimen dimensions could be found in Appendix B.
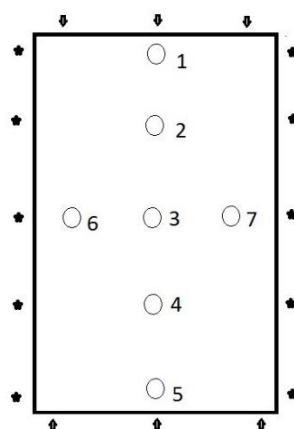
Figure 7.19: measurement positions (circumferences for thickness, arrows for length and stars for width)

7.2 Tests

Quasi Static Indentation tests (QSI, [7.2-7.5]) have been performed on three specimens per each material. Strain data has been collected from a Digital Image Correlation (DIC) sensor.

7.2.1 DIC

Digital Image Correlation is an optical method that employs tracking and image registration techniques for accurate 2D and 3D measurements of changes in images.

To use this kind of sensor, specimens were painted to create a speckle pattern that the sensor uses as reference to collect data:

- Coupons are cleaned with ethanol and painted with a white spray paint (Figure 7.20). This layer has to be uniform and mat in order to create a strong contrast with the speckle pattern and a no-shine surface (the DIC set up needs a couple of lights to illuminate in the best way possible the whole surface and reflecting surfaces block a good data collection in addition to the possibility to ruin cameras sensors).
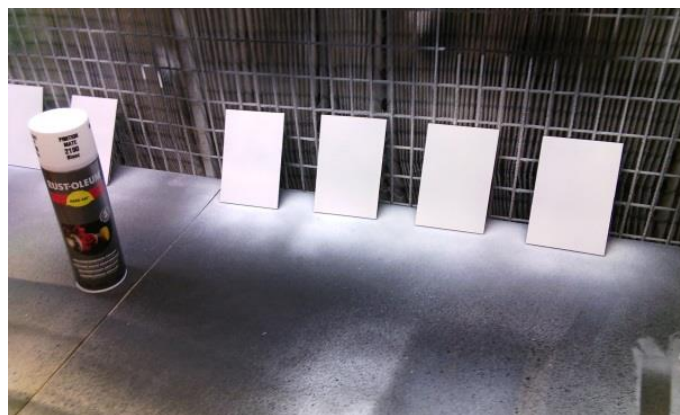
Figure 7.20: Specimens painted with white paint

- After the white paint is dry, a black mat spray paint is used to realize a speckle pattern. Black spots have to be in the right shape and dimensions, thus this step requires a good skilled operator (Figure 7.21).
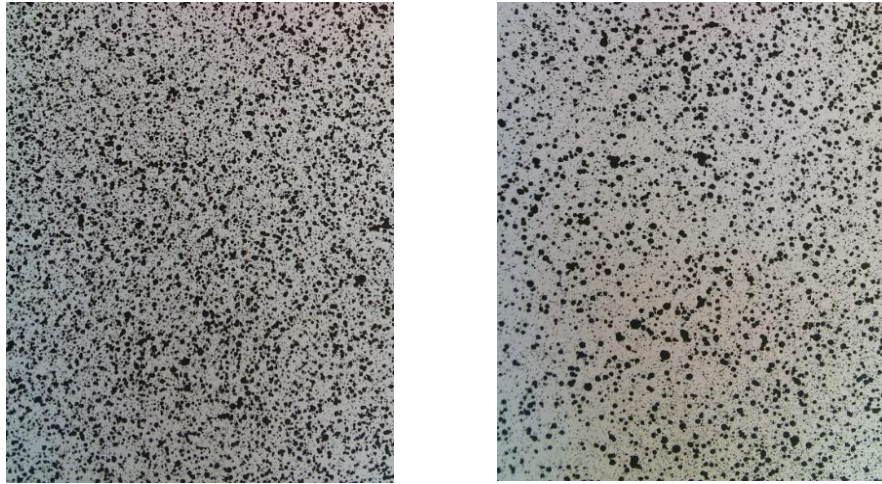
Figure 7.21: Examples of different kind of speckles pattern

After the specimens preparation is done, it is necessary to set up the frame where cameras and lights would take place. This frame will allow camera pursuit of specimens movement. A 20kN Zwick press was used (Figure 7.22a).

(a)

(b)
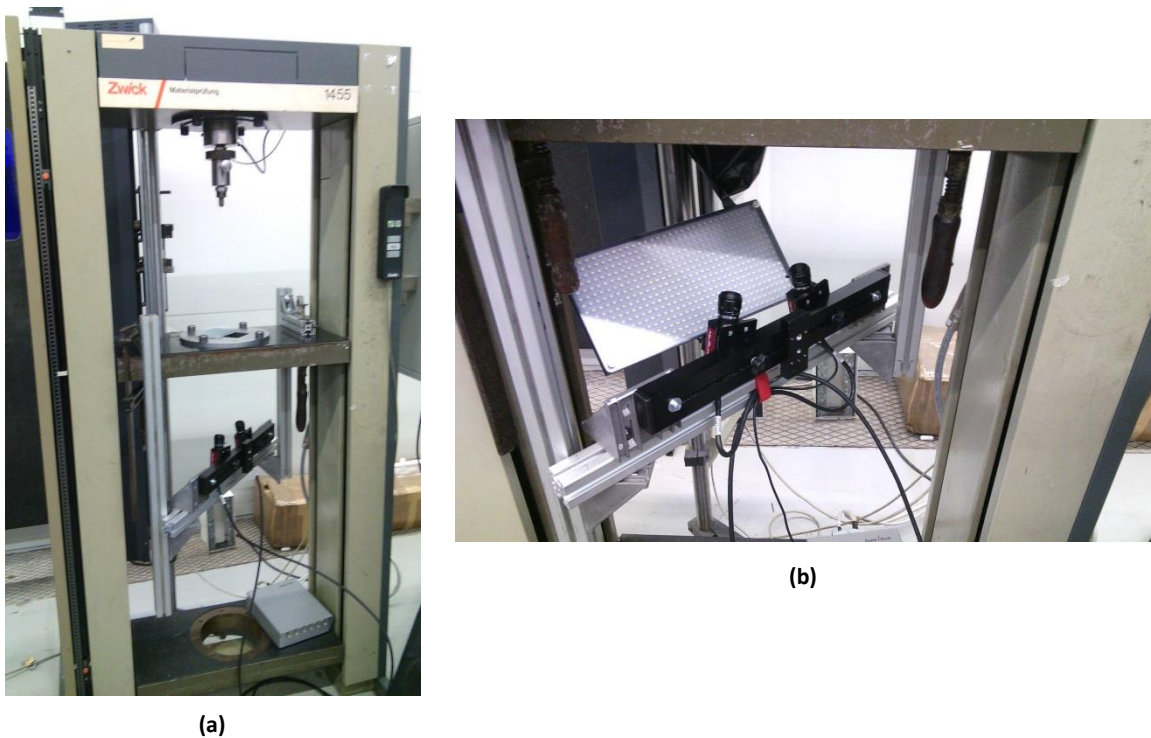
Figure 7.22: Frame set on Zwick press; (a. fixed indenter and specimen fixture can be noticed, b. particular of cameras and lights)

Hence, the frame showed in Figure 7.20 is set up. In the picture 7.20 (b), one of the two lights panels used to light up specimen surface is showed (the other one is set symmetrically).

The two cameras were fixed with an inclination that has to be between 15 and 30 degrees. After focus on both cameras using the specimen surface as reference is done, the cameras are calibrated with a specific panel. To achieve this, many pictures are taken putting the panel in different positions with different inclinations; this is due to the necessity to cover all the space gap the specimen would cover during the test.

After calibration, the specimen is test fixed in the fixture and a moving test is done (the press is started with the test velocity set, meanwhile the DIC sensor takes pictures). This tests is useful to understand if the frame is rigid enough to prevent camera movements and vibrations during tests.

7.2.2   Results

Tests were performed in two different days: calibration data are reported for each configuration set.

Table 7.5: Calibration Data

Calibration Data			
27th January 2016		**4th February**	
Temperature	20.8°C	**Temperature**	21.3°C
α	-20.1°	**α**	0.34°
β	0.18°	**β**	19.30°
γ	-0.77°	**γ**	0.80°
Baseline	169.80 mm	**Baseline**	175.39 mm

A moving velocity of 2 mm/min is set and the test end is decided to be at an 80% decrease of the maximum force.

Indenter is a cylinder with a diameter of 12.5mm and a length of 25mm; the end that will push against specimens is hemispherical.

Data are recorded by both compression machine and DIC Sensor by means of an analogical connection. Results regarding Maximum Force before failure starts and indenter displacement are reported in the following tables.

Between data recorded by compressive machine and DIC analogical data capture there is a good correspondence thus, from now on, we will address only to Zwich data which shows less background noise.

The strength and stiffness of No-Metal laminate is lower than FML composites. The EXT coupons have a higher bending stiffness due to the numbers of layers; therefore, a comparison is not possible. Thus, a normalization of the results has been carried out by dividing maximum forces for bending stiffness.

Table 7.5: Comparison parameter calculation

Material	F_{MAX} [N]	Bending Stiffness [Pa*m³]	Comparison Parameter
No-Metal	4397.1	108	40.71
EXT	6316.0	132	47.84
MID	4800.7	98	48.99
INT	5713.7	107	53.40

Looking at the comparison parameter, the aluminium layers insertion leads to a higher failure force. This is higher when aluminium layers move towards the centre of the material: maximum force of the specimen with aluminium layers outside (EXT) is lower than specimen with aluminium in the middle part (MID), that is, in turn, less than that of specimen with the core in aluminium (INT).
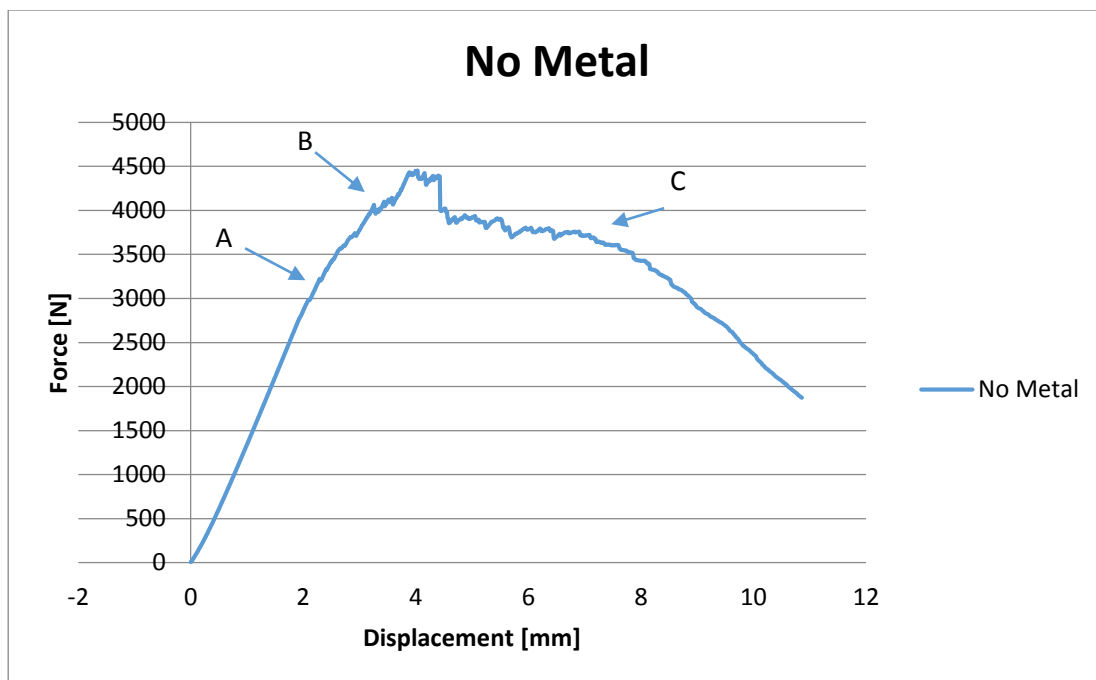
Figure 7.23: Force-Displacement diagram for no metal specimen
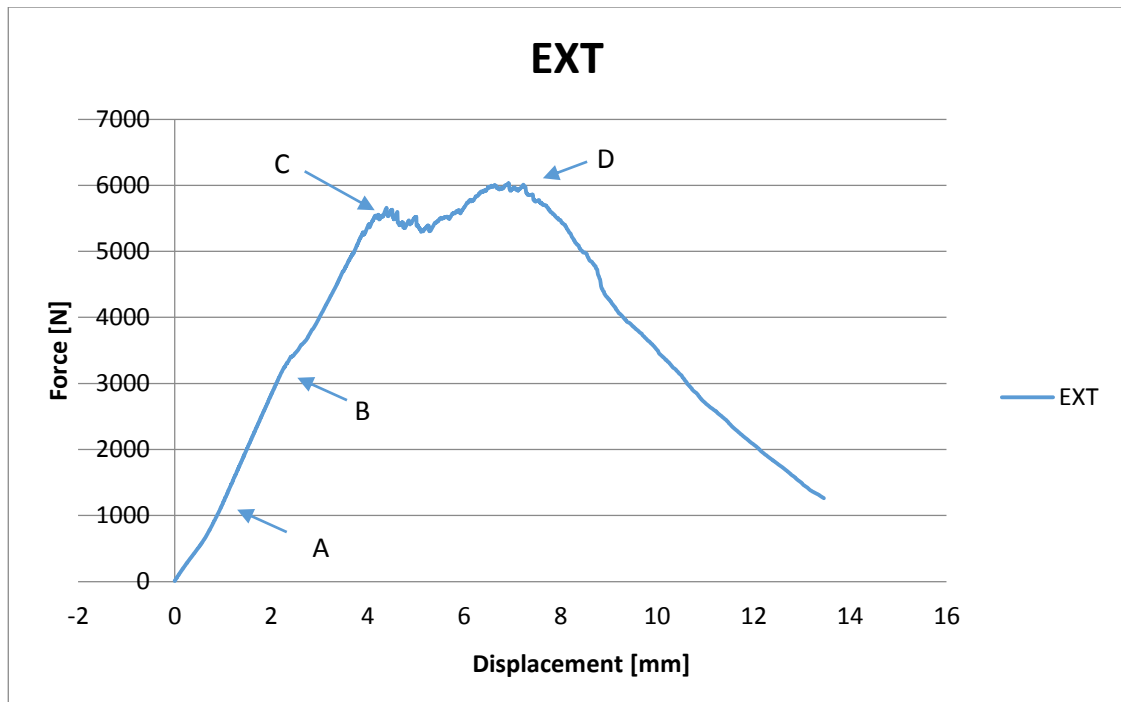
Figure 7.24: Force-Displacement diagram for EXT specimen
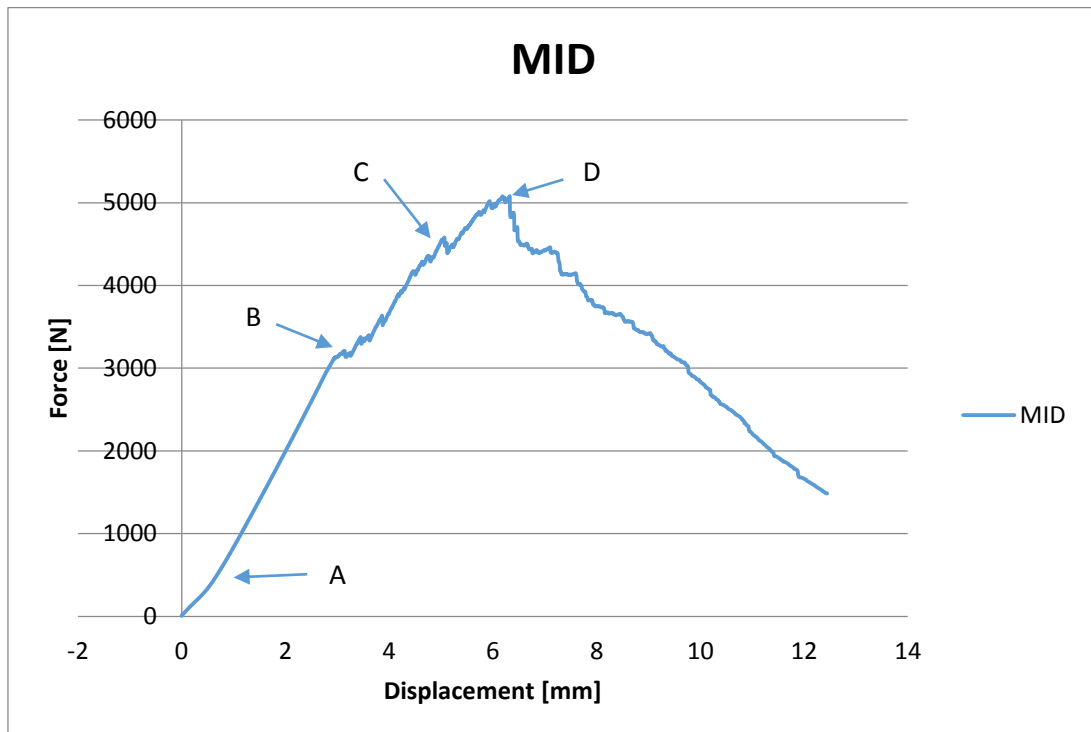
Figure 7.25: Force-Displacement diagram for MID specimen
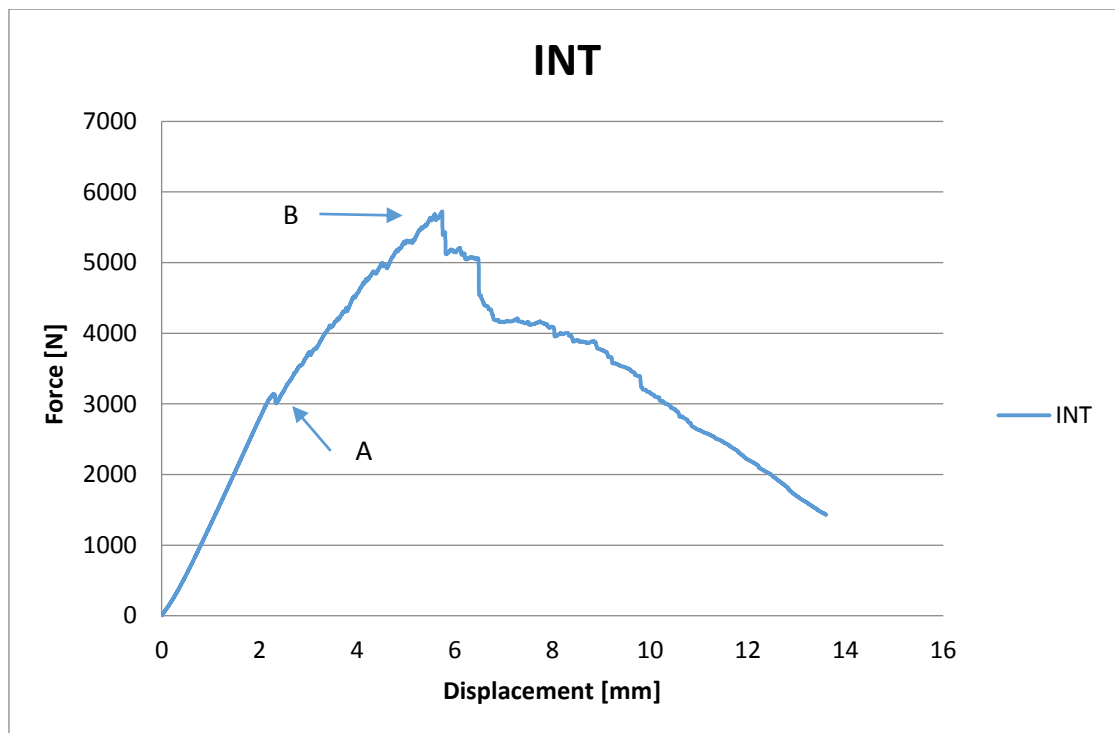
Figure 7.26: Force-Displacement diagram for INT specimen

Looking at Force-Displacement graphs obtain by analogical DIC data, a pure laminate has a more stable behaviour after failure beginning: it can carry a high load for a longer time compared with others specimens, where the load resistance starts to decrease quite soon.

Furthermore, analysing in detail each graph [7.2-7.9]:

- looking at No-Metal material behaviour (Figure 7.23), there is a little load drop at instant named point A: given that 'fixture dimensions/specimen thickness' rate is quite high, at that point matrix failure starts and evolves until point B, where the damage starts to involve also fibres; damage progression is then pretty stable until point C where the maximum failure strain is reached.
- In EXT graph (Figure 7.24) there is a change of slope (point A) attributable to yield of the Al layer at the specimen face opposite to the indenter. This is due to the small thickness of specimen and relative small bending stiffness of the material. Hence yield point is firstly reached on the specimen back face. Point B shows matrix cracks onset, visible due to change of curve slope. Matrix cracks growth ends at point C where fibres failure occurs. Since this instant until failure maximum force (point D), failure is stable.
- MID specimens have a slightly different behaviour (Figure 7.25): there is a first yield point (A) where first Al layer yields while matrix crack onsets are at points B and C. This is due to the peculiar stacking sequence that results in more groups of

carbon/epoxy plies: point B refers to external back-face carbon/epoxy layers, while point C is linked to internal carbon/epoxy layers. Point D describes max load and max displacement that the specimen can carry and the point where fibre failure takes place.

- For INT specimens (Figure 7.26), a matrix cracks growth onset at point A, which propagates until point B, where fibre failure occurs. This is also the max displacement: after this point all back-face carbon/epoxy layers are heavily damaged and hence load bearing capacity is much lower.

A plot of all averaged QSI behaviour is showed in Figure 7.27. The same graph is proposed with normalised values (Figure 7.28), for a better comparison of different materials behaviour. Normalization was obtained dividing loading force by material bending stiffness.

The most important feature raising from these plots, is failure progression. No-Metal material has a more stable failure progression. Also EXT has a quite stable damage propagation (better load bearing also after first fibre damage).

Moreover, yield loads are almost the same while failure load is higher in INT and MID materials (looking at normalised graph, where results are independent from bending stiffness small differences).
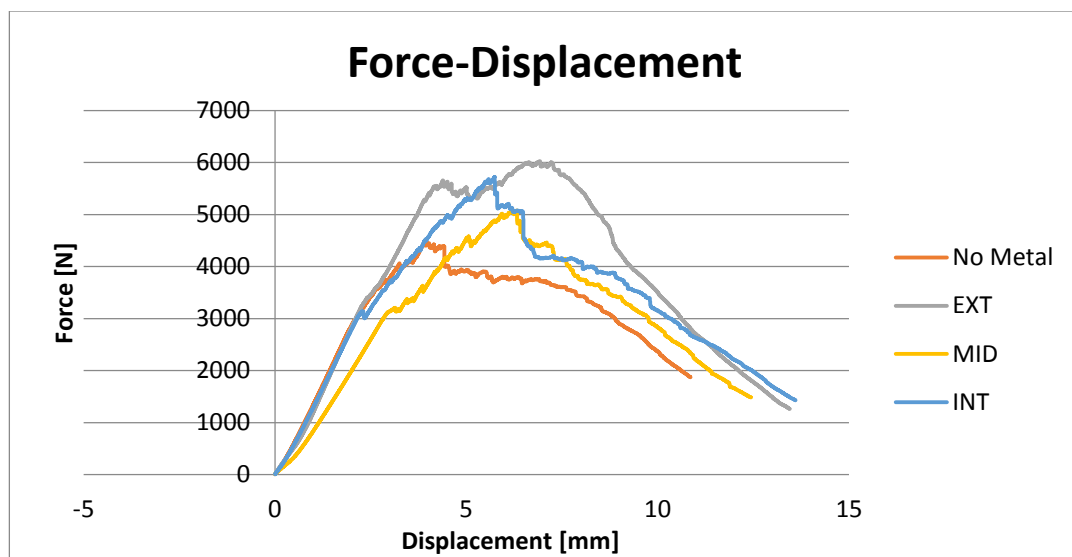
Figure 7.27: QSI tests average results
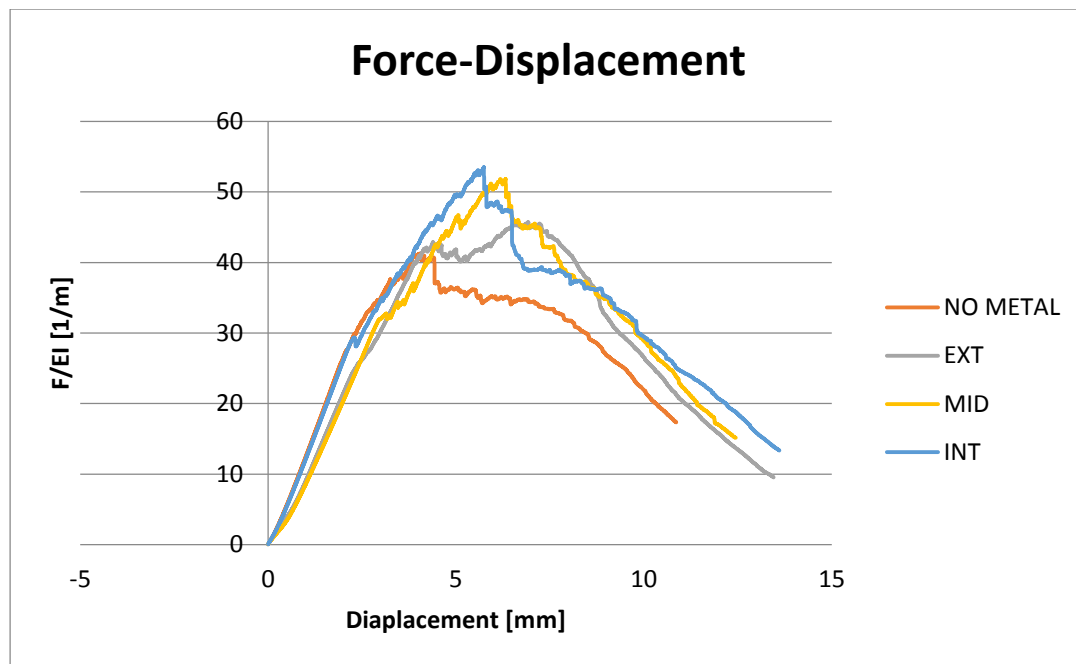
Figure 7.28: QSI tests, normalised average results

It is also evident how the elastic modulus is really sensitive to bending stiffness: in raw data graph MID material has a less rigid behaviour compared to other materials, while in the normalised graphs this difference is not present anymore. This is due to MID bending stiffness: normalizing by this value, hence, it is possible to erase this parameter effects on material data.

Looking at the decreasing load slope, after max force, No-Metal and INT materials have the same kind of slope that is less stiff than that of MID and EXT specimens. This is another proof of the more gradually failure evolution in materials where composite part has a higher contribution to mechanical characteristics.

In the following picture (Figure 7.30-7.37) strain results per each material are presented. In Figure 7.29 are represented direction on which strains are acquired: Longitudinal strains are collected on the transversal specimen symmetry axis, while Transversal strains on the vertical specimen axis.

Strains have been analysed with Vic3D Software of Correlated Solutions. This software performs a correlation between pictures taken by the two cameras resulting in a complete displacement and strain field measurements. This correlation is possible thanks to the speckle pattern painted on specimens; therefore, when this paint fails data in that area are unavailable. Hence, to be able to capture a complete strain screening until the very material failure, extensometer tool in Vic3D Software was used. Two measurements per each direction were made: for Transversal strains, extensometer were implemented just above and under indentation area (where paint would first fail), while for Longitudinal strains on the right and left of it.
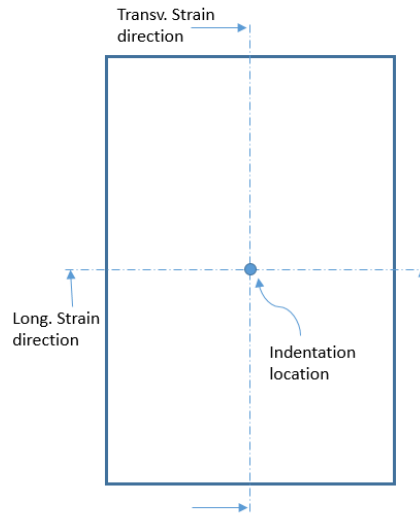
Figure 7.29: Directions for strain plot
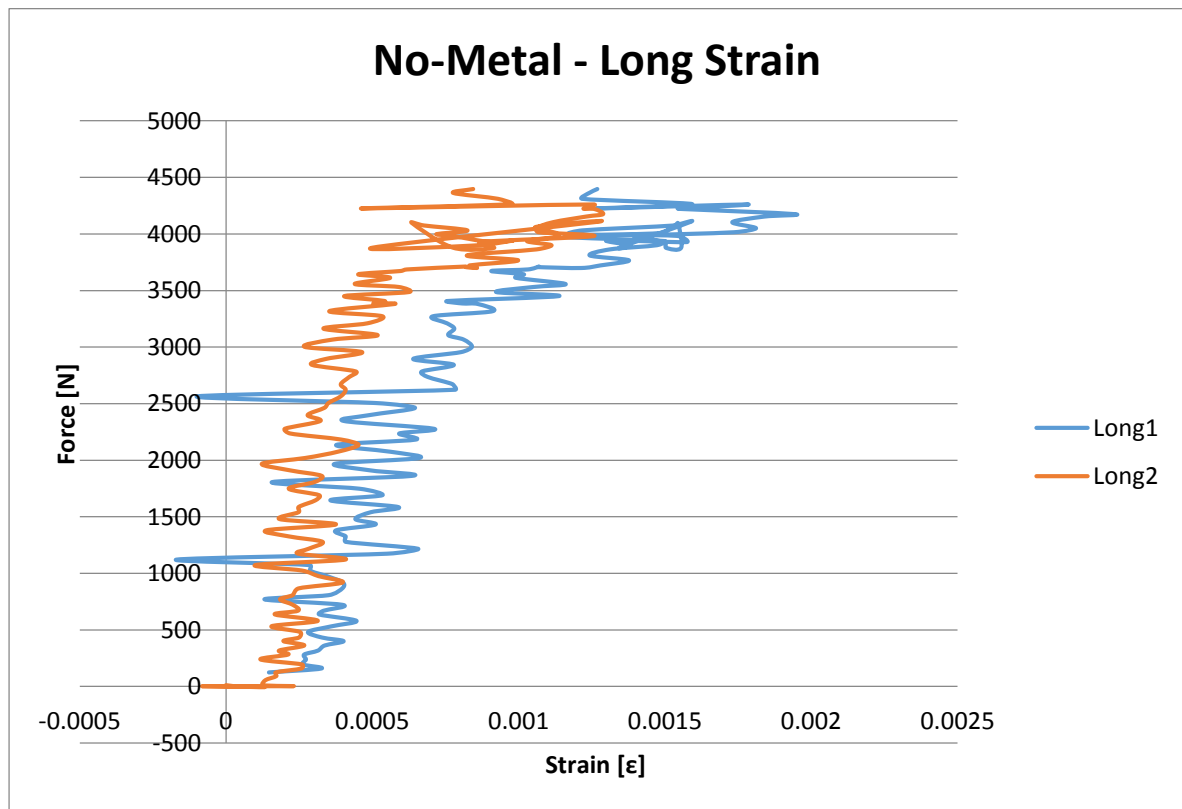
Figure 7.30: Longitudinal strain in No-Metal specimen
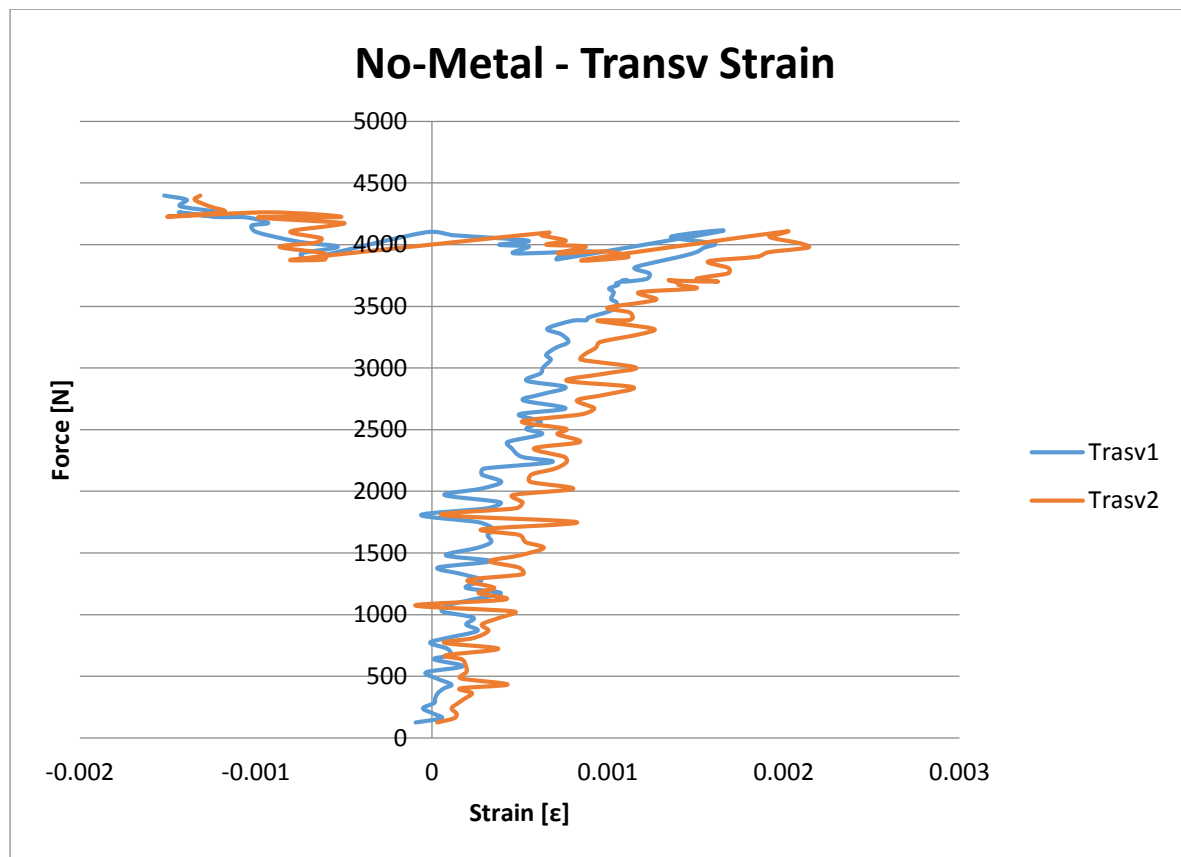
Figure 7.31: Transversal strain in No-Metal specimen
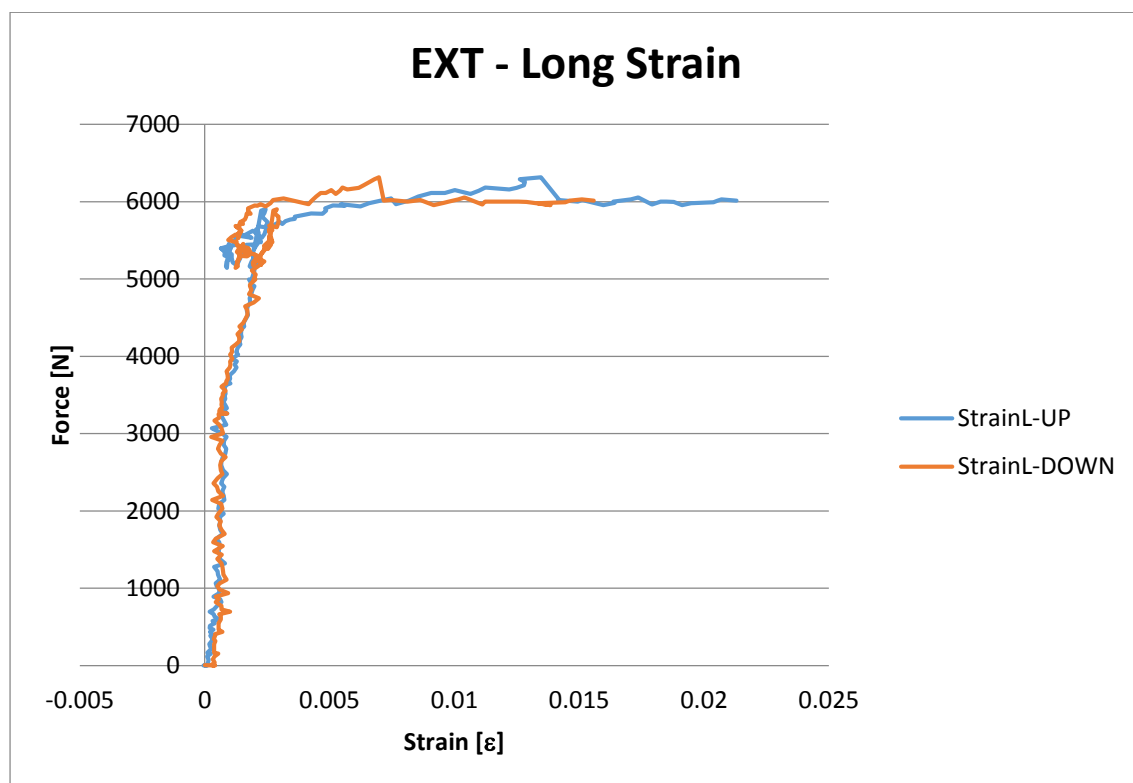
Figure 7.32: Longitudinal strain in EXT specimen
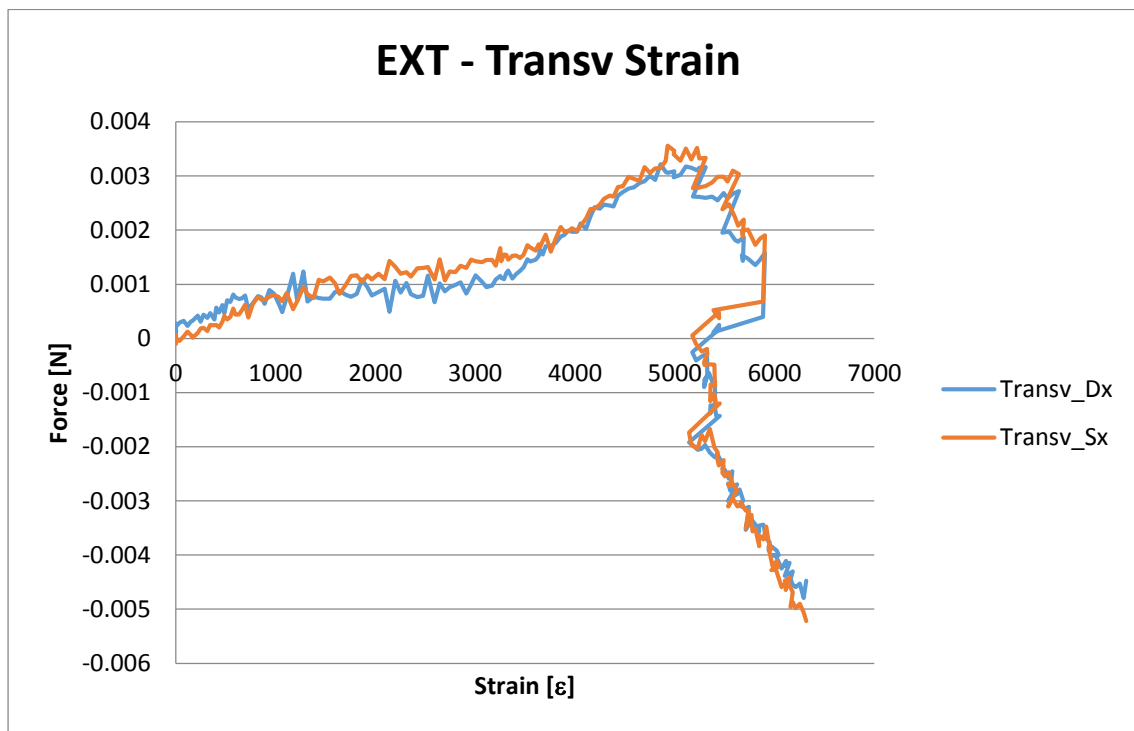
Figure 7.33: Transversal strain in EXT specimen
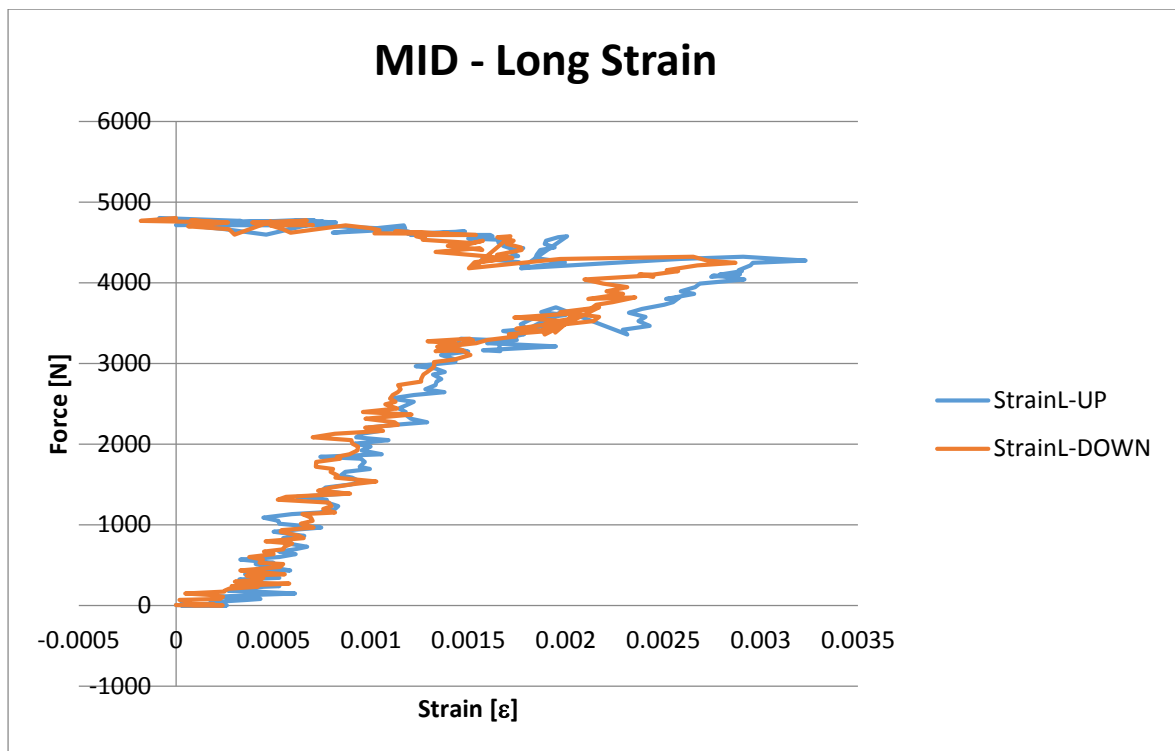
Figure 7.34: Longitudinal strain in MID specimen
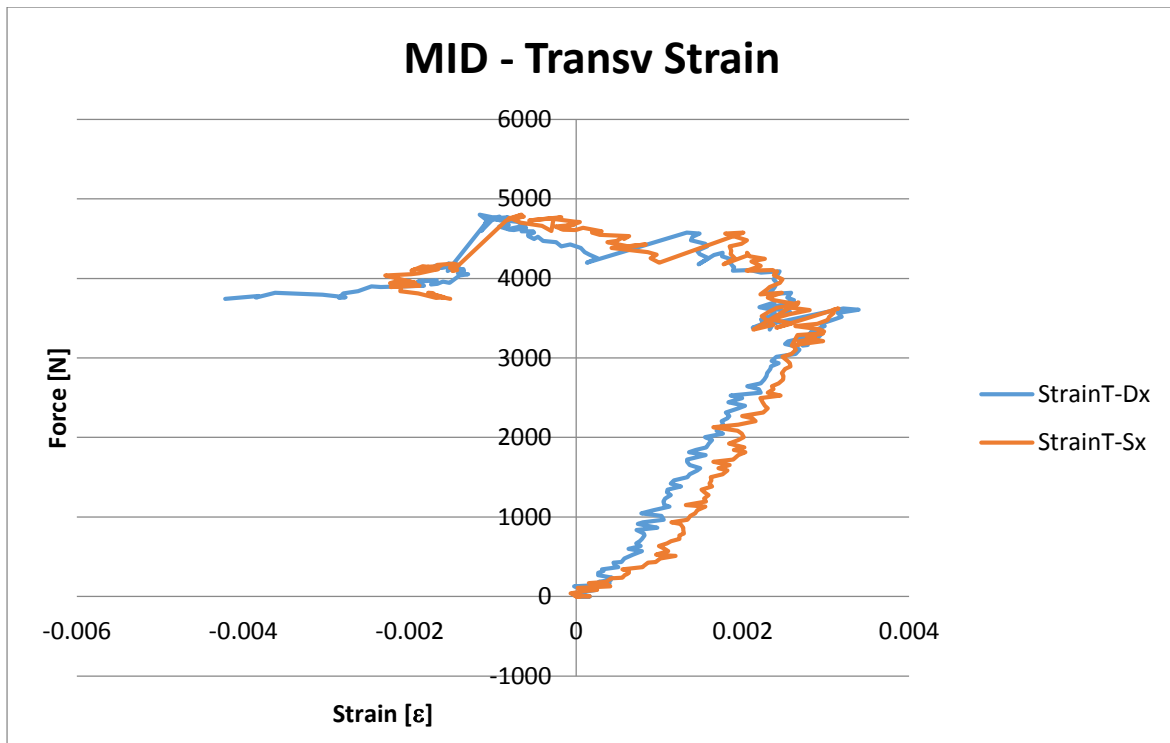
Figure 7.35: Transversal strain in MID specimen
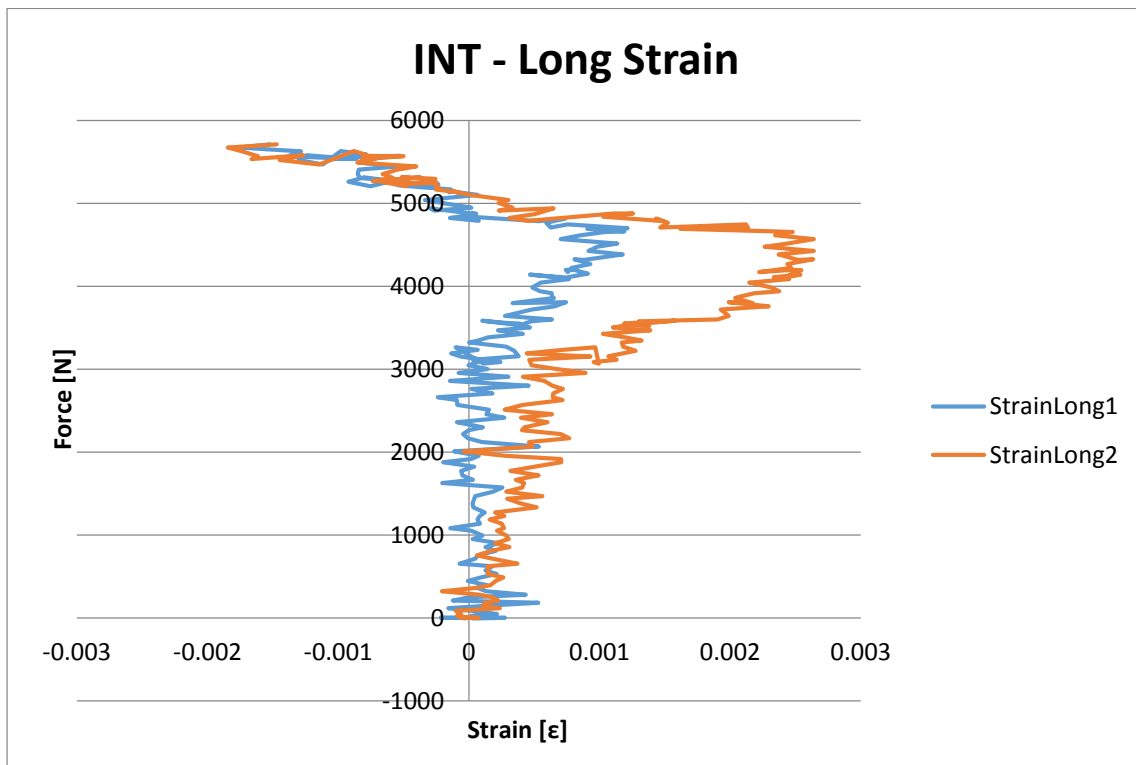
Figure 7.36: Longitudinal strain in INT specimen
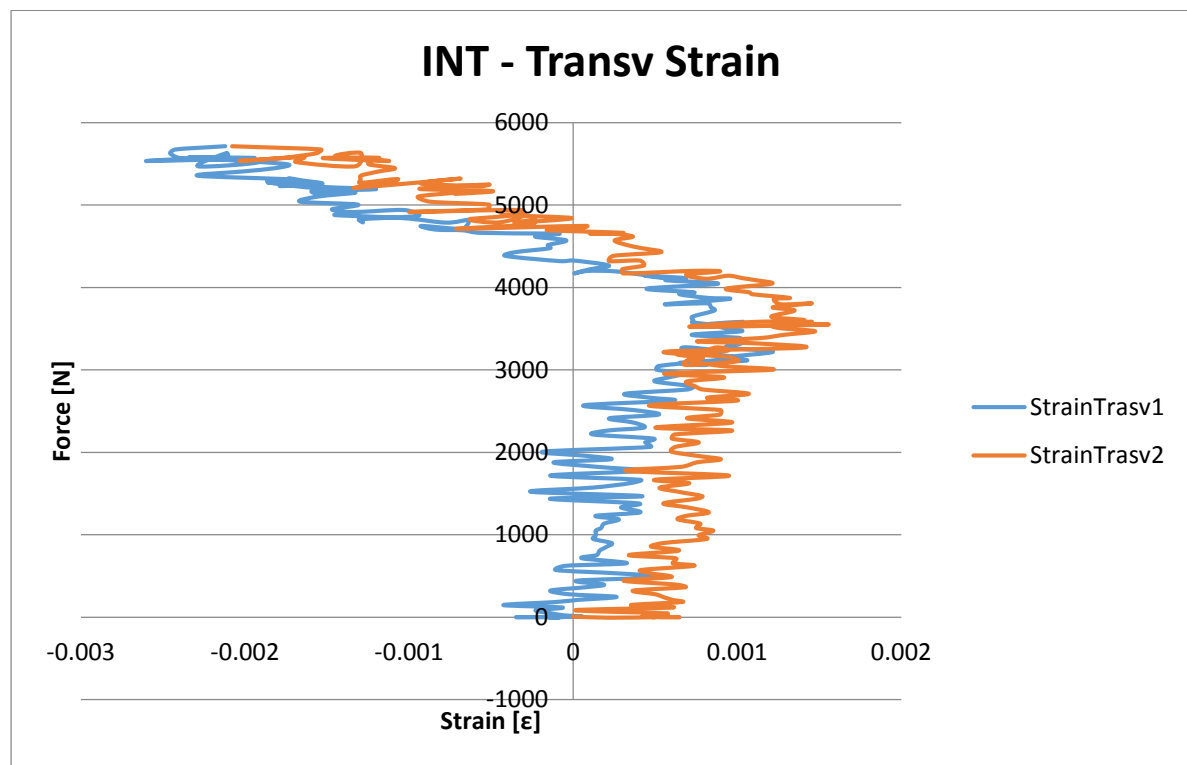
Figure 7.37: Transversal strain in INT specimen

Looking at strain plots, materials with carbon/epoxy on the outer part show a higher noise than the EXT one. This could be ascribable to fragile behaviour of composite. Another result that could be deduced from these plots is the nonlinear behaviour of strains for all material kinds.

7.3 Discussion

Data analysis has shown that the presence of aluminium layers inside a carbon/epoxy composite results in a higher maximum force and displacement at failure. In particular the max force is higher when the metal layers are in the laminate inner part. At the same time, however, a pure carbon/epoxy composite shows a better energy dissipation, noticeable in the stable high force that the laminate can resist after main failure. This is the principal reason that brought carbon/epoxy composite to replace metal structures in crashworthiness tools. This stable failure has been discovered also for EXT material with even a higher peak indentation resistance value. This result together with an easier detectability of the impact location, due to Al plasticity, are the reasons why it could be said that having metal layers in the outer part of a composite stacking sequence can be the best configuration possible.

This material has other advantages that don't not really come from this experimental campaign but they represent important matters that can't be ignored during an aircraft design project. These are lightning strike and surface painting.

A composite structure is usually not conductive and, therefore, in order to avoid issues related to lightning strikes, metallic nets are embedded into the composite material. This approach could be avoided using a material with metallic layers on the outside; hence EXT is once again pointed out as the best configuration obtained.

Another convenience in this material application could come from the painting requirements: composite structures have to be treated to have a good adhesion between its surface and varnish, while this is easier when it comes to metallic structures. Hence, EXT materials seems to be the best choice.

References

[7.1] ASTM D7136 / D7136M – 15, Standard Test Method for Measuring the Damage Resistance of a Fiber-Reinforced Polymer Matrix Composite to a Drop-Weight Impact Event

[7.2] L.S.Sutherland, C. Guedes Soares, The use of quasi static testing to obtain the low-velocity impact damage resistance of marine GRP laminates, Composites: Part B, 2012.

[7.3] A. Wagih, P- Maimì, N. Blanco, J. Costa, A quasi static indentation test to elucidate the sequence of damage events in low velocity impacts on composite laminates, Composites: Part A, 2016.

[7.4] L.S. Sutherland, Contact indentation of marine composites, 2004.

[7.5] A. T. Nettles, A comparison of Quasi-Static Indentation to Low-Velocity Impact, 2000.

[7.6] M. Sadighi, R.C. Alderliesten, R. Benedictus, Impact resistance of fiber-metal laminates: A review, International Journal of Impact Engineering, 2012.

[7.7] F.D. Moriniere, R.C. Alderliesten, R. Benedictus, Low-Velocity impact energy partition in GLARE, Mechanics of Materials, 2013.

[7.8] M Sadighi, RC Alderliesten, R Benedictus, Impact resistance of fiber-metal laminates: a review, International Journal of Impact Engineering, 2012.

[7.9] Shengqing Zhu, Gin Boay Chai, Low-Velocity impact response of fibre-metal laminate – Experimental and finite element analysis, Composites Science and Technology, 2012.

8

FEM analysis:

Cohesive Zone Model

In this chapter, main characteristics of a Finite Element Method analysis are presented. Cohesive zone model, used in developed models in order to obtain delamination damages, characteristics are described.

8.1 Introduction

Experimental campaign are the best way to study materials mechanical characteristics. They are done at different design levels (Figure 8.1) involving different kinds of tests and specimens, different materials and structure features.
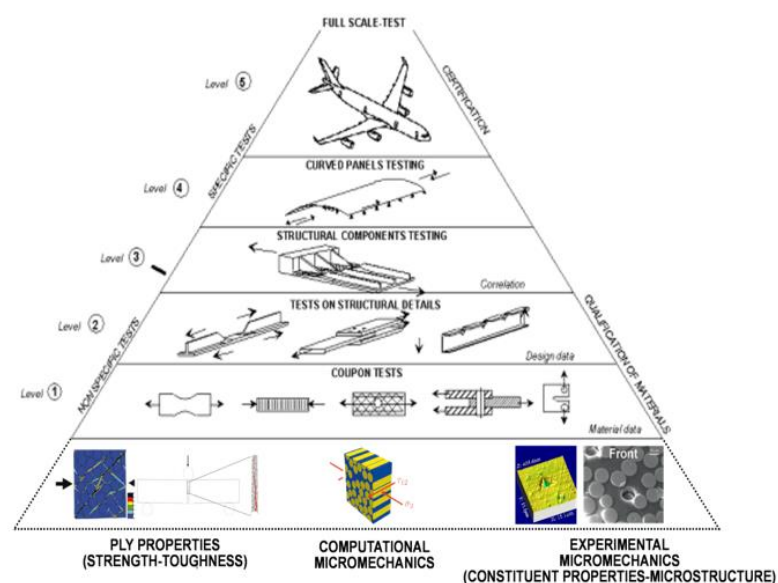
Figure 8.1: Design tests pyramid

Realising a complete and reliable experimental campaign for each level, and for each material property, is a really expensive and difficult procedure, and, therefore, it is not always possible.

Fortunately, in the last forty years, computational capacity have seen a huge improvement, giving powerful means to engineers. Thanks to different commercial softwares of Finite Element Method, it is possible to recreate same conditions and loads of an experimental test, without all its drawbacks.

On one hand, in fact, FEM is a cheap and flexible way to obtain reliable results. On the other hand, model design and tuning is not an easy step and it requires many data that have to be found experimentally. Therefore, practical test can not be completely replaced by an FEM software.

In particular, talking about composite materials this is even more complicated: composites properties studies are still in an evolving phase and many different condition behaviours and their causes are still unknown.

Due to this complexity, and referring to which properties and behaviour is going to be studied, there are different ways to model a laminate or a composite structure. In the following, only FEM features strictly connected with this thesis are described, leaving to the reader a deeper study of this powerful mean [8.1].

FEM analysis described in this thesis was carried out by means of commercial software Abaqus; specific terminology and properties refer to this but similar can be found in other kinds of FE software, even if with different names.

8.2 Model overlook

Finite element simulations can be divided into 3 different steps:

- Pre-processor, where intial geometry, material description and initial condition are implemented. For model and conditions, these have to be as equal to reality as possible in order to obtain reliable results. However, assumptions need to be done in order to deal with numerical programming issues and computational costs. For what concerns material it has to be described by many values, depending on which kind of material is used (isotropic, orthotropic, etc.). Moreover damage criterion and failure mode should be described as practice as possible; therefore, many parameters are needed.
- Main Programme, where all test parameters, i.e. loads and boundary conditions, are implemented, materials are assigned to each part (defining orientation, if needed), mesh size and shape are assigned, output variable are chosen depending on which results need to be underlined.

- Post-processor, where all information coming from the run simulation are analysed (deformations, contacts, energies, damages, etc).

Many variables can influence FEM results: first, it is necessary to know and understand all parameter involved in the simulation; this also depends on which kind of simulation is running (static, dynamic, etc.) and which kind of loads and boundary conditions are involved. Moreover, mesh size and shape influence model results and, therefore, they should be carefully chosen.

For deeper information about Abaqus software and its characteristics, please refer to [8.1-8.2].

8.3 Cohesive zone model

Cohesive Zone Model (CZM) was developed to simulate composite fracture mechanics. It is nowadays quite widely used as an alternative to other fracture mechanics approaches (e.g. Linear Elastic Fracture Mechanics LEFM or Virtual Crack Closure Technics VCCT). In fact, it shows many advantages: it can be applied to analyse uncracked structures (for predicting delamination or disbonding in composites); non-linear zones can be analysed with a more realistic approach; progressive material damages are simulated thanks to its properties deterioration; it can predict multiple cracking and allow mixed-mode behaviour.

With Cohesive Zone Models, damages are supposed to take place between two fictional surfaces and they are suitable for modelling thin layers. Therefore, they are widely used in composite delaminations modelling.

Damage is strictly connected with CZM tensile resistance and it happens when the last goes to zero. Therefore, cohesive region behaviour is usually modelled with traction-separation laws: this relationship is based on link between surfaces displacement and traction that cohesive can carry on to resist that separation. Traction-separation law can have different expression depending on which form the damage law assumes. Usually, traction separation laws are divided into two parts (Figure 8.2): a beginning part where traction has an increasing trend and cohesive zone still is able to handle surfaces separation; a decreasing slope, after a maximum traction value that defines damage onset, where damage evolutions takes place and therefore, material property decreases, until it reaches zero value, defining crack tip. Depending on which functions are used to describe these two parts, there have been developed many different kinds of traction separation laws (Figure 8.1): trapezoidal, linear, exponential, polynomial, etc.
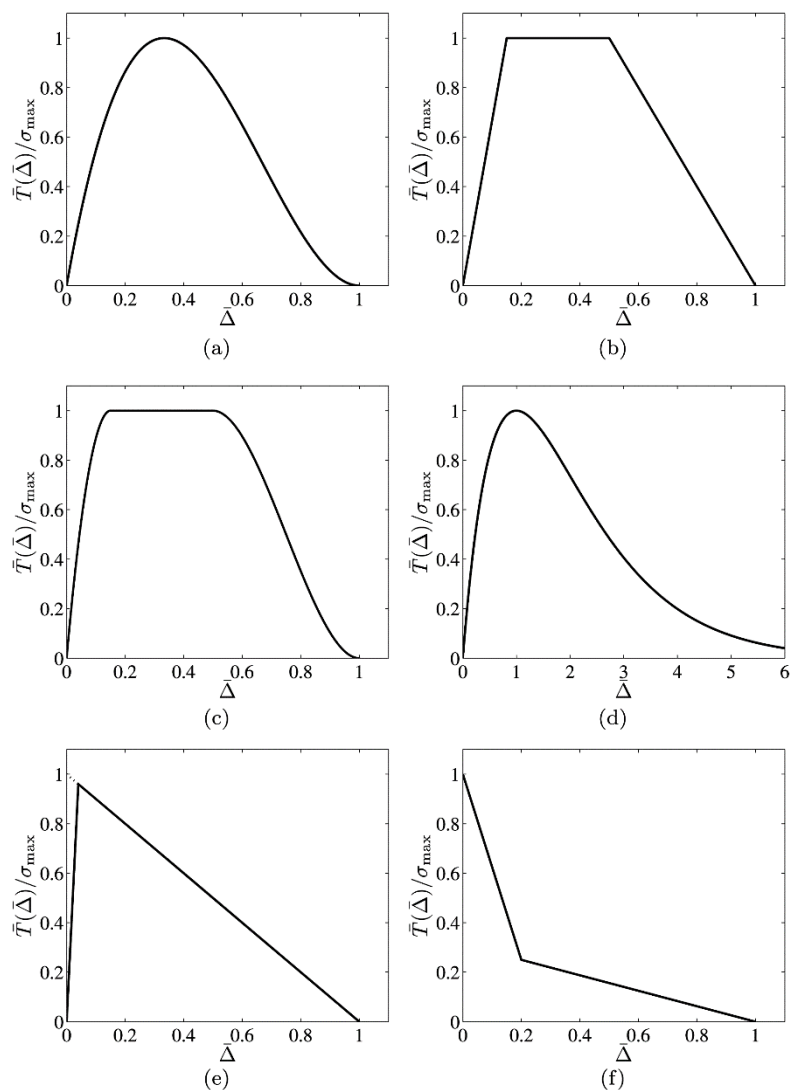
Figure 8.1: Different kinds of Traction-Separation laws

Irrespective of which kind of law is used, there are some parameters to be defined: first of all, cohesive strength, i.e. threshold value of traction; characteristic length, i.e. displacement at which maximum traction value is reached; parameter (related to displacement or dissipated energy) at which surfaces are completely separated and, therefore, cohesive fails.

There parameters are related to material properties and model characteristics: cohesive strength is usually related to material yield stress; characteristic length is related to material brittleness and can be obtain from cohesive strength, by means of inverse function (after the latter is chosen). As previously said, last parameter could be related to maximum displacement or energy dissipation in fracture evolution. Choosing one over the other depends on problem physical mechanisms: if damage is linked to displacement, it would occur when the maximum displacement between surfaces is reached, while, if it is linked to energy dissipation, it would occur when a threshold value, i.e. fracture energy,

is exceeded. Dissipated energy refers to the area under traction-separation curve and it depends on which mode element is loaded (mode I, mode II, mode III, mixed mode).

Linear traction-separation law has been used for models developed for this thesis aim; therefore, involved parameter and characteristics are described.

As shown in Figure 8.2, initial part follows a linear-elastic behaviour (that is expressed with a matrix form stress-strain relation, due to a better implementation in FEM software) until damage initiation point is reached. Stress vector σ id given by force components divided by section area of unloaded cohesive element. At the same time, strain vector ε is obtained dividing displacement components (δ_n ; δ_s ; δ_t) by the element thickness (T), as shown in (8.1).

$$(8.1) \qquad \varepsilon_n = \frac{\delta_n}{T} \; ; \; \varepsilon_s = \frac{\delta_s}{T} \; ; \; \varepsilon_t = \frac{\delta_t}{T}$$

The subscripts, s n and t, refer to the perpendicular directions of a three axis reference system; usually n indicates normal direction, s and t transversal ones.

In the same way, elastic modulus can be expressed in its components, forming the constitutive matrix $\boldsymbol{K}$ (that is called penalty stiffness in Abaqus) obtaining (8.2):

$$(8.2) \qquad \boldsymbol{\sigma} = \begin{bmatrix} \sigma_n \\ \sigma_s \\ \sigma_t \end{bmatrix} = \begin{bmatrix} K_{nn} & K_{ns} & K_{nt} \\ K_{sn} & K_{ss} & K_{st} \\ K_{tn} & K_{ts} & K_{tt} \end{bmatrix} \begin{bmatrix} \varepsilon_n \\ \varepsilon_s \\ \varepsilon_t \end{bmatrix} = \boldsymbol{K}\varepsilon$$
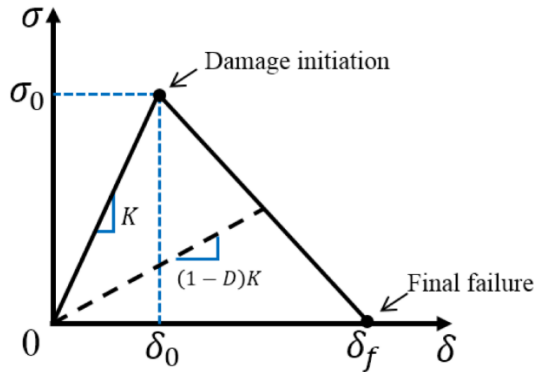
Figure 8.1: Linear Traction-Separation law example

Figure 8.2 shows an example of this law and could be referred to normal or shear directions (just adding s, n or t subscripts). Characteristic length is described as δ_0 and corresponds to cohesive strength (σ_0). Different criteria can be adopted to describe damage initiation referring to strains ratio or stresses. The commonest among these are:

- maximum nominal stress criterion, where $max \left\{ \frac{\sigma_n}{\sigma_n^0}, \frac{\sigma_s}{\sigma_s^0}, \frac{\sigma_t}{\sigma_t^0} \right\} = 1$

- maximum nominal strain criterion, where $max \left\{ \frac{\varepsilon_n}{\varepsilon_n^0}, \frac{\varepsilon_s}{\varepsilon_s^0}, \frac{\varepsilon_t}{\varepsilon_t^0} \right\} = 1$

- quadratic nominal stress criterion: $\left(\frac{\sigma_n}{\sigma_n^0}\right)^2 + \left(\frac{\sigma_s}{\sigma_s^0}\right)^2 + \left(\frac{\sigma_t}{\sigma_t^0}\right)^2 = 1$

- quadratic nominal strain criterion: $\left(\frac{\varepsilon_n}{\varepsilon_n^0}\right)^2 + \left(\frac{\varepsilon_s}{\varepsilon_s^0}\right)^2 + \left(\frac{\varepsilon_t}{\varepsilon_t^0}\right)^2 = 1$

In simulations developed for this thesis aim, maximum nominal stress criterion was used.

Damage evolution is represented by materials softening and damage is represented by a variable called D: this is equal to 0 at the beginning when material is undamaged; at damage initiation, D increases up to 1 that corresponds to complete facture. Stress-strain relation becomes (8.3):

(8.3) $$\sigma = (1 - D)K\varepsilon$$

With a linear softening relation, damage is given by (8.4):

(8.4) $$D = \frac{\delta_m^f(\delta_m^{max} - \delta_m^0)}{\delta_m^{max}(\delta_m^f - \delta_m^0)}$$

where $\delta_m = \sqrt{\delta_n^2 + \delta_s^2 + \delta_t^2}$ is the effective displacement, δ_{max} is the maximum value obtained and δ_m^f is the value at which total failure takes place. Therefore, it would be:

(8.5) $$D = \begin{cases} 0 & \delta \leq \delta_0 \\ 0 < D < 1 & \delta_0 \leq \delta < \delta_f \\ 1 & \delta \geq \delta_f \end{cases}$$

Relating to failure, an energetic criterion is taken, i.e. complete fracture happens when critical energy G_c is exceeded; hence, maximum displacement is:

(8.6) $$\delta_f = \frac{2G_c}{\sigma_0}$$

References

[8.1] Abaqus 6.13 user manual

[8.2] A. Khennane, 'Introduction to Finite Element Analysis Using MATLAB® and Abaqus', CRC Press, 2013

[8.3] Luca Boni, 'Modello numerico per la valutazione del comportamento di pannelli irrigiditi in materiali compositi soggetti ad impatto', 2010

[8.4] Z. Hashin, 'Failure Criteria for Unidirectional Fiber Composites', 1980

[8.5] C.G. Davila, P.P. Camanho, A. Turon, 'Effective Simulation of Delamination in Aeronautical Structures Using Shells and Cohesive Elements'.

[8.6] E.V: Gonzalez, P. Maimi, P.P. Camanho, A.Turon, J.A. Mayugo, 'Simulation of drop-weight impact and compression after impact tests on composite laminates, Composite Structures, 2012.

[8.7] C.G. Davila, P.P. Camanho, C.A. Rose, Failure criteria for FRP laminates, Journal of composite materials, 2007.

[8.8] S. Abrate, 'Impact on laminated composite materials,

[8.9] Barbero!

9

FEM analysis:

Impacts on Carbon/Epoxy and FML coupons

FEM models have been realised to simulate impact tests on a carbon/epoxy laminate and FML materials described in chapter 5 and 7. These models aimed to a better understanding of inner damages kinds and evolution that could rise from a low energy impact, implementing cohesive plies in between pre-pregs layers.

9.1   Carbon/epoxy developed model

Taking into account impact tests described in Chapter 5, a FE Model was developed. The main aim was to show low energy impact damages, i.e. delamination and small matrix cracks. Hence, it was decided to use cohesive model implemented in Abaqus and to model each ply in order to understand what happens at plies interface.

Two different model were realised: near-edge and central impact models.

Model characteristics and parameters are described in the following sections.

9.1.1 Impactor geometry and characteristics

Experimental impact tests, as described in Chapter 3, were performed by means of a 'modified Charpy pendulum'; it was not, however, possible to model the whole fixture due to high computational costs and many parameter involved that could influence test results. It was, therefore, modelled only specimen and impactor, reducing holding fixture into proper boundary conditions.

Impactor was realised by means of a rigid body. It is a cylinder with a hemispherical end of 7 mm diameter (Figure 9.1).
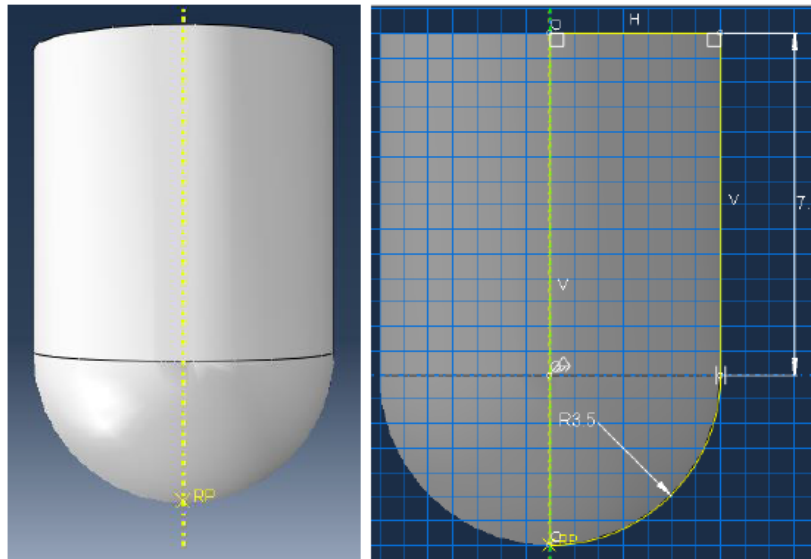
Figure 9.1: Impactor geometry

Taking into account real impactor mass (1.81 kg), density was assigned in order to obtain that mass in the model as well. Typical steel mechanical characteristics (Table 9.1) were set to describe impactor material even if those were not necessary due to rigid body constrain that gives to this part an crushproof nature.

Table 9.1: Impactor mechanical characteristics

Young modulus [GPa]	Poisson modulus
210	0.3

Tetrahedral elements were chosen as mesh shape (Figure 9.2), while its dimensions were not small due to impactor crushproof nature and not necessity to acquire data from its body.
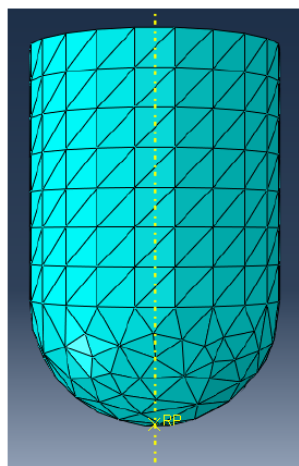
Figure 9.2: Impactor mesh

9.1.2 Laminate geometry and characteristics

Pre-preg plies were modelled with shell element of 100x50 mm dimensions, while their thickness refers to a single ply thickness (0.241 mm). Laminate was made of seven pre-preg laminae, spaced out with cohesive layers. Pre-preg and cohesive material characteristics are list in the following tables (Table 9.2-9.3). This model was used as a preliminary analysis for future more accurate simulations; therefore, materials and stacking sequence involved is different from the one showed in Chapter 5. Qualitative results are still noticeable and were taken into account in the model described in section 9.2.
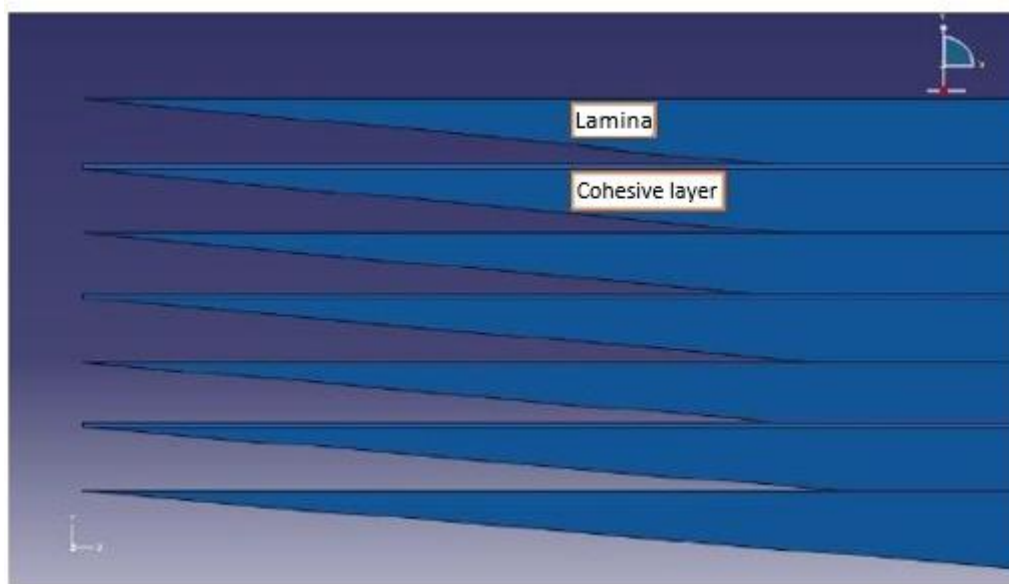
Figure 9.3: Cohesive and Prepreg layers succession

Table 9.2: pre-preg layer properties

Property	
Density (kg/m^3)	1590
Young Modulus (GPa)	E_1=135 , E_2= 9.6
Shear Modulus (GPa)	G_{12}=5.3
Poisson Modulus	v_{12} =0.32 , v_{23}=0.487
Thermal Expansion Coefficient (1/K)	α_1= -3.42x10^{-7} , α_2= 2.58x10^{-5}
Strength (MPa)	X^T=2207, X^c=1531, Y^c=199.8, Y^T=80.7, S^L=114.5
Fracture Toughness (N/mm)	G_{2+}=0.28, G_6=0.79, G_{1-}=106.3, G_{1+}=81.5

Table 9.3: cohesive elements properties

Property	
Density (kg/m^3)	P=1
Thickness (m)	K =10^{-6}
Mechanical properties (GPa/m)	E/K$_{nn}$=1.92e^{15}
	G$_1$/K$_{ss}$=645595158e^6
	G$_2$/K$_{tt}$= 645595158e^6
Damage Initiation (MPa)	Y^T=80.7, S^L=114.5
Damage Evolution (N/mm)	G$_{2+}$=0.28, G$_6$=0.79
B-K parameter	μ=1.45

The pre-preg fracture toughness G is material capacity to bear fracture growth. For orthotropic materials it is necessary to measure five toughnesses: two in longitudinal direction (one for compression, indicated with '-', and one for traction, indicated with '+'), two in transversal direction ('-' sign underlines compression and '+' tensile one); G$_6$ refers to shear toughness. G$_{2-}$ (transversal direction compressive fracture toughness) is obtain by calculation:

(9.1) $$G_{2-} = \frac{G_6}{\cos\alpha_0}$$

where α_0 is the angle which fracture tends to grow inside the material. It is usually considered equal to 53°.

X and Y are strength measured in fibre direction and transversal direction respectively. S^L is the lamina longitudinal shear strength. S^T has to be calculated by means of:

(9.2) $$S^T = \frac{Y^C}{2}$$

Laminate stacking sequence is $[(0/-45/+45/\overline{90}]_s$. Fibre angles refer to x axis (Figure 9.4).
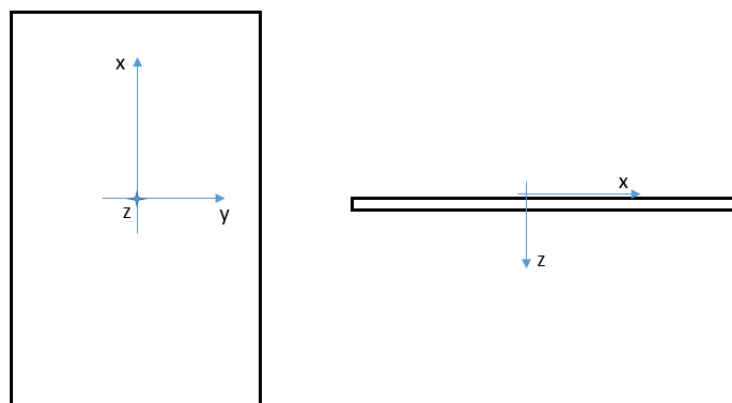
Figure 9.4: Cohordinate system

As already said, every lamina is modelled by means of shell elements. In this way it is possible to apply Hashin failure criteria [9.4], that could be applied only to 2D element.

Cohesive layers are modelled as solid elements with 5 μm thickness.

9.1.3 Mesh

Mesh size and shape was chosen in order to have more detailed results in the impact area (Figure 9.5). To achieve this a circular partition was made on cohesive and shell elements. In order to link shell mesh elements movement to cohesive ones, a tie constrain was added between these parts.
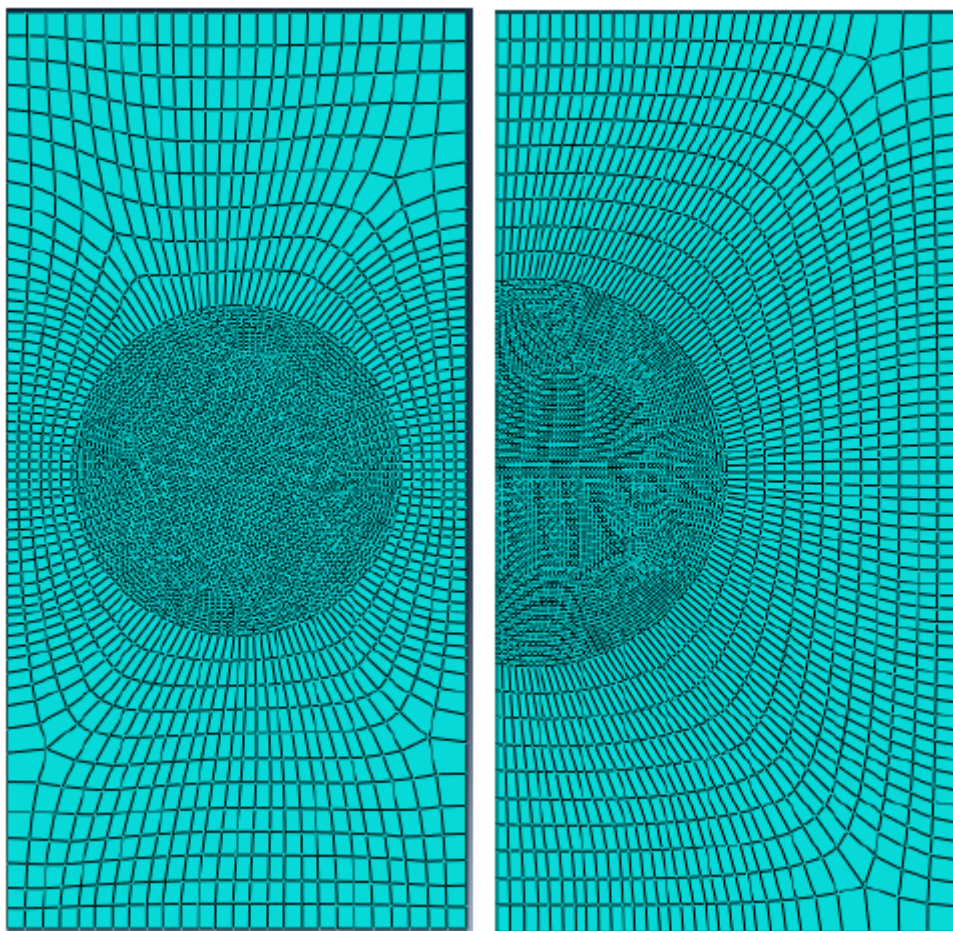
Figure 9.5: Mesh shape of layers for central and near-edge impact

9.1.4 Boundary conditions

Boundary condition setting is an important step into a FE analysis: in fact, they simulate loads and limits on structure degrees of freedom (DoF) and, therefore, wrong boundary conditions could invalidate simulation results.

First of all, it is fundamental to describe impact load: it was chosen a 6 J energy impact and, hence, a proper velocity was calculated by (9.4):

(9.3) $\qquad E_{imp} = \frac{1}{2} m_{imp} v_{imp}^2$

(9.4) $\qquad v_{imp} = \sqrt{\dfrac{2\,E_{imp}}{m_{imp}}}$

where E_{imp} is the impact energy, m_{imp} is impactor mass, v_{imp} is the velocity assigned to impactor to obtain E_{imp}.

As previously said, impactor was modelled as a rigid crushproof body and, therefore, it is possible to refer all data related to it only on a reference point. This was set at the hemispherical summit.

Modelled impactor could move only in z directions: other DoFs were limited. In fact, it was not reproduced the pendulum impact trajectory. This is not misleading because even in experimental tests, specimen was fixed where the impactor hit it orthogonally to its medium plane.

Contact properties were implemented (Figure 9.6), as well. In particular, hard contact between all close surfaces and friction properties (between impactor surface and first pre-preg ply, μ=0.3; between laminae, μ=0.5).
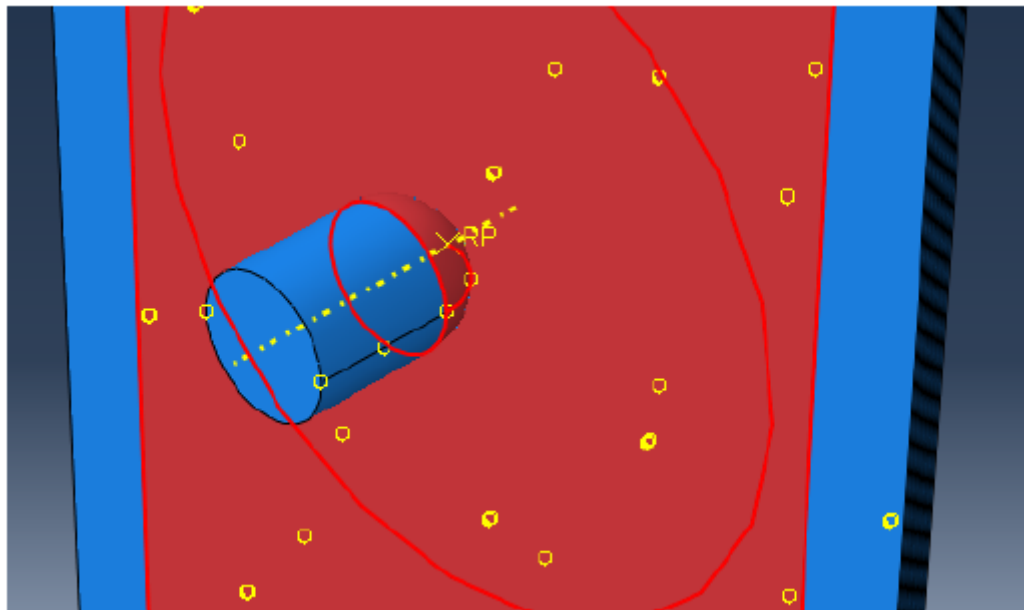
Figure 9.6: Detail of impactor and fist lamina surfaces contact properties definition

Moreover, boundary condition for holding fixture were implemented on specimen surfaces. External plies were partitioned, taking into account experimental fixture dimensions, and DoF were limited in the areas underlined in Figure 9.7). It was, therefore, modelled as a built-in.
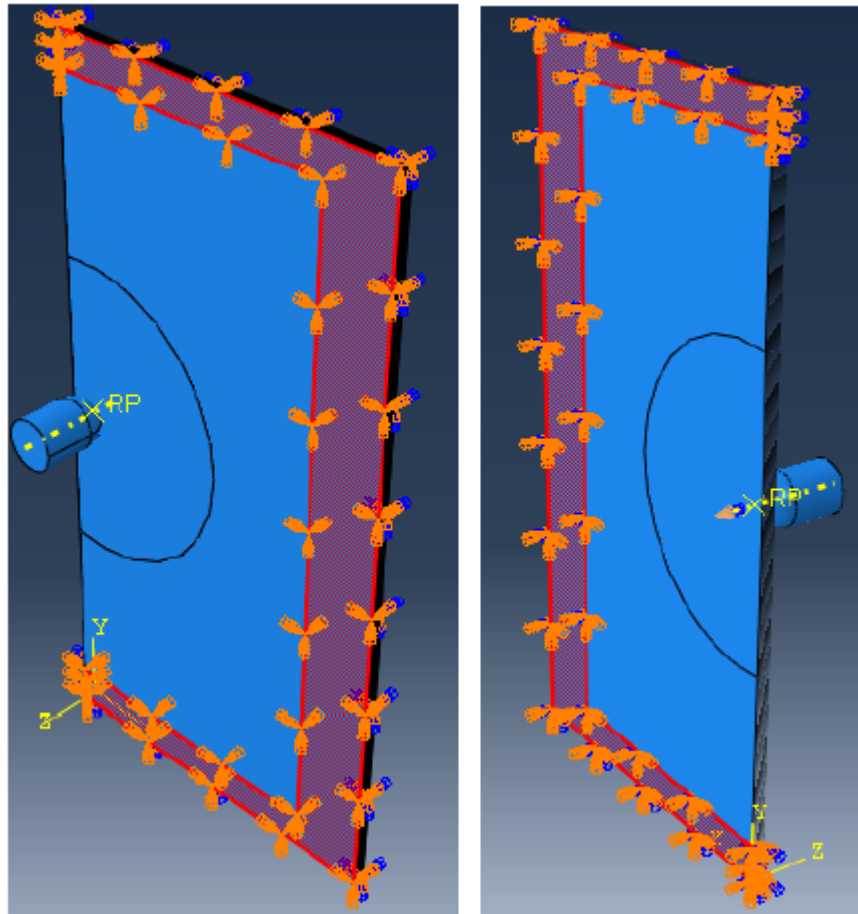
Figure 9.7: Holding fixture modellation by means of boundary conditions

A dynamic explicit step was created: step time was assigned in order to simulate impact and bounce event.

9.1.5 Results

- First model, Central Impact

In the following pictures (Figure 9.8-9.14), first model simulation sequence is presented. At t =1 ms, contact between impactor and laminate has taken place: first effect of this contact is deformation of laminate, and in particular of the bottom ply due to membranal behaviour. At t =2 ms, impactor starts to go back and laminate starts to gain its initial form, thanks to its elastic properties; from this moment on, some cohesive elements start to deform in an improper way: due to element damage but not complete failure, a numerical error occurs. At t =10 ms, laminate is still reacting to impact load: there is a small deformation in opposite impact direction. If simulation was left run longer, this effects could have finished and laminate could have gain its straight form. To check

cohesive layers damages, it was decided to stop simulation at this point, where all damages are already developed.
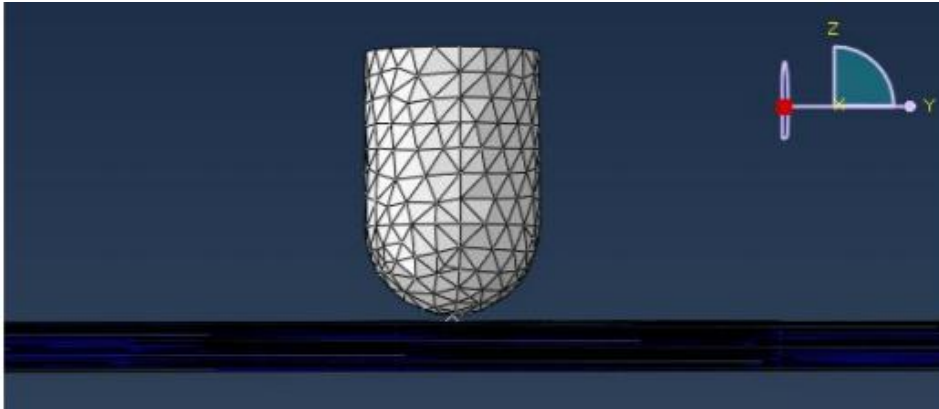
Figure 9.8: CI model (t=0ms)
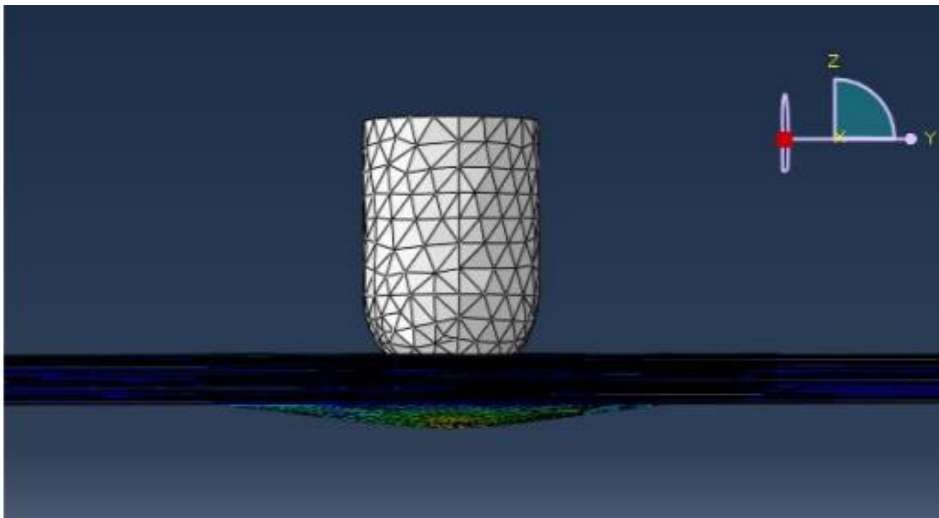
Figure 9.9: CI model (t=1ms)
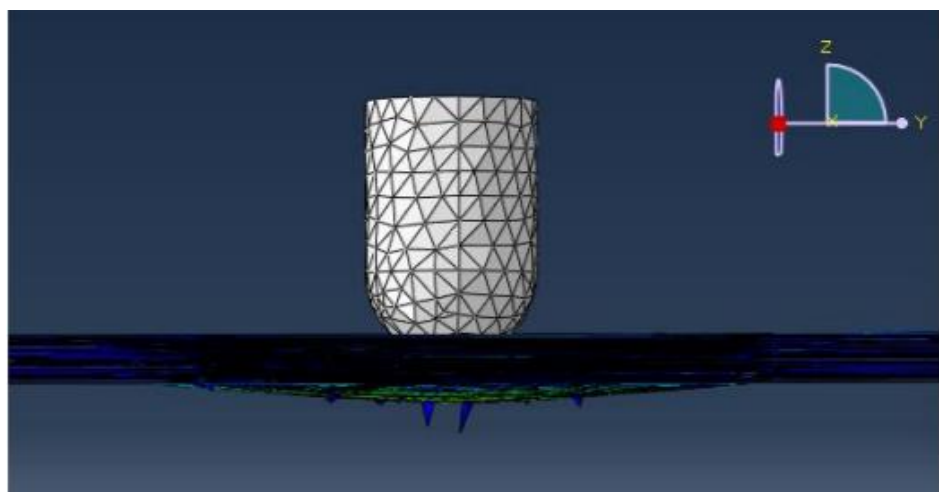
Figure 9.10: CI model (t=2ms**)**
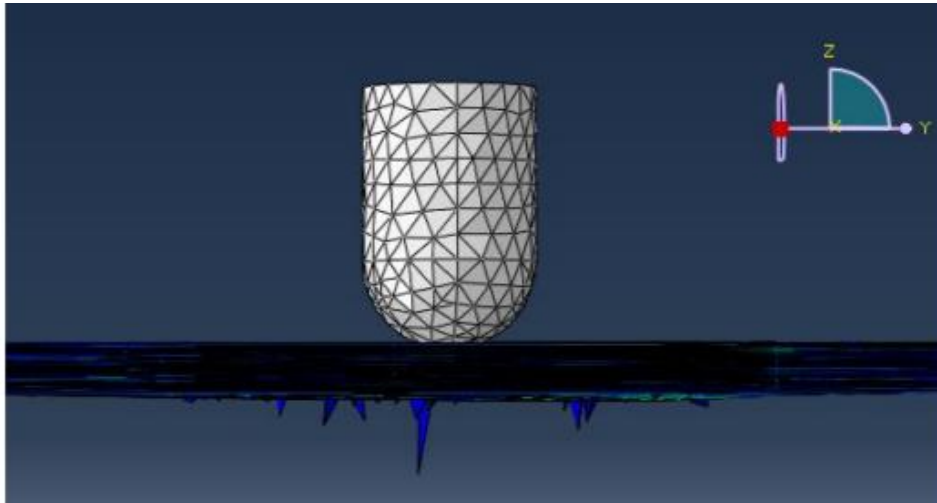
Figure 9.11: CI model (t=3.5ms)
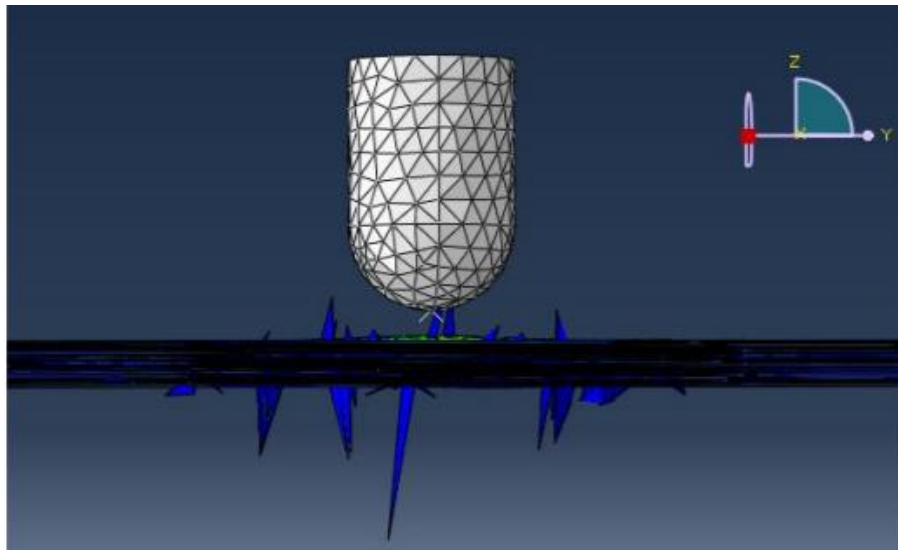
Figure 9.12: CI model (t=6.5ms)
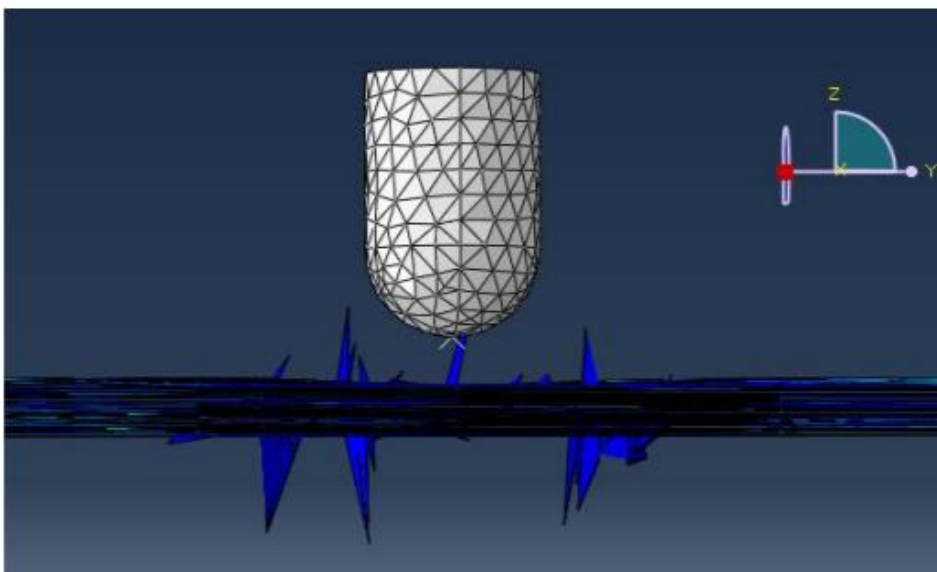
Figure 9.13: CI model (t=8ms)
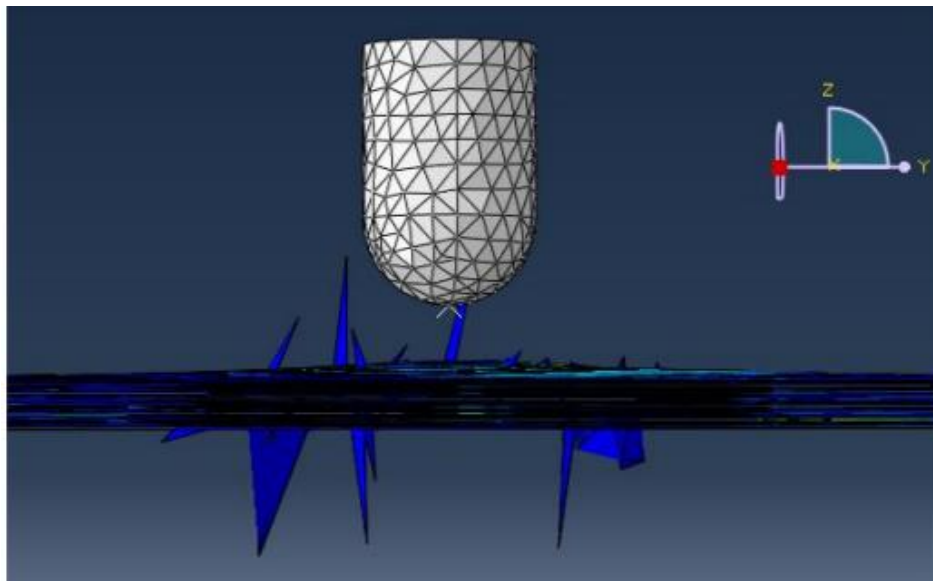
Figure 9.14: CI model (t=10ms)

Cohesive damaged zones are showed in Figure 9.15 – 9.18. Thanks to cohesive elements implementation, impact damages are obtained: delaminations are wider for layers further from impact location (membranal behaviour) while their shape are influenced by prepreg layers orientation. They, in fact, assume a 'peanut' shape oriented along next layer fibre direction.
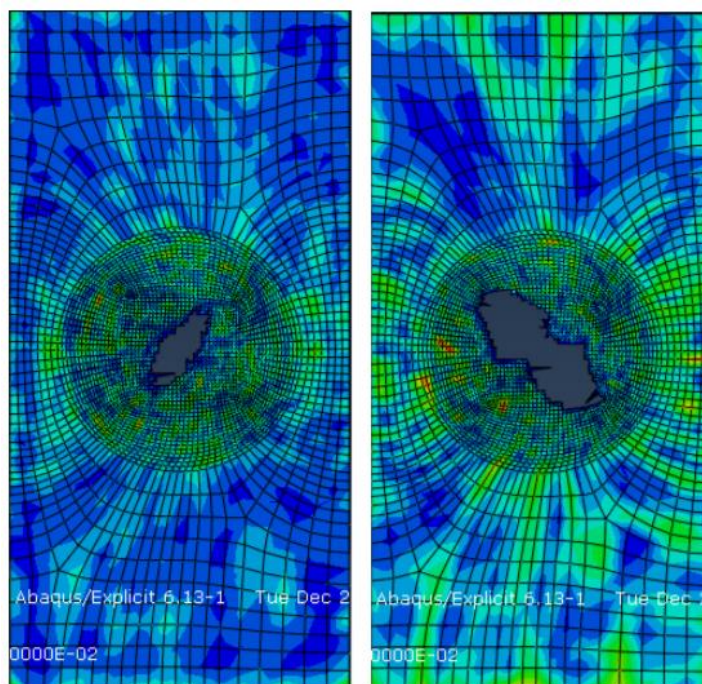
Figure 9.15: CI model: cohesive layers (between 1-2 plies, and 2-3 plies)
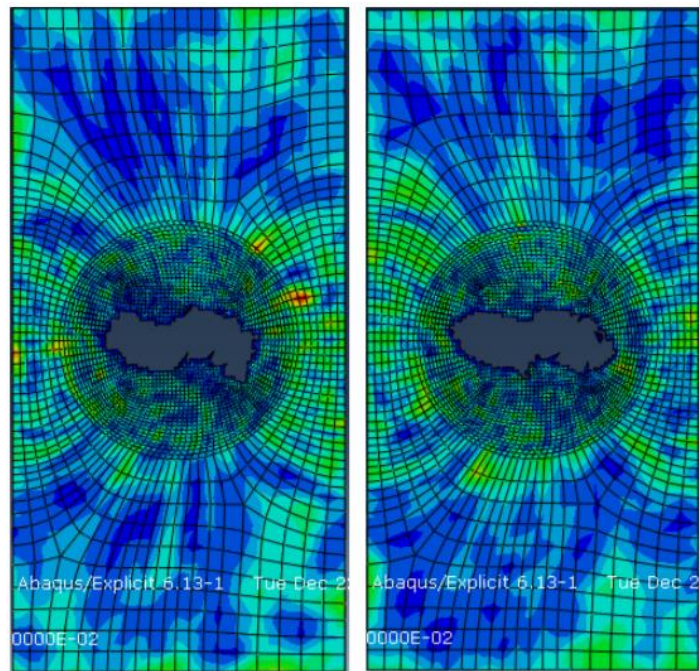
Figure 9.16: CI model: cohesive layers (between 3-4 plies, and 4-5 plies)
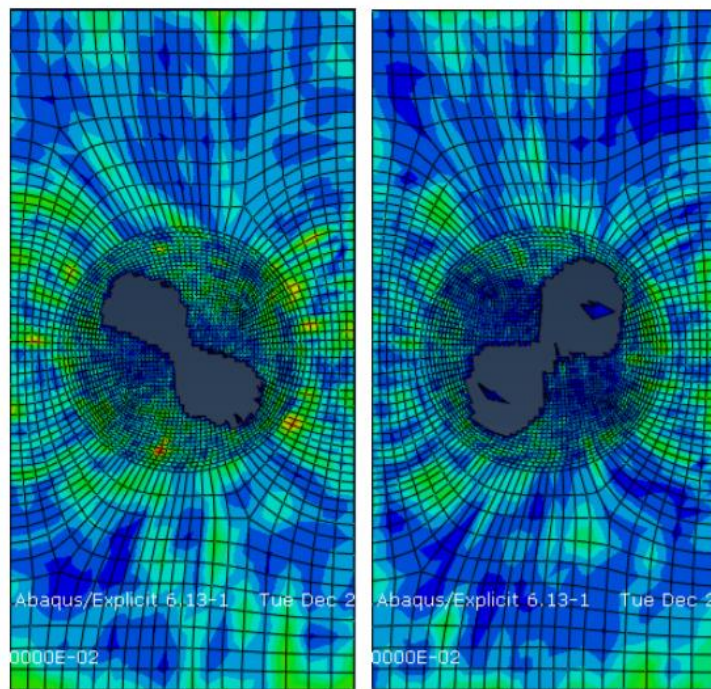
Figure 9.17: CI model: cohesive layers (between 5-6 plies, and 6-7 plies)
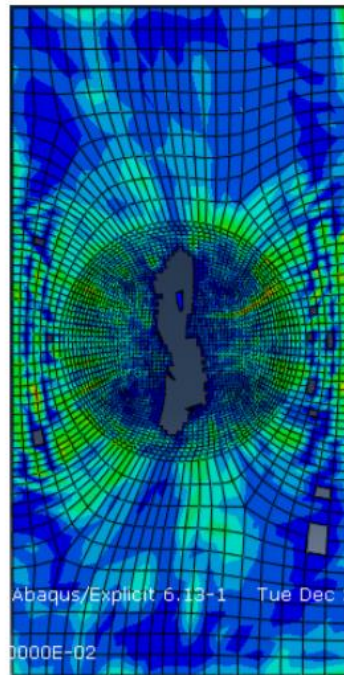
Figure 9.18: CI model: cohesive layers (between 7-8 plies)

Pre-preg failure has been implemented by means of Hashin criteria [9.4], but it was observed that, while cohesive layers are subjected to damages, there is not any failure on pre-preg plies. Therefore, as expected and experimentally proved, this energy impact (6 J) do not create any damage on material surface but inner delaminations.

- **First model, Near-Edge impact**

From Figure 9.19 to Figure 9.24 Near-Edge impact sequences are presented: deformation is evident and bigger than for central impact, previously presented. At t = 4.5 ms, impactor bounce starts and specimen gains its shape back.
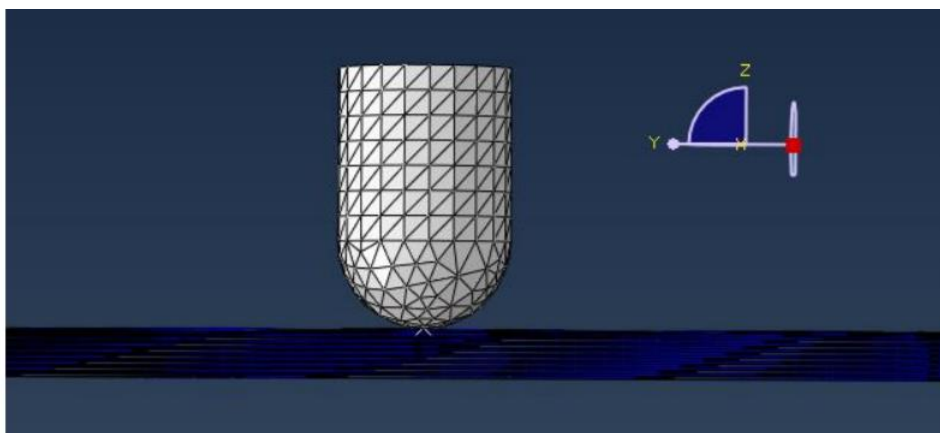
Figure 9.19: NE model (t=0ms)
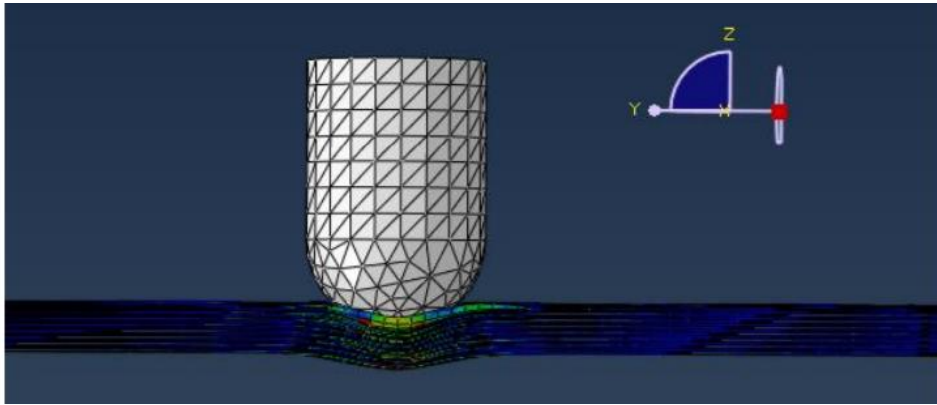
Figure 9.20: NE model (t=0.5ms)
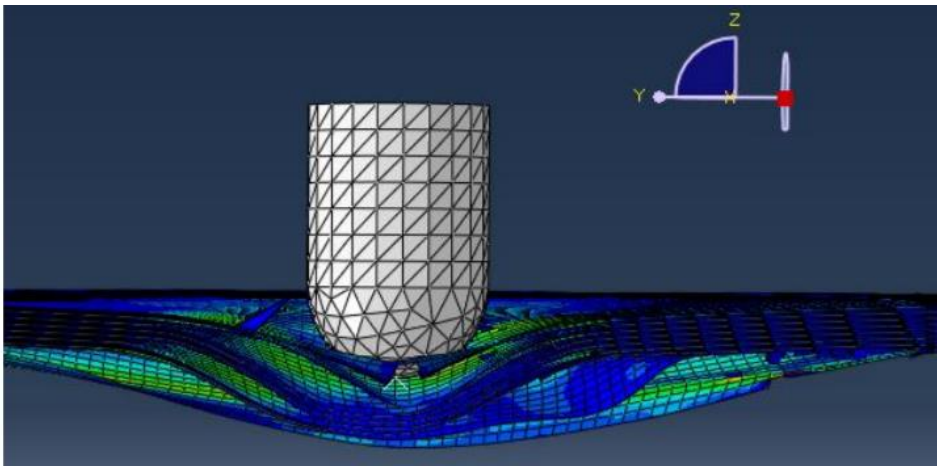
Figure 9.21: NE model (t=3.5ms)
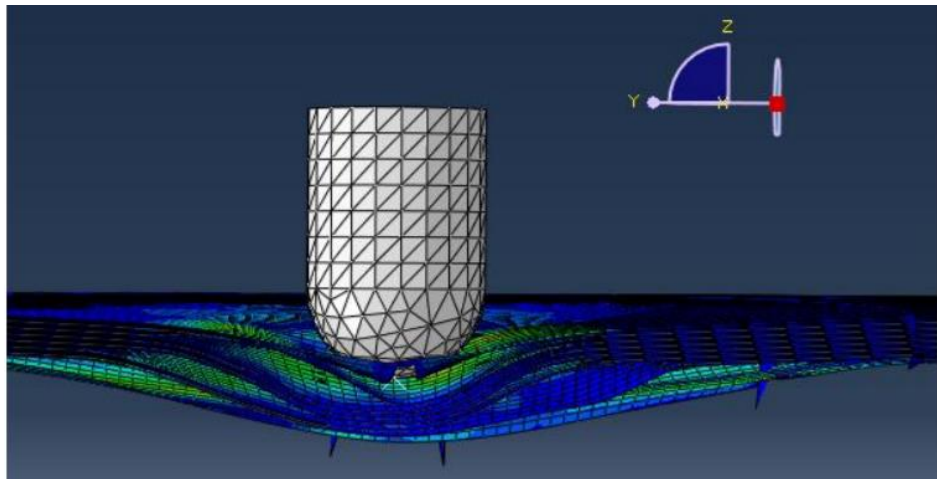
Figure 9.22: NE model (t=4.5ms)
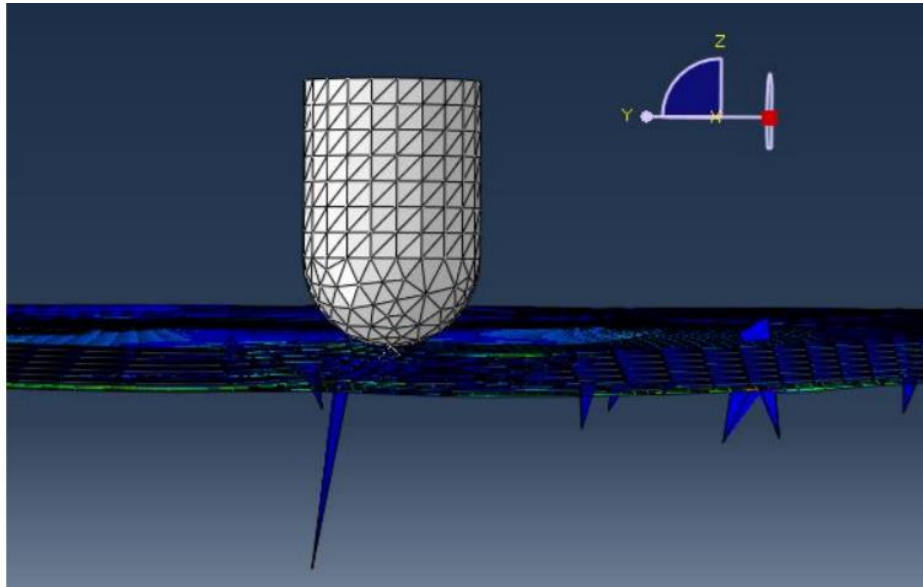
Figure 9.23: NE model (t=8ms)
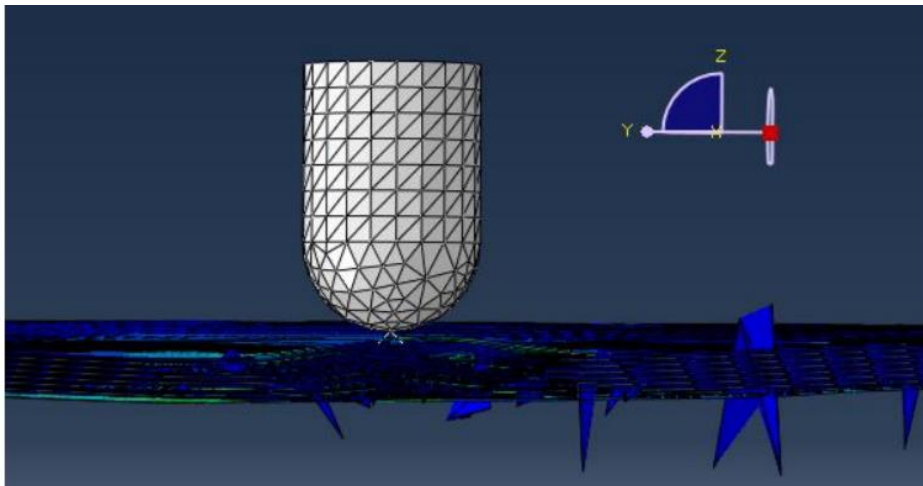
Figure 9.24: NE model (t=10ms)

Looking at cohesive layers damages, they follow same behaviour described for central impact: 'peanut' shapes oriented as close layer fibres direction (Figure 9.25-9.28).

In this case, a small fibre damage has occurred on the first pre-preg ply (Figure 9.29), right under impact location (2 mm distance from specimen edge).
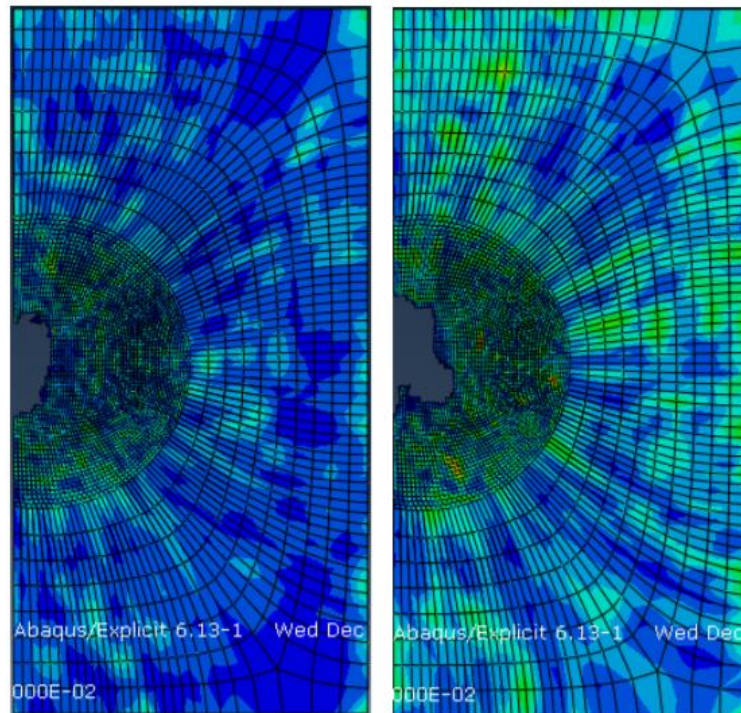
Figure 9.25: NE model: cohesive layers (between 1-2 plies, and 2-3 plies)
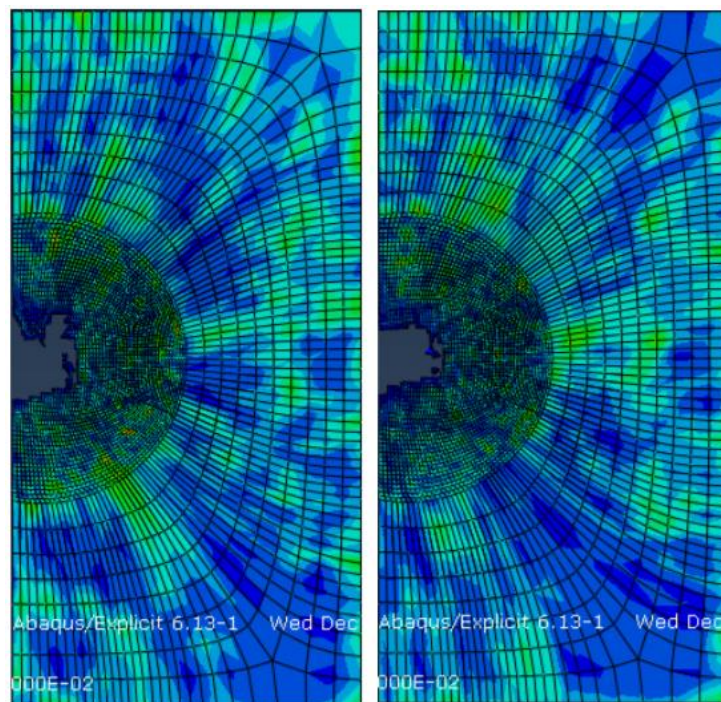
Figure 9.26: NE model: cohesive layers (between 3-4 plies, and 4-5 plies)
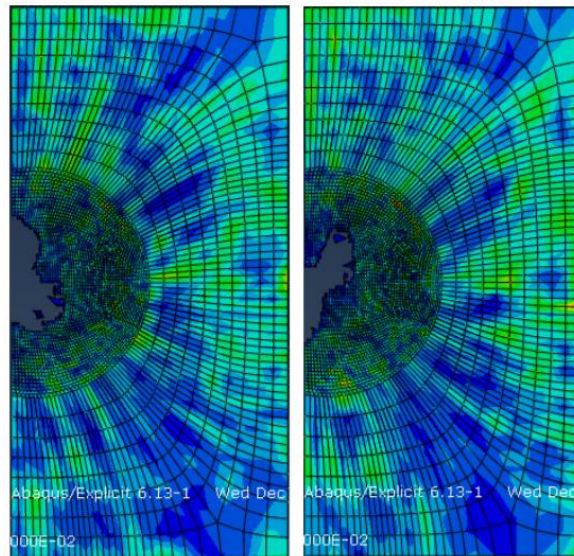
Figure 9.27: NE model: cohesive layers (between 5-6 plies, and 6-7 plies)
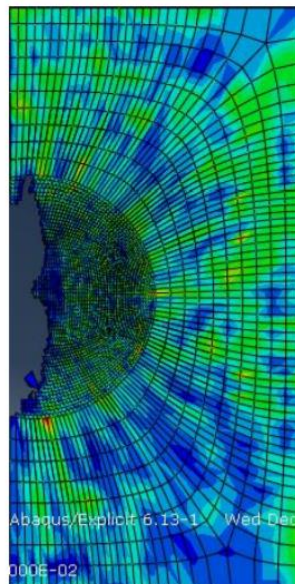
Figure 9.28: NE model: cohesive layers (between 7-8 plies)
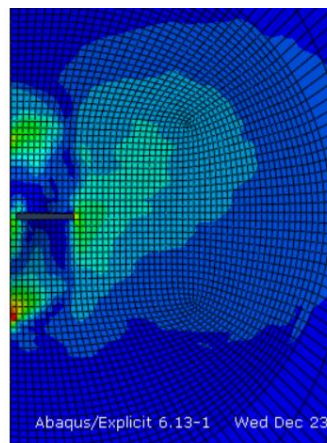
Figure 9.29: fibre damage on first pre-preg lamina

- **Comparison: Central Impact – Near-Edge Impact**

A comparison between Central and Near-Edge impact simulations can help in a better understanding of this two different events.

First of all, maximum displacements are different (Figure 9.30): Central impacted specimen shows a deformation along z axis smaller than for near-edge impact due to surrounding material contributing to load response.

Cohesive layers damages add another interesting parameter to this comparison. Looking at same cohesive layer level, it looks like Near-Edge impact could cause less damage than central one. But a more attentive analysis, Near-Edge impact creates a damage that could be compared to only one lobe of the 'peanut' delamination in the central impacted specimen. Therefore, it is worth a comparison between these two areas: in Near-Edge impacts, that area is wider than the corresponding one on a central impact damage. This underlines one more time the more effectiveness of Near-Edge impacts compared to Central ones.

Another detail, worth to notice, is delamination size growth through the thickness direction. For Near-Edge impacted specimens, delamination size grows form the first cohesive layer to the last one emphasizing more specimen flexibility, due to boundary conditions.
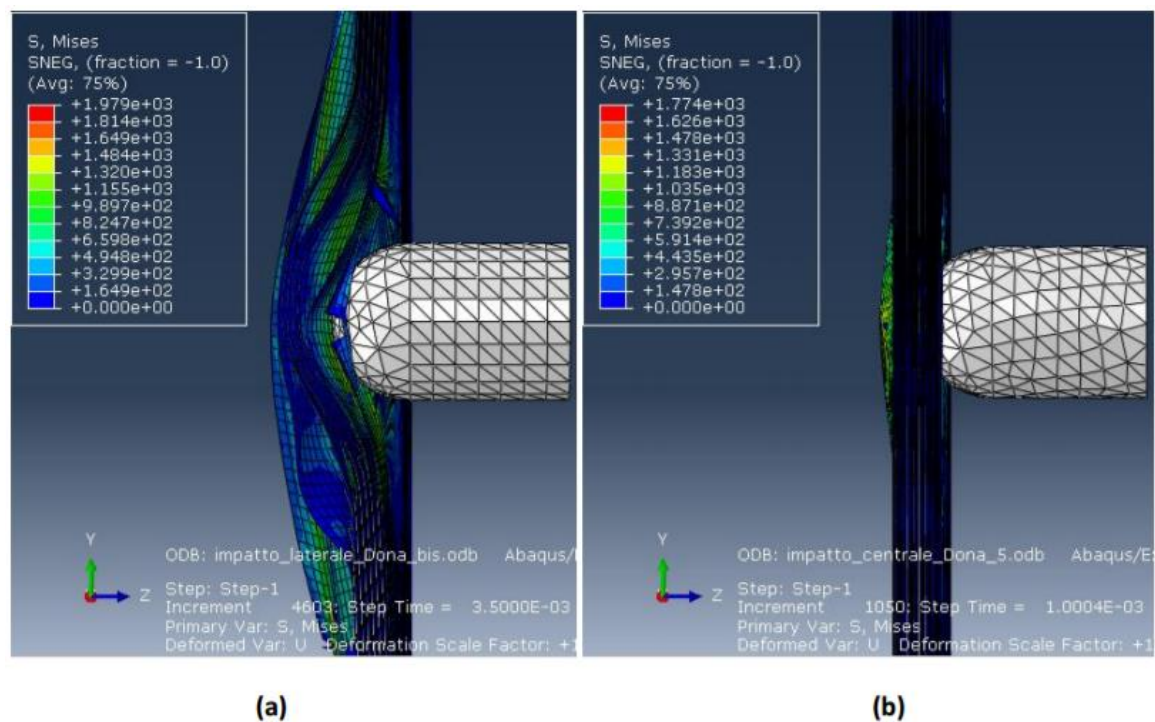
Figure 9.30: Max Displacement(a. NE impact, b. CI)
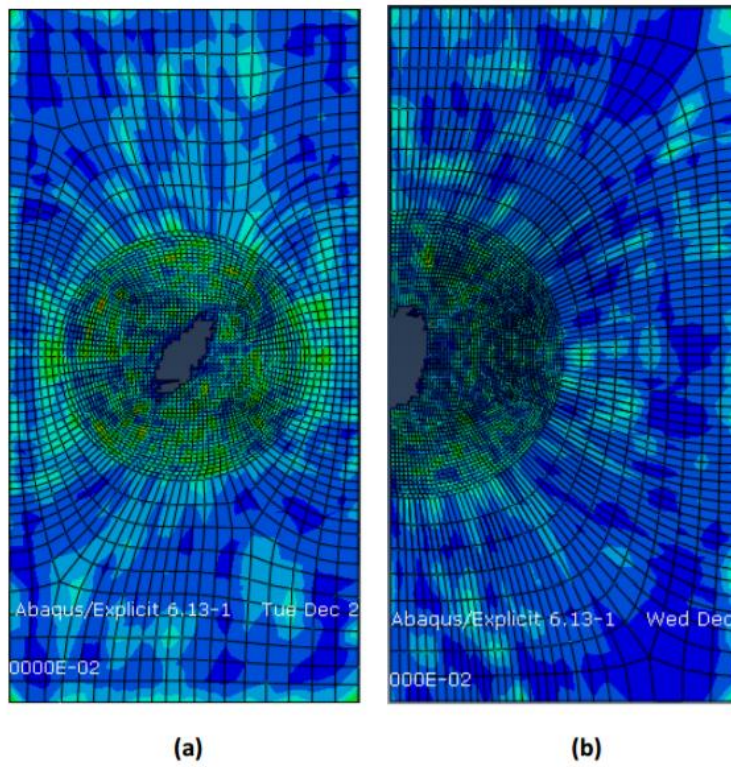
Figure 9.31: cohesive layer 1 damage (a. CI, b. NE)
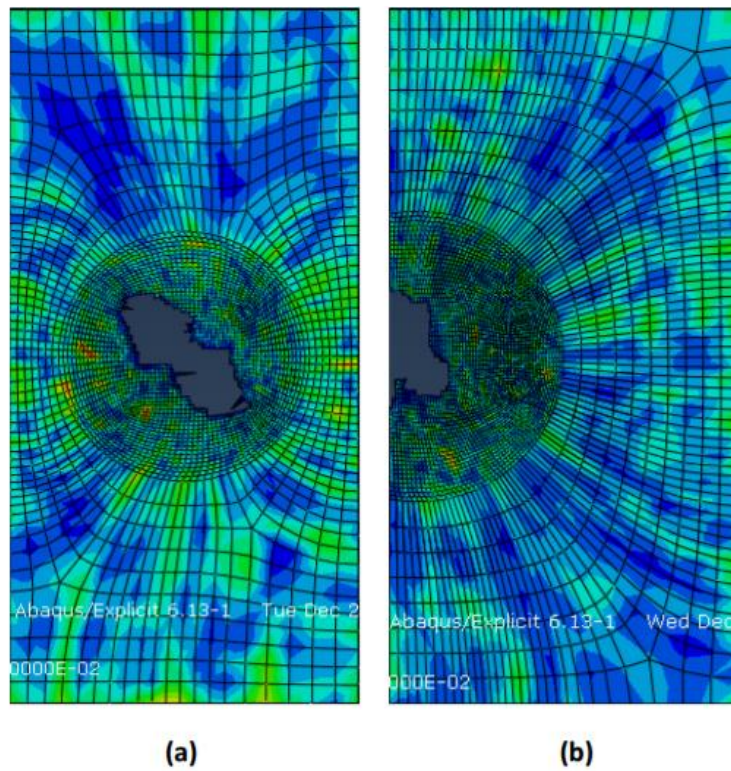
Figure 9.32: Cohesive layer 2 damage (a. CI, b. NE)
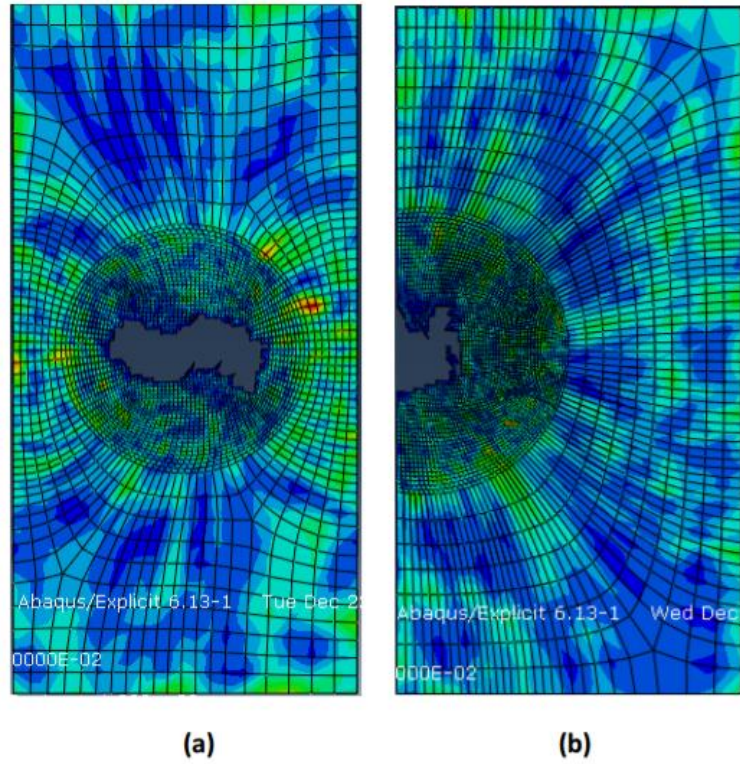
Figure 9.33: cohesive layer 3 damage (a. CI, b. NE)
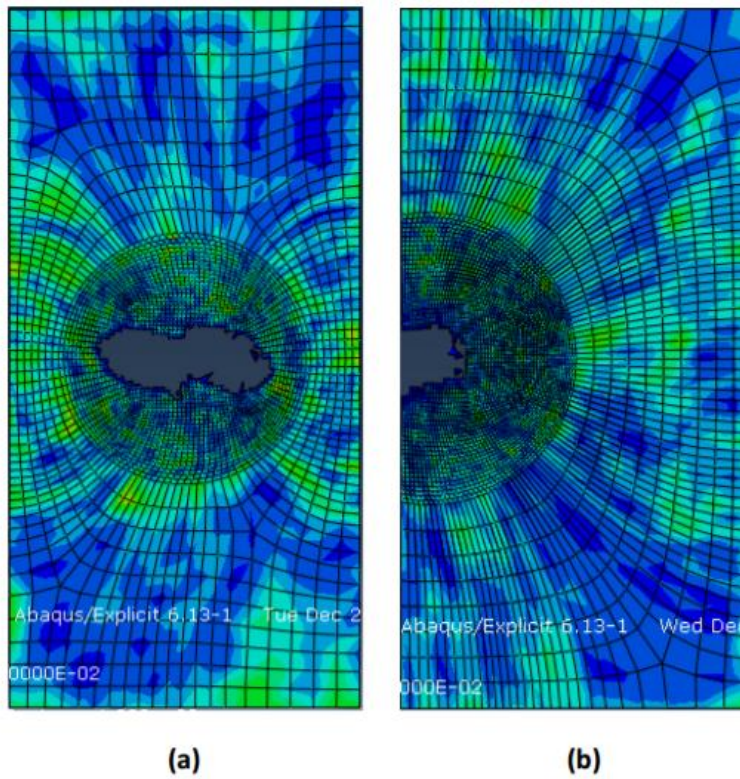
Figure 9.34: *cohesive layer 4 damage (a. CI, b. NE)*
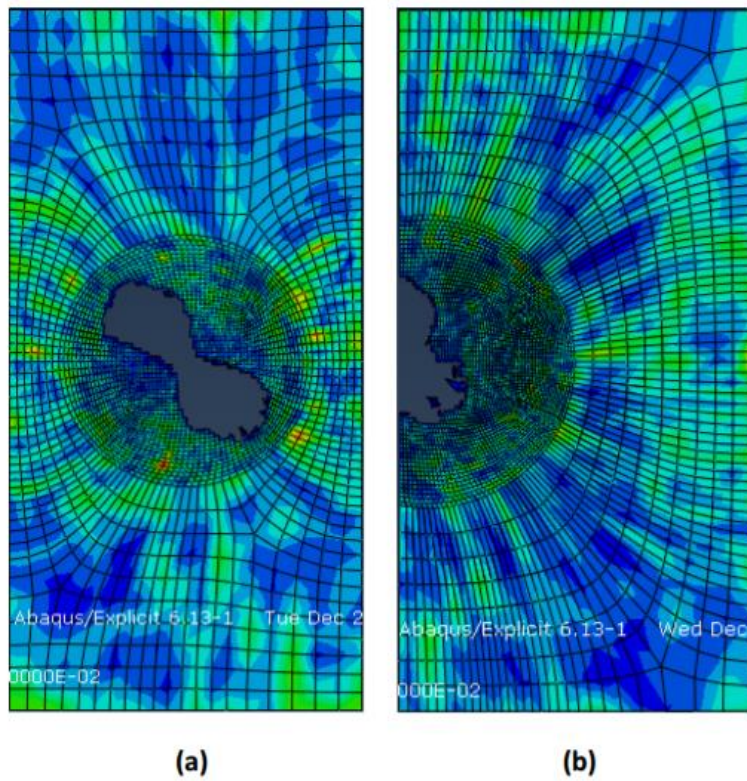
Figure 9.35: cohesive layer 5 damage (a. CI, b. NE)
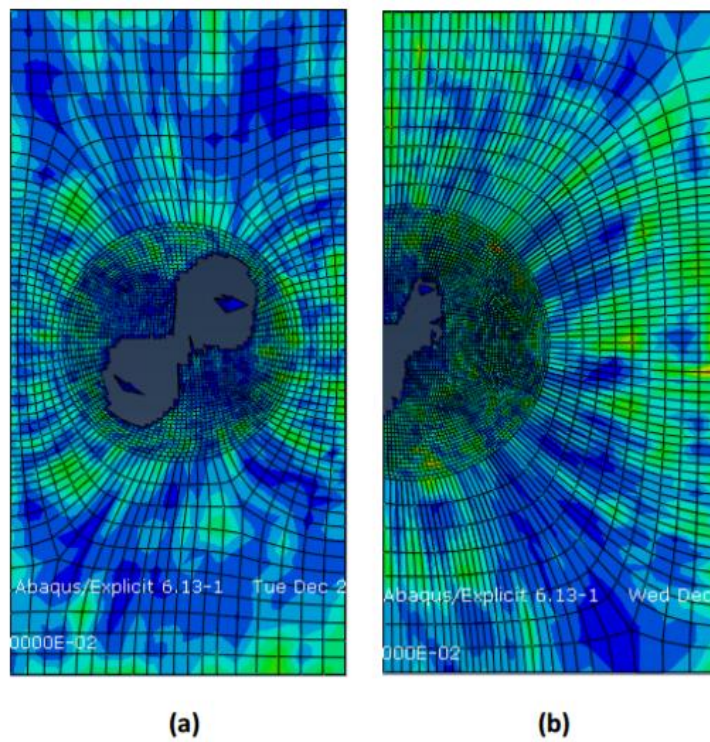
Figure 9.36: cohesive layer 6 damage (a. CI, b. NE)
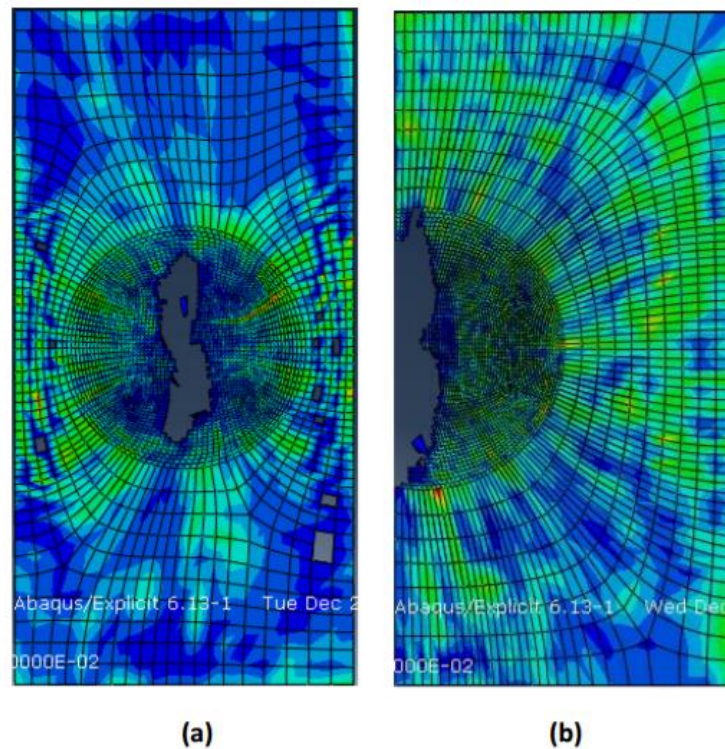
Figure 9.37: cohesive layer 7 damage (a. CI, b. NE)

9.2 FML developed model

For FML material impact model, materials described in chapter 7 have been taken into account. Specimens dimensions are different from the QSI experimental campaign carried out at TU Delft: 140x30 mm big specimens were modelled in order to be able to implement also compression after impact step in future simulations. Therefore, the necessity to have specimens dimensions in accordance with [8.10].

As for the previous model, cohesive elements were used in between fabric pre-preg layers.

Four different models were realised (Figure 9.38):

(a) 12 Carbon/Epoxy fabric and 11 cohesive regions (as No-Metal);
(b) 2 external Al foils, 8 Crbon fabrics and 9 cohesive regions (as EXT);
(c) 2 Al foils in the middle, 8 composite plies and 9 cohesive layers (as MID);
(d) 2 Al laminates in an intermediate potision compared to previous configurations, 8 carbon/epoxy and 9 cohesive layers.
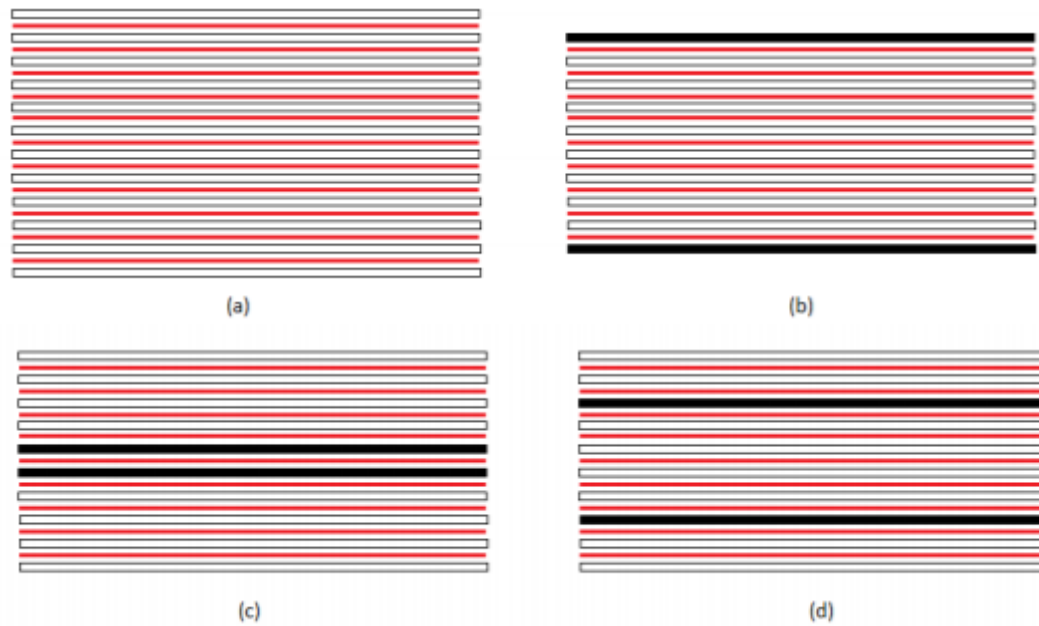
Figure 9.38: Schematic representation of FML FE Model (Black, Al layers; Red, cohesive layers; White, carbon/epoxy fabric)

For an easier dissertation, reference system has been chosen like showed in Figure 9.39; therefore, plies numerations starts from the first lamina on the upper part of each specimen.
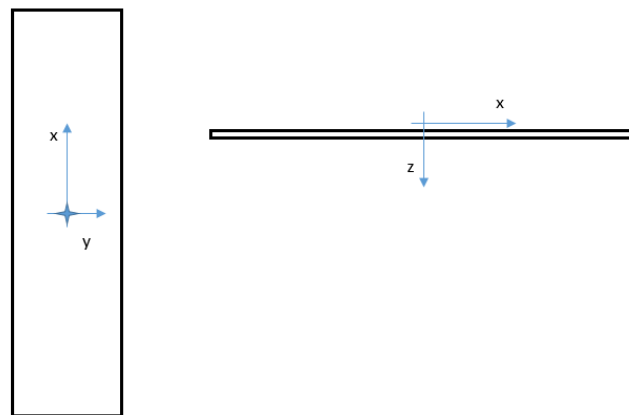
Figure 9.39: FML FE Model reference system

9.2.1 Impactor geometry and characteristics

As in the previous model, impactor was modelled as a steel cylinder with a 7 mm diameter hemispherical end (Figure 9.40). Impact energy was set at 10 J, with an impactor mass of 0.8 kg and velocity of 5 m/s.

Figure 9.40: impactor model

9.2.2 Laminate geometry and boundary conditions

No-Metal specimen thickness was of 2.73 mm while others specimens were 2.62 mm thick.

Implemented materials are described in chapter 7. Cohesive characteristics are reported in the following table (Table 9.4).

Table 9.4: cohesive elements characteristics

Cohesive Strengths		Fracture Energies		Penalty stiffness values	
σ_n^0	50 MPa	G_{I_C}	0.28 N/mm	K_{nn}	3000 MPa/mm
σ_s^0	30 MPa	G_{II_C}	0.79 N/mm	K_{ss}	1200 MPa/mm
σ_t^0	30 MPa	G_{III_C}	0.79 N/mm	K_{tt}	1200 MPa/mm

Specimens were fixed only along short edges (Figure 9.41).
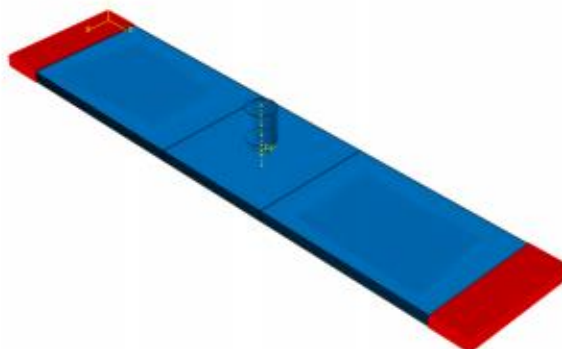
Figure 9.41: Boundary conditions (red edges clamped)

9.2.3 Mesh

Pre-preg plies were discretized with solid Continuum Shell Elements while SCR8 element (solid element) was used for Al and cohesive layers.

Mesh size has been defined in order to have a finer mesh in the central part of specimens where the impact takes place. The in-plane dimensions of the elements in this zone are 1 mm x 1 mm, while in further zones a rarer discretization has been used (2.5 mm x 1 mm). The cohesive region has been meshed in a finer way to obtain a smoother stress distribution (0.2 mm x 0.2 mm in the finer spacing zone, 2.5 mm x 0.2 mm in other zones). COH3D8 element have been chosen.

Impactor elements, being modelled as a rigid body, have not be set because no deformations and no stresses are evaluated for this. Concerning its interaction with the impacted surface an approximated friction coefficient of 0.3 has been used and it has been necessary to impose a "hard" contact to avoid the penetration of the target. Surface-to-surface constraints have been employed to tie cohesive and laminates interfaces due to unmatched meshes.

9.2.4 Results

In the following pictures, main simulations results are reported.

In Figure 9.42-9.52, No-Metal specimen simulation results are showed. Maximum deformation is reached (5.9 mm) before 2 ms of simulation; thereafter the impactor moves back, starting the unloading phase. Von Mises stress distribution in the first cohesive region is presented; deletion of damaged elements occurs when damage parameter reaches value equal to 1.
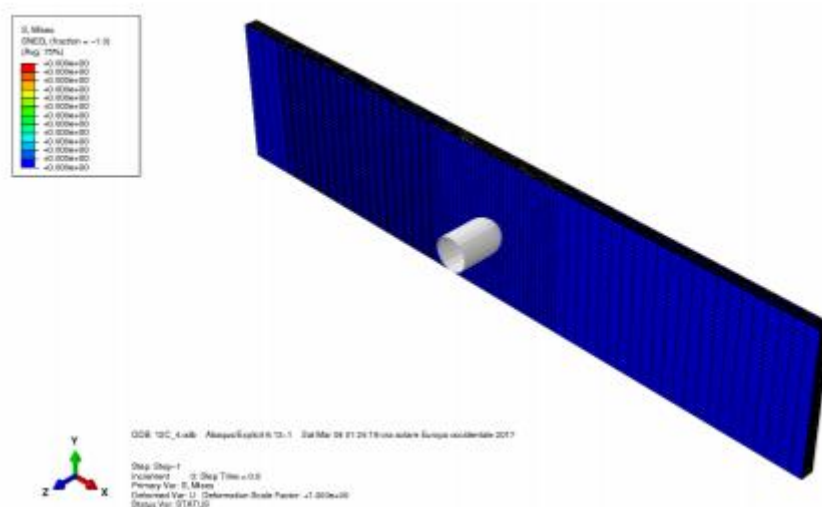
Figure 9.42: No-Metal Model
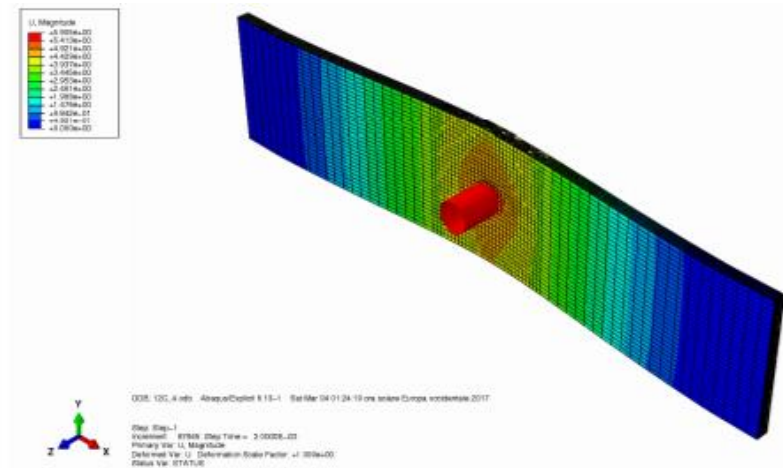
Figure 9.43: Max deformation for No-Metal specimen

(a)

(b)

(c)

(d)

(e)
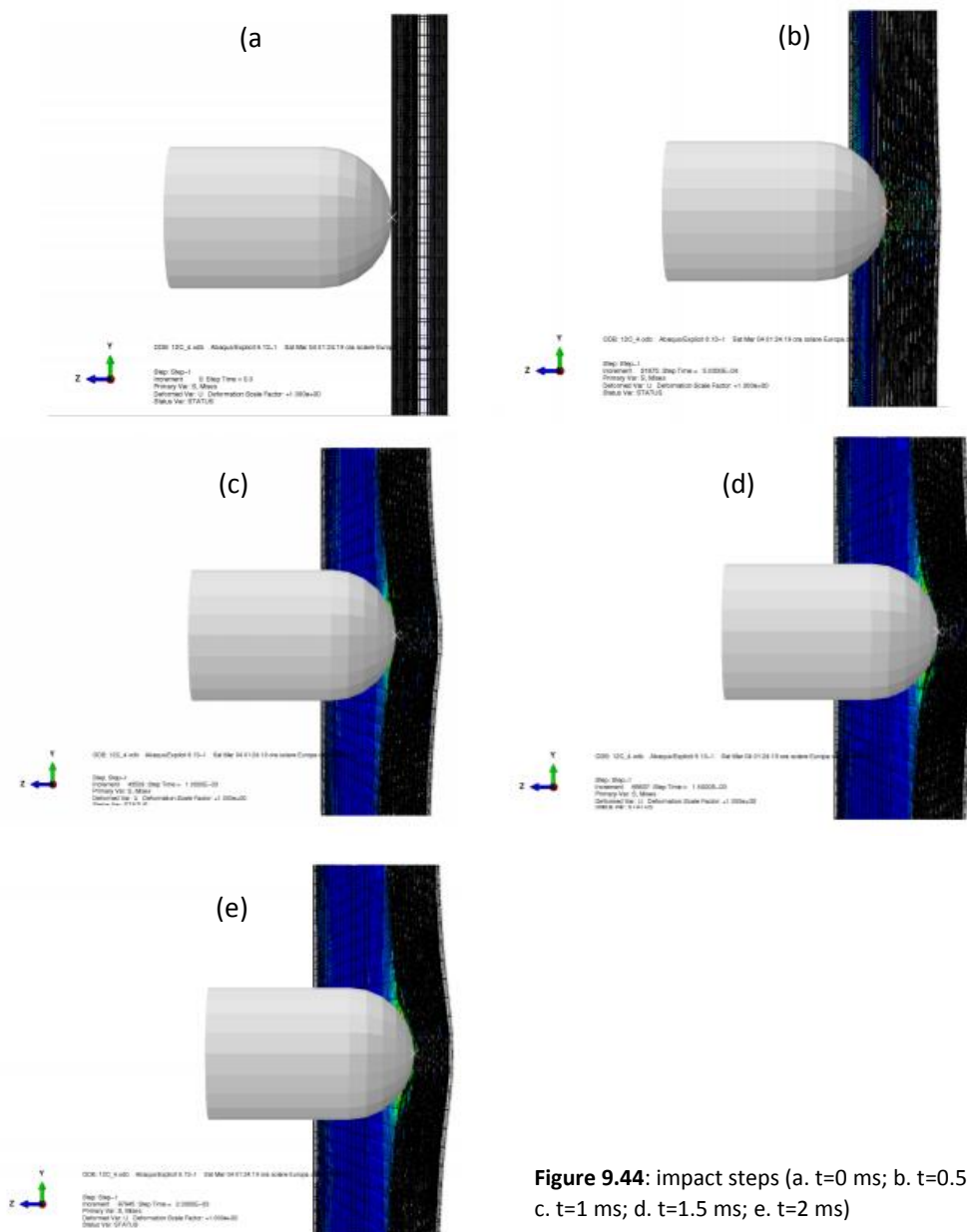
Figure 9.44: impact steps (a. t=0 ms; b. t=0.5 ms; c. t=1 ms; d. t=1.5 ms; e. t=2 ms)
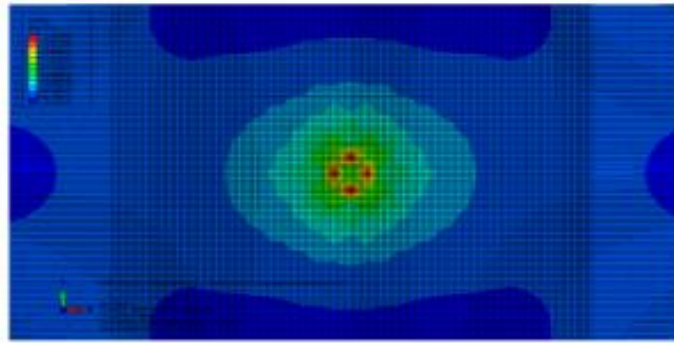
Figure 9.45: Von Mises stresses in cohesive first layer
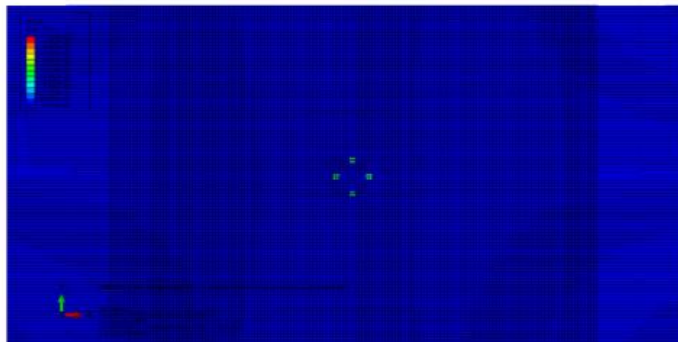
Figure 9.46: Damage parameter (D) at t=0.5 ms
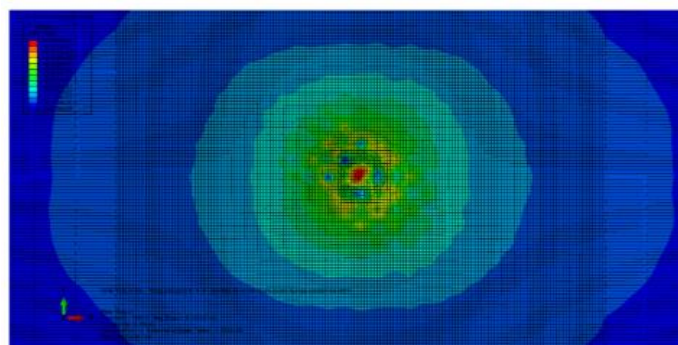
Figure 9.47: Stress distribution first cohesive layer at t=0.85 ms
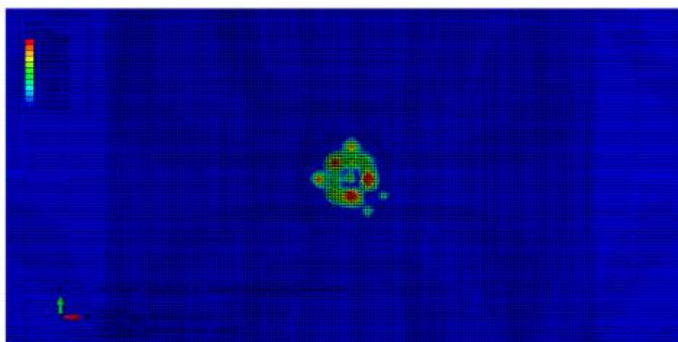
Figure 9.48: Damage parameter at t=0.85 ms
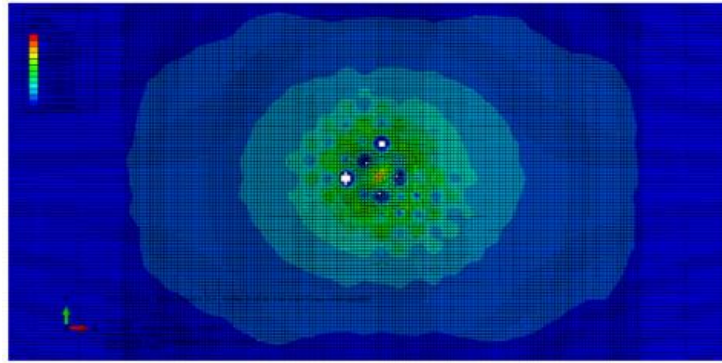
Figure 9.49: Stress distribution cohesive layer 1, at t=0.9 ms
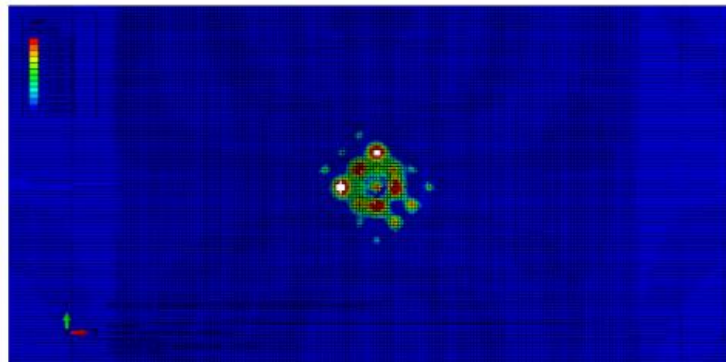
Figure 9.50: Damage parameter cohesive layer 1, at t= 0.9 ms
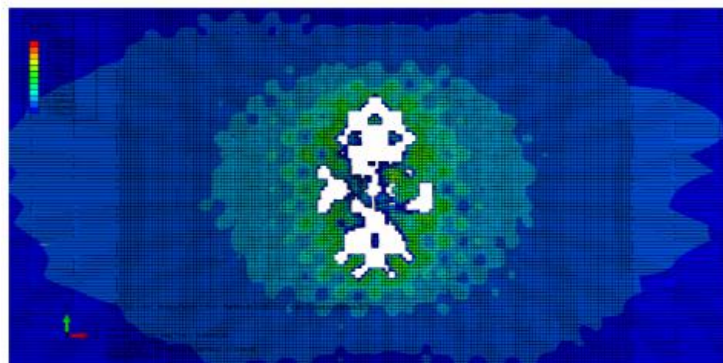
Figure 9.51: Stress distribution cohesive layer 1, at t= 2ms
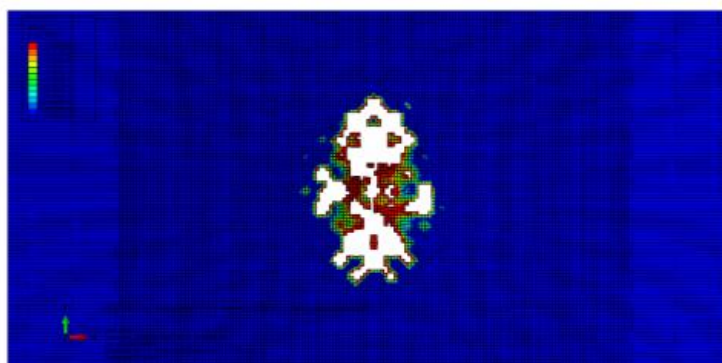
Figure 9.52: Damage parameter cohesive layer 1, at t=2 ms

In the following pictures (Figure 9.53-9.62) stresses in pre-preg plies and damaged zones on cohesive layers are presented. Hashin damage criterion is applied for pre-preg layers. In Cohesive layer 4, some cohesive elements are damages but not deleted: this is because damage was not reached in the whole element. The central part of these regions results damaged simulating matrix cracks caused by compressive damage.
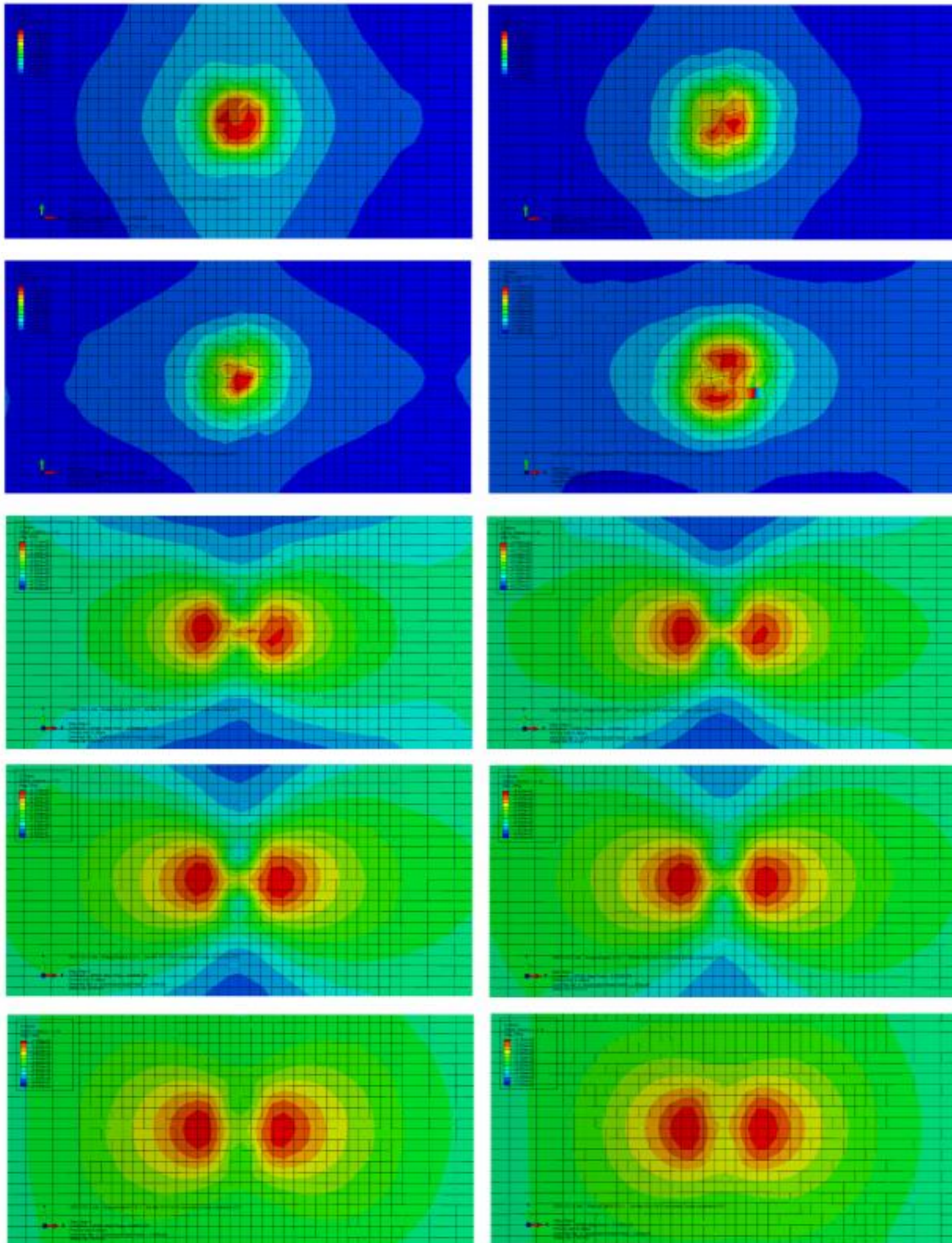
Figure 9.53: No-Metal simulation **-** Pre-preg layers, Von Mises stresses (No-Metal specimen)
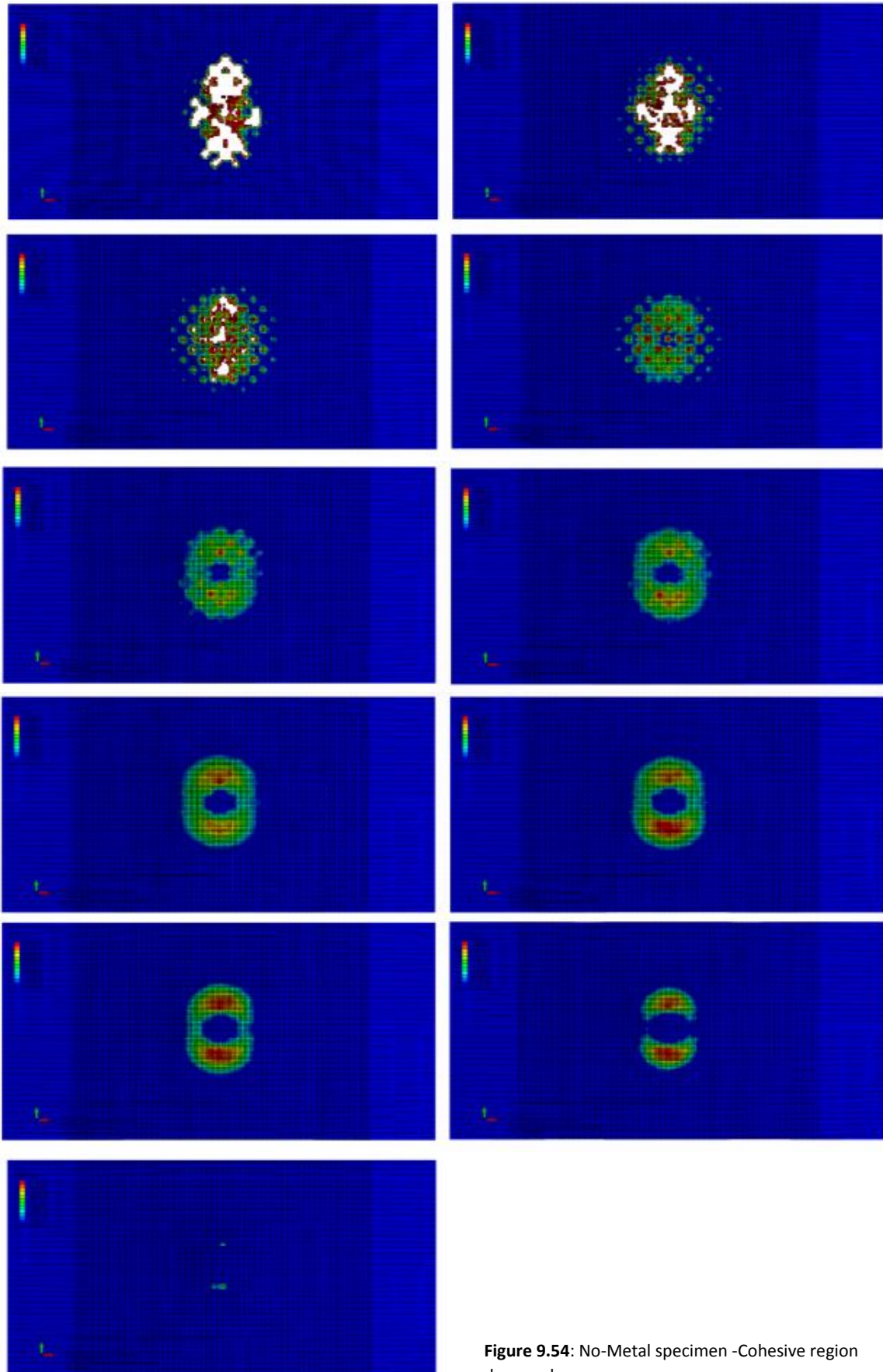
Figure 9.54: No-Metal specimen -Cohesive region damaged zone
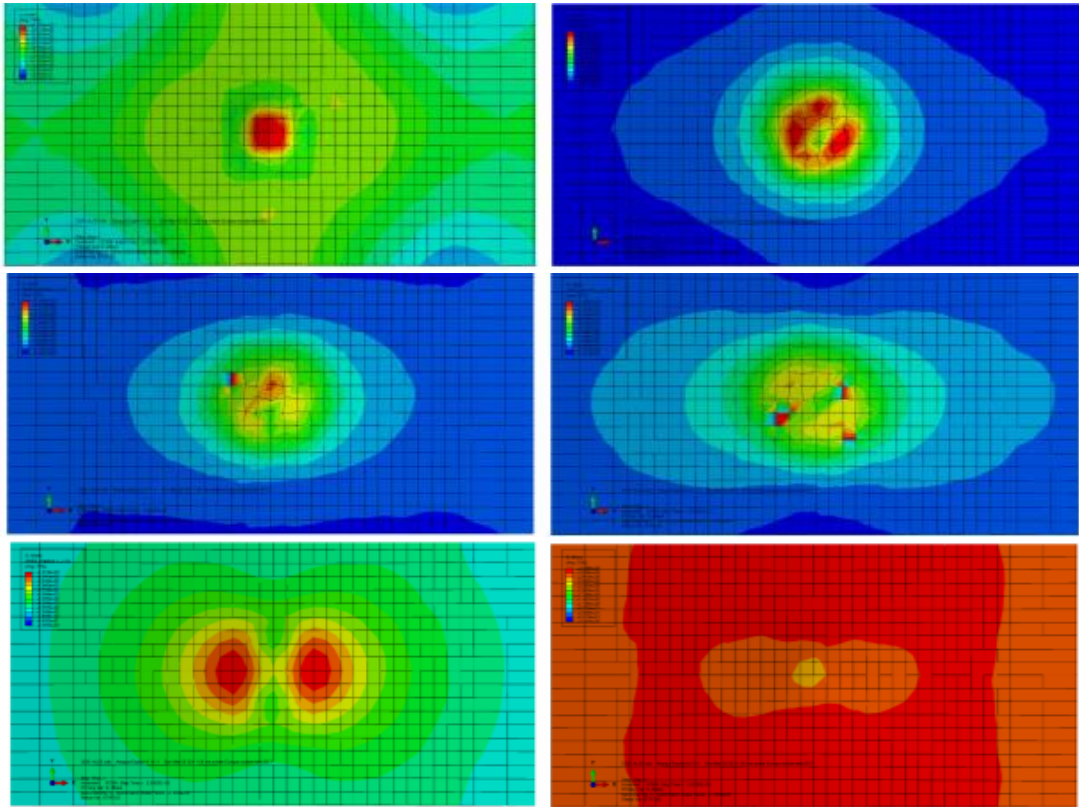
Figure 9.55: EXT specimen test (from left to right and from top to the bottom: Al layer 1, pre-preg layers 1-2-3-4, Al layer at the bottom of the specimen)
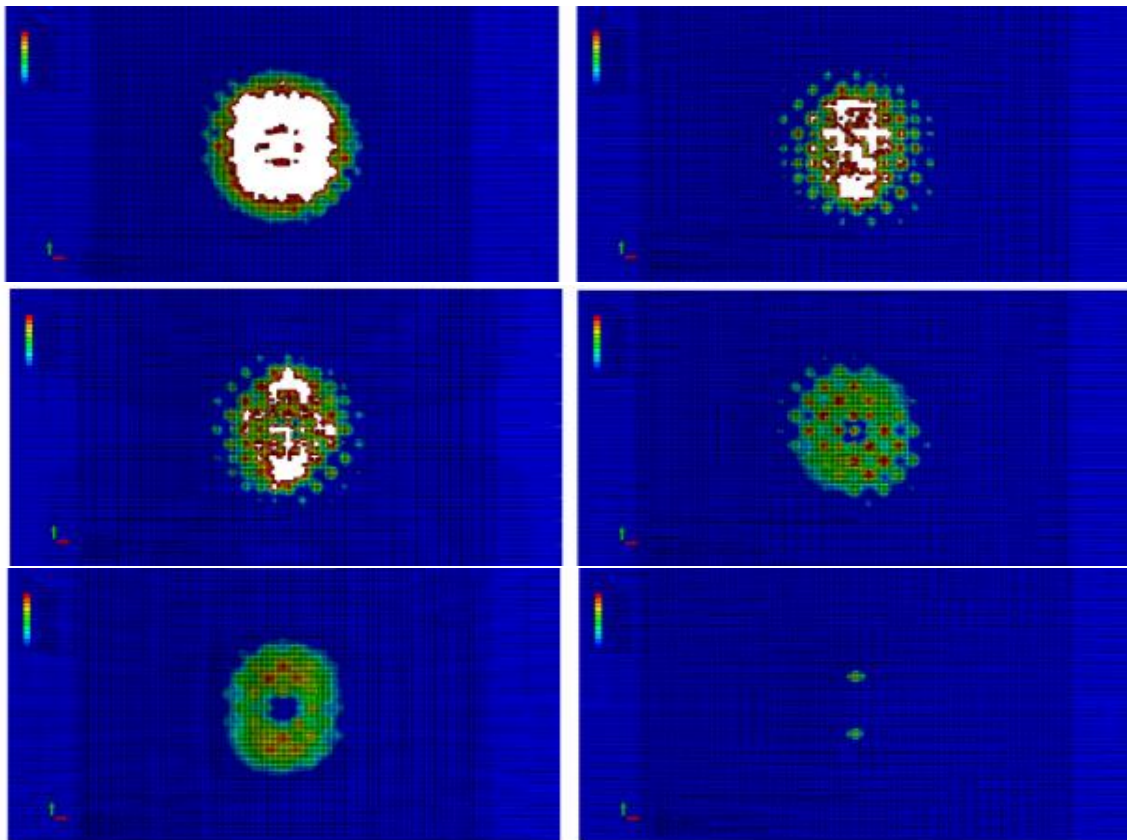
Figure 9.56: EXT simulation - Cohesive layers damaged zones
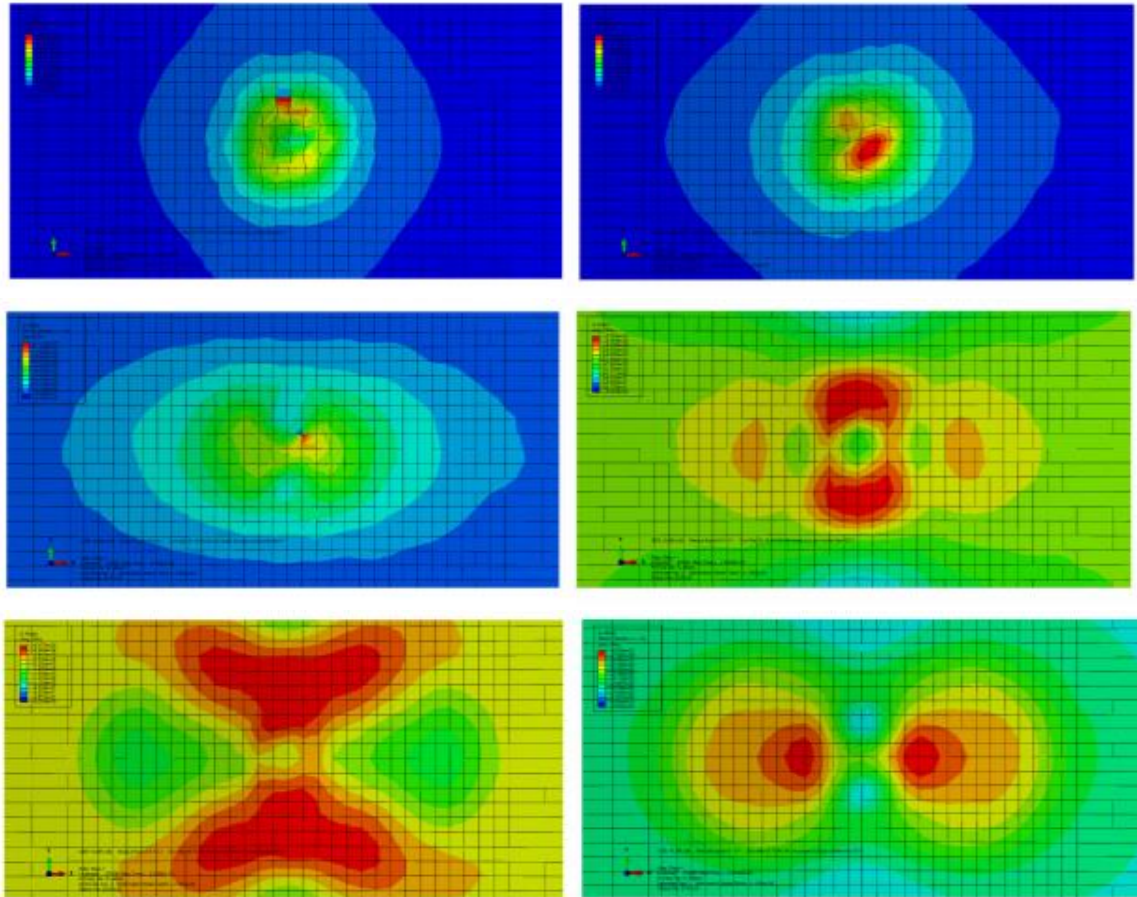
Figure 9.57: MID specimen simulation (from left to right and from top to the bottom: pre-preg layers 1-2-4, Al layers 1-2, pre-preg layer 7) Von Mises stresses
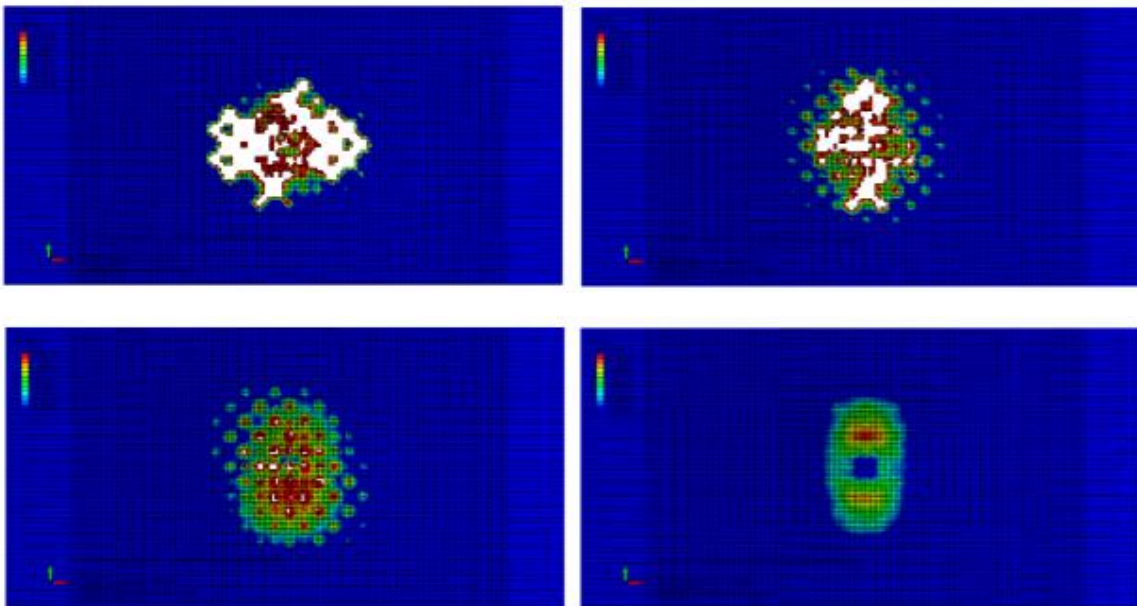
Figure 9.58: MID specimen – cohesive damaged zone layers 1-2-3-4
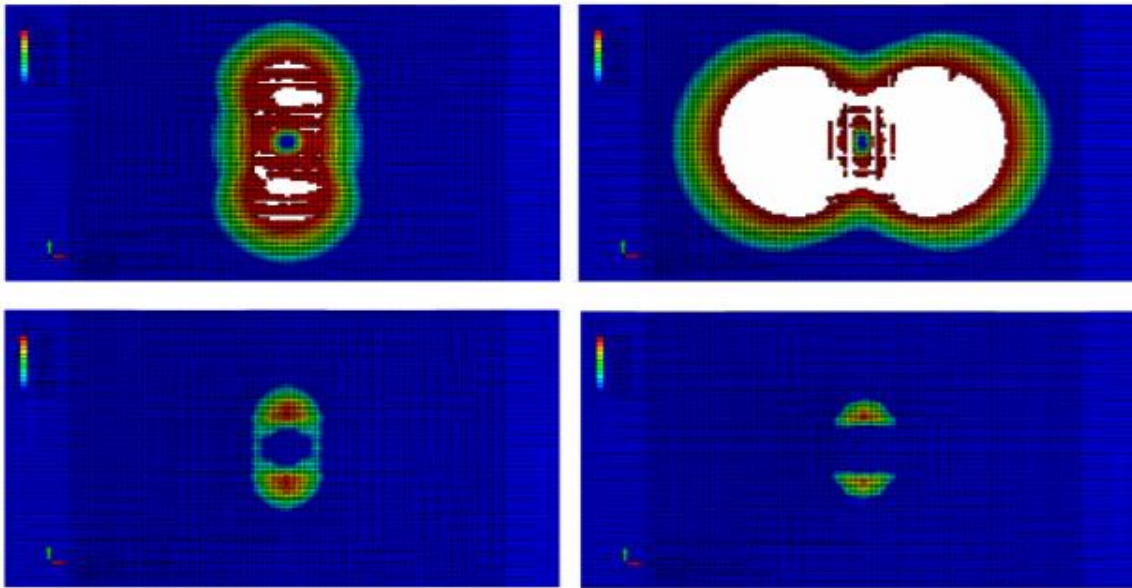
Figure 9.59: MID specimen – cohesive damaged zone layers 5-6-7-9
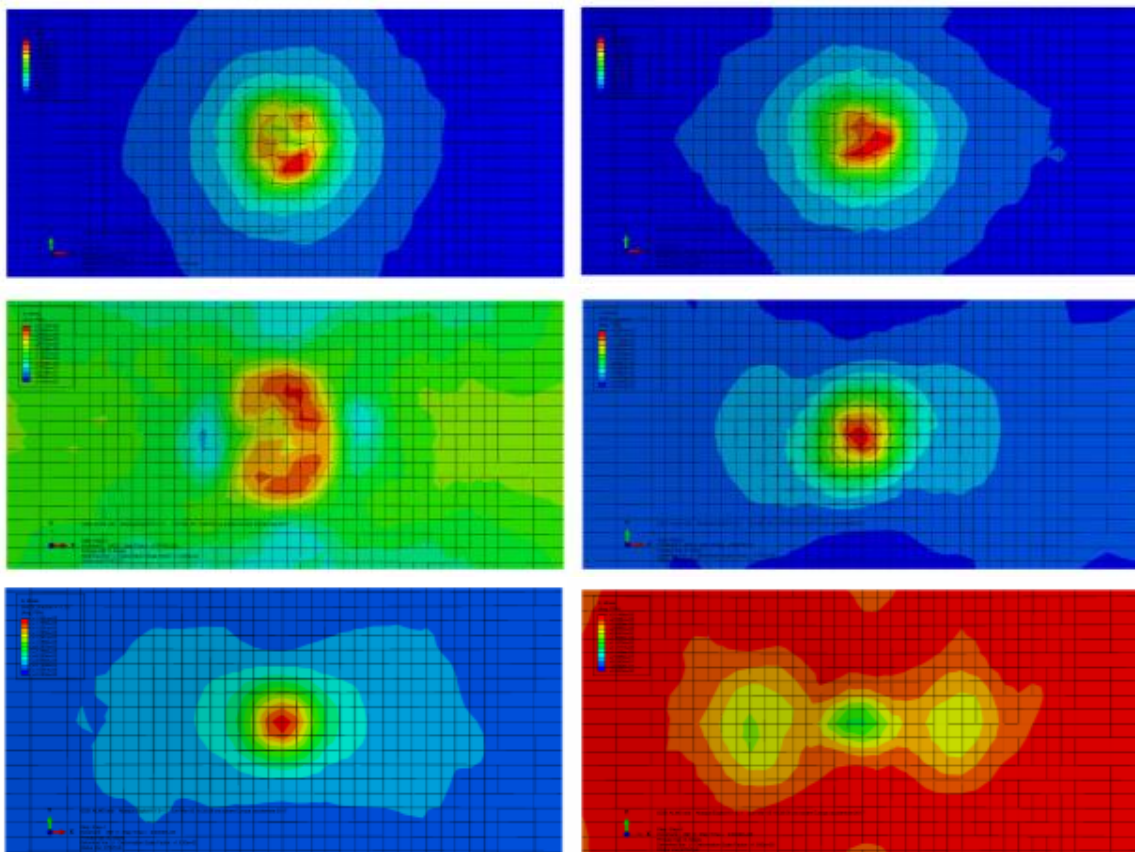
Figure 9.60: INT specimen Von Mises stresses (from left to right and from the top to the bottom, pre-preg layers 1-2, Al layer 1, pre-preg layers 4-6, Al layer 8)
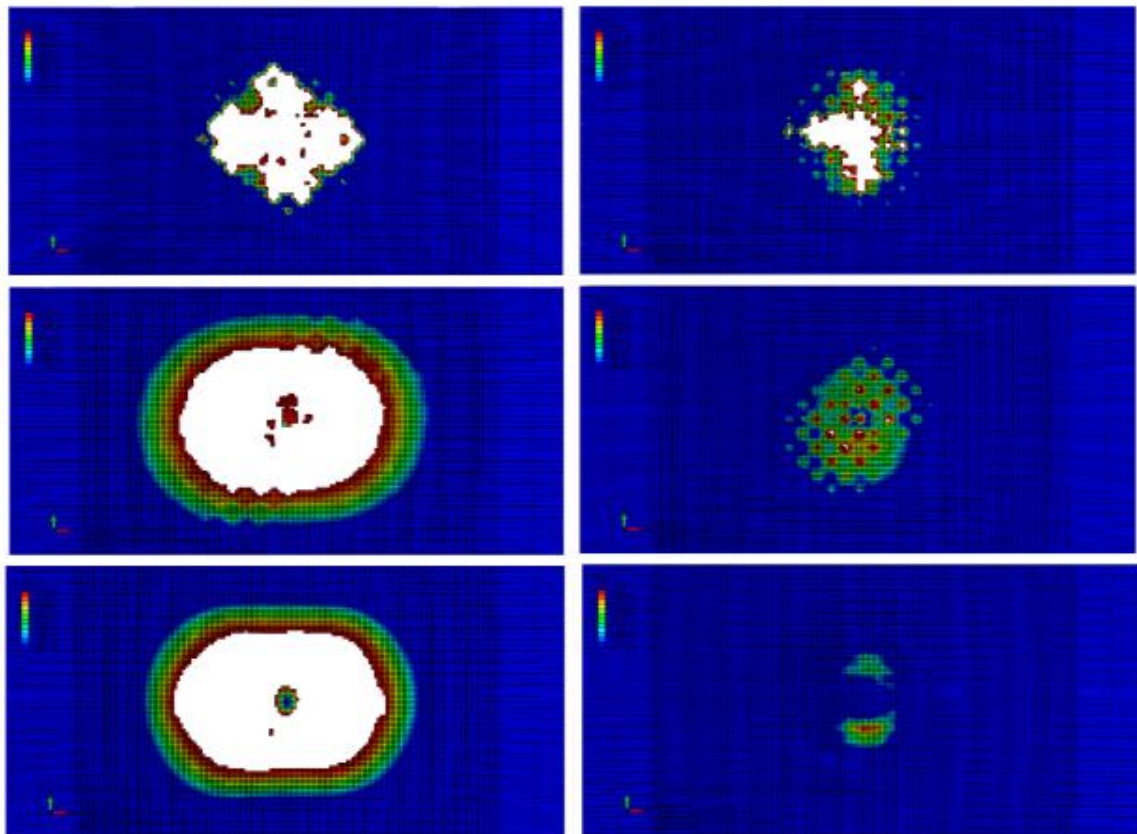
Figure 9.61: INT specimen cohesive demaged zone (layers 1-2-3-4-8-9)

In Figure 9.55-9.56 EXT material simulation results are reported (Von Mises stresses and cohesive damages zone). Al layers behaviour is ruled by plasticity, clearly evident looking at lower peak values. The last Al foil is not plastically deformed as the one impacted, but flexure stresses are wider spread. Cohesive region 1 presents a delaminated squared shape area, while a more irregular delamination and larger damaged areas can be identified in region 3. Totally failed areas decrease in dimension moving away from the impacted ply, through the thickness direction.

MID specimen results are showed in Figure 9.57-9.59. Stress distribution is strongly different between pre-preg layer 4 and close Al foil. Wide delamination in cohesive region 5 may be the consequence of this difference. In this analysis the non-deleted elements corresponding to damage parameter higher than 0.9, are considered totally failed. Same assumption could be made for lamina 6 and 7.

INT material is presented in Figure 9.60-9.61. Al layer 8 shows a large propagation of stresses as pre-preg layer under Al 3. Cohesive layers show quite wide delaminated area with a rectangular shape.

9.3 Overall discussion

Main FE Models developed during Author's PhD research were presented.

The first one was a preliminary analysis to understand carbon/epoxy simulation characteristics under impact loads: cohesive elements were implemented in order to be able to check plies interface damages under quite low loads, which could not create any fibre damage. This model was quite reliable: only few numerical instabilities that created an unpleasant visualization of the results, but had no influence on main material behaviour.

All points came out from this first FE Model were taken into account in a more accurate simulation. Different kinds of composites were implemented starting to add metal layers into a carbon/epoxy stacking sequence. Fibre Metal Laminate were, therefore, simulated as well as a pure 'classical' composite. Results showed a really interesting influence of material interface integrity to low energy impacts: wide damaged areas were obtained on cohesive layers, exhibiting plies interfaces weakness.

Noticeable is that each damaged cohesive layer showed an orientation that followed lower pre-preg layer: in the first model, pre-preg layers modelling unidirectional plies, delaminations had a 'peanut' shape oriented as lower ply and that is experimentally proved. In the second model, due to the use of fabric pre-pregs, delaminations resulted rectangular shaped (following fibres, both orthogonally and transversally oriented).

This behaviour, combined with realistic stress values and distributions, verify developed models reliability.

References

[9.1] Abaqus 6.13 user manual

[9.2] A. Khennane, 'Introduction to Finite Element Analysis Using MATLAB® and Abaqus', CRC Press, 2013

[9.3] Luca Boni, 'Modello numerico per la valutazione del comportamento di pannelli irrigiditi in materiali compositi soggetti ad impatto', 2010

[9.4] Z. Hashin, 'Failure Criteria for Unidirectional Fiber Composites', 1980

[9.5] C.G. Davila, P.P. Camanho, A. Turon, 'Effective Simulation of Delamination in Aeronautical Structures Using Shells and Cohesive Elements'.

[9.6] E.V: Gonzalez, P. Maimi, P.P. Camanho, A.Turon, J.A. Mayugo, 'Simulation of drop-weight impact and compression after impact tests on composite laminates, Composite Structures, 2012.

[9.7] C.G. Davila, P.P. Camanho, C.A. Rose, Failure criteria for FRP laminates, Journal of composite materials, 2007.

[9.8] S. Abrate, 'Impact on laminated composite materials,

[9.9] Barbero!

[9.10] ASTM 6641

Conclusions and future research

Nowadays, aircraft are designed to bear all range of impacts during operational life but there still is a small knowledge on how these materials respond: design standards, in fact, envisage high safety factors, which reduce the proper application of advanced materials, such as composites.

Aircrafts structures are exposed to many different causes of impact events that could have different energies, velocities and location. Damages that could result from these impacts can lead to brittle and sudden failure, up to a catastrophic event. Therefore, it is important to understand composite characteristics against this threat, in order to be able to design safer and lighter structures.

One of the most dangerous impact kind is the Low Velocity Impact: in fact, this may cause no or feeble damage on hit surface (which could be easily missed during normal visual aircraft inspection) but quite wide inner detriment. The latter could deeply influence material characteristics leading to unsafe operative conditions.

This threat was widely discussed in the present work trying to analyse it from experimental and numerical points of view.

Main work focused on carbon/epoxy impact damage tolerance: two experimental campaigns were conducted on cross-ply laminate, involving different thicknesses and impact energies. Purpose was to identify low energy impact influence on compressive residual strength of a carbon/epoxy laminate depending on material thickness and impact locations.

By means of these experimental tests it was proved that even a low energy impact, which does not cause evidence on laminate surface, can result in a not negligible reduction of compressive residual strength. Moreover, a near-edge impact resulted in a higher reduction, stressing impact location importance. This acquires even more relevance when it comes to thinking how more common are near-edge impact on an airplane, compared to central ones.

It was also proved that not every low energy influences material characteristics: there is an energy threshold under which, even a damage was created, this is irrelevant (compressive residual strength remains under material data scatter). This threshold depends on composite characteristics, laminate stacking sequence and thickness.

It was, therefore, necessary to figure out which meliorations were possible to improve composite impact resistance. Thanks to a collaboration between Forlì research group MaSTeR Lab and Structure Integrity and Composites group at Aerospace Engineering Faculty of TU Delft, it was possible to start a research on Fibre Metal Laminates. This composite has been developed and studied at TU Delft, in collaboration with some of the bigger airplanes builders, and shows good properties, combining metal foils and composite plies advantages.

A Quasi Static Indentation experimental campaign was conducted on four different laminate: they were made of carbon/epoxy fabric and Aluminium 2024 T3 foils, which were located in different position inside the stacking sequence. This led to an evaluation of Al layers position influence on material indentation resistance. Results showed that a carbon/epoxy laminate, reinforced with Al layers on the outer part, has a better behaviour under indentation loads due to a more stable failure mode and a higher resistance. Therefore, this Al location could led to a better impact behaviour (it is, in fact, proved in literature that accordance between Quasi Static Indentation and Low Velocity Impact tests results). Moreover, an external Al layer can give more chances in impact individuation due to plastically deformation.

A numerical investigation took place as well. Using Abaqus software, two models were developed: the first one was intended as a preliminary analysis of software reliability on impact event simulation results; in the second, Fibre Metal Laminate were modelled. In both of them, cohesive elements were used in order to simulate laminae interfaces damages and, therefore, delaminations. Good accordance with experimental tests was obtained and, therefore, models were considered reliable.

This research has shown that impacts are a real threat for composite materials and that near-edge impacts are even more dangerous. But there still are many knowledge gap that need to be fill up by further research. Many could be recommended:

- Individuation of energy thresholds for different laminate thicknesses, in order to correlate these two quantities;
- Use of different impactor shapes, in order to test different real objects impact;
- Multiple impact tests, in order to analyse which impact waves cooperation would be;
- Further FE analysis, implementing compression after impact test.

Acknowledgement

Appendix A: Carbon/Epoxy specimens dimensions

Dimensions of Carbon/Epoxy specimens used in experimental campaigns described in Chapter 5.

> **2.6 mm thick specimens**

Material A	n° measure	Width [mm]	Thickness [mm]	Length [mm]	Mass [g]
A0	1	29.65	2.93	-	-
	2	29.60	2.94	-	-
	3	29.60	2.93	-	-
	4	29.89	2.92	-	-
	5	29.83	2.91	-	-
	Mean value	29.71	2.93	139.67	-
	St. Deviation	0.14	0.01		
A1	1	29.61	2.93	-	-
	2	29.56	2.94	-	-
	3	29.54	2.93	-	-
	4	29.80	2.92	-	-
	5	29.80	2.91	-	-
	Mean value	29.66	2.93	139.66	18.2
	St. Deviation	0.13	0.01		
A2	1	29.63	2.95	-	-
	2	29.60	2.97	-	-
	3	29.50	2.97	-	-
	4	29.72	2.96	-	-
	5	29.67	2.97	-	-
	Mean value	29.62	2.96	139.7	18.3
	St. Deviation	0.08	0.01		
A3	1	29.75	2.92	-	-
	2	29.80	2.92	-	-
	3	29.74	2.94	-	-
	4	29.87	2.91	-	-
	5	29.92	2.90	-	-
	Mean value	29.82	2.92	139.69	18.3
	St. Deviation	0.08	0.01		
A4	1	29.99	2.57	-	-
	2	29.93	2.91	-	-
	3	29.83	2.99	-	-
	4	29.78	2.94	-	-
	5	29.75	2.96	-	-
	Mean value	29.86	2.87	139.66	18.0
	St. Deviation	0.10	0.17		
A5	1	30.03	2.63	-	-
	2	30.03	2.53	-	-
	3	30.00	2.89	-	-
	4	30.00	3.00	-	-
	5	29.99	2.95	-	-
	Mean value	30.01	2.80	138.29	17.5

	St. Deviation	0.02	0.21		
Material B	**n° measure**	**Width [mm]**	**Thickness [mm]**	**Length [mm]**	**Mass [g]**
B1	1	29.88	2.46	-	-
	2	29.90	2.43	-	-
	3	29.98	2.25	-	-
	4	29.98	2.30	-	-
	5	29.97	2.22	-	-
	Mean value	29.94	2.33	139.54	16.4
	St. Deviation	0.05	0.11		
B2	1	29.97	2.50	-	-
	2	29.91	2.74	-	-
	3	29.87	2.87	-	-
	4	29.85	2.80	-	-
	5	29.78	2.80	-	-
	Mean value	29.88	2.74	139.55	17.4
	St. Deviation	0.07	0.14		
B3	1	29.93	2.93	-	-
	2	29.95	2.91	-	-
	3	29.97	2.95	-	-
	4	29.98	2.78	-	-
	5	30.01	2.51	-	-
	Mean value	29.97	2.82	139.56	17.9
	St. Deviation	0.03	0.18		
B4	1	29.72	2.99	-	-
	2	29.73	3.00	-	-
	3	29.69	3.00	-	-
	4	29.95	3.00	-	-
	5	29.97	2.97	-	-
	Mean value	29.81	2.99	139.63	18.5
	St. Deviation	0.14	0.01		
B5	1	29.98	2.95	-	-
	2	29.97	2.96	-	-
	3	29.70	2.96	-	-
	4	29.60	2.97	-	-
	5	29.60	2.95	-	-
	Mean value	29.77	2.96	139.61	18.3
	St. Deviation	0.19	0.01		

Material C	**n° measure**	**Width [mm]**	**Thickness [mm]**	**Length [mm]**	**Mass [g]**
C1	1	29.58	2.65	-	-
	2	29.67	2.57	-	-
	3	29.68	2.94	-	-
	4	29.75	3.00	-	-
	5	29.90	2.98	-	-
	Mean value	29.72	2.83	139.68	17.4
	St. Deviation	0.12	0.20		
C2	1	29.99	2.55	-	-
	2	29.98	2.76	-	-
	3	29.89	2.95	-	-
	4	29.84	2.97	-	-
	5	29.87	2.97	-	-
	Mean value	29.91	2.84	139.67	18.1

	n° measure			
	St. Deviation	0.07	0.18		
C3	1	29.68	2.93	-	-
	2	29.75	2.93	-	-
	3	29.80	2.97	-	-
	4	29.89	2.81	-	-
	5	29.95	2.50	-	-
	Mean value	29.81	2.83	139.67	17.9
	St. Deviation	0.11	0.19		
C4	1	29.80	2.91	-	-
	2	29.74	2.93	-	-
	3	29.72	2.92	-	-
	4	29.92	2.91	-	-
	5	29.90	2.90	-	-
	Mean value	29.82	2.91	139.7	18.4
	St. Deviation	0.09	0.01		
C5	1	29.68	2.93	-	-
	2	29.69	2.95	-	-
	3	29.62	2.93	-	-
	4	29.84	2.93	-	-
	5	29.88	2.91	-	-
	Mean value	29.74	2.93	139.67	18.3
	St. Deviation	0.11	0.01		

Material D	**n° measure**	**Width [mm]**	**Thickness [mm]**	**Length [mm]**	**Mass [g]**
D1	1	29.76	2.43	-	-
	2	29.70	2.44	-	-
	3	29.68	2.39	-	-
	4	29.53	2.15	-	-
	5	29.33	2.18	-	-
	Mean value	29.60	2.32	139.59	14.6
	St. Deviation	0.17	0.14		
D2	1	29.48	2.57	-	-
	2	29.84	2.56	-	-
	3	29.88	2.85	-	-
	4	29.95	2.96	-	-
	5	29.99	2.92	-	-
	Mean value	29.83	2.77	138.16	17.2
	St. Deviation	0.20	0.19		
D3	1	29.86	2.43	-	-
	2	29.84	2.41	-	-
	3	29.82	2.44	-	-
	4	29.75	2.44	-	-
	5	29.80	2.41	-	-
	Mean value	29.81	2.43	139.6	15.3
	St. Deviation	0.04	0.02		
D4	1	29.47	2.56	-	-
	2	29.53	2.50	-	-
	3	29.60	2.85	-	-
	4	29.63	2.96	-	-
	5	29.74	2.91	-	-
	Mean value	29.59	2.76	138.05	17.2

	St. Deviation	0.10	0.21		
D5	1	29.84	2.40	-	-
	2	29.88	2.44	-	-
	3	29.90	2.51	-	-
	4	29.94	2.38	-	-
	5	29.00	2.20	-	-
	Mean value	29.71	2.39	139.69	15.4
	St. Deviation	0.40	0.12		

Material E	**n° measure**	**Width [mm]**	**Thickness [mm]**	**Length [mm]**	**Mass [g]**
E1	1	29.22	2.58	-	-
	2	29.38	2.52	-	-
	3	29.42	2.85	-	-
	4	29.68	2.95	-	-
	5	29.82	2.89	-	-
	Mean value	29.50	2.76	138.03	17
	St. Deviation	0.24	0.19		
E2	1	29.93	2.50	-	-
	2	29.87	2.80	-	-
	3	29.89	2.99	-	-
	4	29.84	2.95	-	-
	5	29.74	2.97	-	-
	Mean value	29.85	2.84	139.63	17.8
	St. Deviation	0.07	0.21		
E3	1	29.60	2.99	-	-
	2	29.84	2.94	-	-
	3	29.86	2.96	-	-
	4	29.93	2.66	-	-
	5	30.01	2.47	-	-
	Mean value	29.85	2.80	139.68	17.8
	St. Deviation	0.15	0.23		
E4	1	29.72	2.93	-	-
	2	29.80	2.93	-	-
	3	29.88	2.98	-	-
	4	29.94	2.75	-	-
	5	30.00	2.49	-	-
	Mean value	29.87	2.82	139.68	17.8
	St. Deviation	0.11	0.20		
E5	1	29.57	2.76	-	-
	2	29.67	2.80	-	-
	3	29.78	2.77	-	-
	4	29.85	2.75	-	-
	5	29.87	2.72	-	-
	Mean value	29.75	2.76	139.61	17.1
	St. Deviation	0.13	0.03		

Group A	Width [mm]	Thickness [mm]	Length [mm]	Mass [g]
Mean value	29.79	2.90	139.4	18.1
St. Uncertainty	0.04	0.02		

Group B	Width [mm]	Thickness [mm]	Length [mm]	Mass [g]
Mean value	29.87	2.77	139.578	17.7
St. Uncertainty	0.05	0.02		

Group C	Width [mm]	Thickness [mm]	Length [mm]	Mass [g]
Mean value	29.80	2.87	139.678	18.0
St. Uncertainty	0.05	0.03		

Group D	Width [mm]	Thickness [mm]	Length [mm]	Mass [g]
Mean value	29.71	2.53	139.018	15.9
St. Uncertainty	0.10	0.03		

Group E	Width [mm]	Thickness [mm]	Length [mm]	Mass [g]
Mean value	29.76	2.80	139.326	17.5
St. Uncertainty	0.07	0.03		

> **5.5 mm thick specimens**

Group A	n° measure	Width [mm]	Thickness [mm]	Length [mm]	Mass [g]
	1	30.10	5.345	-	-
	2	30.15	5.385	-	-
	3	30.00	5.440	-	-
A1	4	30.00	5.350	-	-
	5	29.95	5.380	-	-
	Mean value	30.04	5.380	140.05	32.8
	St. Deviation	0.08	0.038		
	1	30.05	5.410	-	-
	2	30.10	5.420	-	-
	3	30.10	5.400	-	-
A2	4	30.05	5.400	-	-
	5	30.05	5.450	-	-
	Mean value	30.07	5.416	140.00	33.7

	St. Deviation	0.03	0.021		
A3	1	30.05	5.440	-	-
	2	30.10	5.440	-	-
	3	30.05	5.390	-	-
	4	30.05	5.450	-	-
	5	30.05	5.450	-	-
	Mean value	30.06	5.434	140.05	33.7
	St. Deviation	0.02	0.025		
A4	1	30.05	5.430	-	-
	2	30.05	5.430	-	-
	3	30.10	5.440	-	-
	4	30.00	5.430	-	-
	5	30.00	5.450	-	-
	Mean value	30.04	5.436	139.90	33.8
	St. Deviation	0.04	0.009		
A5	1	30.05	5.410	-	-
	2	30.00	5.420	-	-
	3	30.05	5.410	-	-
	4	30.05	5.415	-	-
	5	30.05	5.455	-	-
	Mean value	30.04	5.422	139.90	33.8
	St. Deviation	0.02	0.019		
A6	1	30.10	5.425	-	-
	2	30.05	5.435	-	-
	3	30.05	5.500	-	-
	4	30.05	5.410	-	-
	5	30.00	5.410	-	-
	Mean value	30.05	5.436	139.85	33.8
	St. Deviation	0.04	0.037		

Group B	**n° measure**	**Width [mm]**	**Thickness [mm]**	**Length [mm]**	**Mass [g]**
B1	1	29.90	5.550	-	-
	2	30.00	5.570	-	-
	3	30.00	5.650	-	-
	4	30.00	5.550	-	-
	5	30.00	5.580	-	-
	Mean value	29.98	5.580	140.05	34.2
	St. Deviation	0.04	0.041		
B2	1	30.00	5.590	-	-
	2	30.05	5.680	-	-
	3	30.00	5.600	-	-
	4	30.00	5.630	-	-
	5	30.00	5.620	-	-
	Mean value	30.01	5.624	140.00	34.2
	St. Deviation	0.02	0.035		
B3	1	30.00	5.560	-	-
	2	30.00	5.580	-	-
	3	30.05	5.570	-	-
	4	30.05	5.550	-	-
	5	30.05	5.600	-	-
	Mean value	30.03	5.572	139.95	34.3

	n° measure	Width [mm]	Thickness [mm]	Length [mm]	Mass [g]
	St. Deviation	0.03	0.019		
B4	1	29.95	5.570	-	-
	2	30.00	5.610	-	-
	3	30.00	5.670	-	-
	4	30.00	5.590	-	-
	5	30.00	5.670	-	-
	Mean value	29.99	5.622	140.00	34.1
	St. Deviation	0.02	0.046		
B5	1	29.85	5.540	-	-
	2	29.95	5.530	-	-
	3	30.00	5.530	-	-
	4	30.00	5.550	-	-
	5	30.05	5.570	-	-
	Mean value	29.97	5.544	140.00	34.1
	St. Deviation	0.08	0.017		

Group C	n° measure	Width [mm]	Thickness [mm]	Length [mm]	Mass [g]
C1	1	29.95	5.560	-	-
	2	29.95	5.570	-	-
	3	29.95	5.680	-	-
	4	30.00	5.530	-	-
	5	30.00	5.560	-	-
	Mean value	29.97	5.580	140.00	34.2
	St. Deviation	0.03	0.058		
C2	1	30.05	5.490	-	-
	2	30.05	5.530	-	-
	3	30.05	5.610	-	-
	4	30.00	5.560	-	-
	5	30.05	5.550	-	-
	Mean value	30.04	5.548	139.95	34.0
	St. Deviation	0.02	0.044		
C3	1	30.00	5.550	-	-
	2	30.05	5.670	-	-
	3	30.05	5.580	-	-
	4	30.05	5.540	-	-
	5	30.10	5.660	-	-
	Mean value	30.05	5.600	140.05	34.1
	St. Deviation	0.04	0.061		
C4	1	30.10	5.670	-	-
	2	30.10	5.660	-	-
	3	30.05	5.530	-	-
	4	30.05	5.520	-	-
	5	30.10	5.560	-	-
	Mean value	30.08	5.588	140.05	34.2
	St. Deviation	0.03	0.072		
C5	1	30.05	5.550	-	-
	2	30.05	5.530	-	-
	3	30.05	5.530	-	-
	4	30.05	5.510	-	-
	5	30.05	5.580	-	-
	Mean value	30.05	5.540	140.00	34.2
	St. Deviation	0.00	0.026		

Group D	n° measure	Width [mm]	Thickness [mm]	Length [mm]	Mass [g]
D1	1	30.05	5.540	-	-
	2	30.05	5.500	-	-
	3	30.05	5.610	-	-
	4	30.05	5.530	-	-
	5	30.05	5.520	-	-
	Mean value	30.05	5.540	139.95	34.2
	St. Deviation	0.00	0.042		
D2	1	30.05	5.580	-	-
	2	30.05	5.550	-	-
	3	30.05	5.540	-	-
	4	30.05	5.510	-	-
	5	30.00	5.510	-	-
	Mean value	30.04	5.538	140.00	34.1
	St. Deviation	0.02	0.029		
D3	1	30.05	5.530	-	-
	2	30.05	5.470	-	-
	3	30.05	5.520	-	-
	4	30.05	5.540	-	-
	5	30.05	5.520	-	-
	Mean value	30.05	5.516	140.00	34.1
	St. Deviation	0.00	0.027		
D4	1	30.05	5.480	-	-
	2	30.05	5.450	-	-
	3	30.05	5.470	-	-
	4	30.05	5.510	-	-
	5	30.05	5.480	-	-
	Mean value	30.05	5.478	140.10	33.9
	St. Deviation	0.00	0.022		
D5	1	29.90	5.510	-	-
	2	29.95	5.580	-	-
	3	30.00	5.540	-	-
	4	30.05	5.560	-	-
	5	30.05	5.620	-	-
	Mean value	29.99	5.562	140.00	33.8
	St. Deviation	0.07	0.041		

Group E	n° measure	Width [mm]	Thickness [mm]	Length [mm]	Mass [g]
E1	1	30.00	5.420	-	-
	2	30.05	5.400	-	-
	3	30.05	5.390	-	-
	4	30.05	5.440	-	-
	5	30.05	5.430	-	-
	Mean value	30.04	5.416	140.00	33.8
	St. Deviation	0.02	0.021		
E2	1	30.05	5.430	-	-
	2	30.05	5.415	-	-
	3	30.05	5.400	-	-
	4	30.05	5.405	-	-
	5	30.05	5.420	-	-
	Mean value	30.05	5.414	139.95	33.9
	St. Deviation	0.00	0.012		

		Width	Thickness	Length	Mass
E3	1	30.05	5.410	-	-
	2	30.10	5.400	-	-
	3	30.05	5.410	-	-
	4	30.05	5.420	-	-
	5	30.05	5.420	-	-
	Mean value	30.06	5.412	140.00	33.8
	St. Deviation	0.02	0.008		
E4	1	30.00	5.380	-	-
	2	30.05	5.400	-	-
	3	30.10	5.390	-	-
	4	30.05	5.400	-	-
	5	30.05	5.420	-	-
	Mean value	30.05	5.398	140.00	33.8
	St. Deviation	0.04	0.015		
E5	1	30.01	5.400	-	-
	2	30.05	5.400	-	-
	3	30.05	5.360	-	-
	4	30.00	5.380	-	-
	5	29.95	5.400	-	-
	Mean value	30.01	5.388	139.85	33.5
	St. Deviation	0.04	0.018		

Group A	**Width [mm]**	**Thickness [mm]**	**Length [mm]**	**Mass [g]**
Mean value	30.05	5.42	139.96	33.60
St. Uncertainty	0.02	0.01		

Group B	**Width [mm]**	**Thickness [mm]**	**Length [mm]**	**Mass [g]**
Mean value	30.00	5.59	140.00	34.18
St. Uncertainty	0.02	0.02		

Group C	**Width [mm]**	**Thickness [mm]**	**Length [mm]**	**Mass [g]**
Mean value	30.04	5.57	140.01	34.14
St. Uncertainty	0.01	0.02		

Group D	**Width [mm]**	**Thickness [mm]**	**Length [mm]**	**Mass [g]**
Mean value	30.04	5.53	140.01	34.02
St. Uncertainty	0.01	0.01		

Group E	**Width [mm]**	**Thickness [mm]**	**Length [mm]**	**Mass [g]**
Mean value	30.04	5.41	139.96	33.76
St. Uncertainty	0.01	0.01		

- x -

Appendix B:
FML specimens dimensions

Dimensions of FML specimens used in experimental campaigns described in Chapter 7.

> **No-Metal specimens**

No-Metal	n° measure	Width [mm]	Thickness [mm]	Length [mm]	Mass [g]
Specimen 1	1	100.70	3.17	150.00	-
	2	100.65	3.16	150.30	-
	3	100.50	3.18	150.45	-
	4	100.30	3.12	-	-
	5	100.25	2.97	-	-
	6		3.18	-	-
	7		3.18	-	-
	Mean value	100.48	3.14	150.25	
	St. Deviation	0.20	0.08	0.23	
Specimen 2	1	100.70	3.16	150.50	-
	2	100.75	3.16	149.90	-
	3	100.95	3.18	149.85	-
	4	101.10	3.08	-	-
	5	101.25	2.95	-	-
	6		3.16	-	-
	7		3.16	-	-
	Mean value	100.95	3.12	150.08	68.67
	St. Deviation	0.23	0.08	0.36	
Specimen 3	1	99.00	3.03	149.35	-
	2	99.20	3.03	149.70	-
	3	99.45	3.03	150.35	-
	4	99.75	2.99	-	-
	5	99.95	2.86	-	-
	6		3.11	-	-
	7		2.87	-	-
	Mean value	99.47	2.99	149.80	64.78
	St. Deviation	0.39	0.09	0.51	

- xii -

> **EXT specimens**

EXT	n° measure	Width [mm]	Thickness [mm]	Length [mm]	Mass [g]
Specimen 1	1	100.05	3.18	150.70	-
	2	99.95	3.15	150.70	-
	3	99.95	3.16	150.90	-
	4	99.85	3.12	-	-
	5	99.80	3.13	-	-
	6		3.14	-	-
	7		3.14	-	-
	Mean value	99.92	3.15	150.77	
	St. Deviation	0.10	0.02	0.12	
Specimen 2	1	100.00	3.17	150.60	-
	2	99.95	3.15	150.60	-
	3	99.90	3.14	150.65	-
	4	99.90	3.11	-	-
	5	99.85	3.11	-	-
	6		3.13	-	-
	7		3.14	-	-
	Mean value	99.92	3.14	150.62	84.11
	St. Deviation	0.06	0.02	0.03	
Specimen 3	1	100.80	3.09	150.60	-
	2	101.00	3.06	150.85	-
	3	101.35	3.06	151.00	-
	4	101.90	3.03	-	-
	5	102.25	3.11	-	-
	6		3.10	-	-
	7		3.11	-	-
	Mean value	101.46	3.08	150.82	84.05
	St. Deviation	0.61	0.03	0.20	

> **MID specimens**

MID	n° measure	Width [mm]	Thickness [mm]	Length [mm]	Mass [g]
Specimen 1	1	100.25	2.90	150.95	-
	2	100.15	2.90	150.60	-
	3	100.00	2.86	150.15	-
	4	99.95	2.84	-	-
	5	99.75	2.85	-	-
			3.66	-	-
			2.90	-	-
	Mean value	100.02	2.99	150.57	
	St. Deviation	0.19	0.30	0.40	
Specimen 2	1	100.70	2.95	150.60	-
	2	100.65	2.90	150.55	-
	3	100.60	2.88	150.55	-
	4	100.50	2.87	-	-
	5	100.35	2.84	-	-
			3.54	-	-
			2.94	-	-
	Mean value	100.56	2.99	150.57	78.97
	St. Deviation	0.14	0.25	0.03	
Specimen 3	1	100.40	2.86	151.00	-
	2	100.55	2.84	150.70	-
	3	100.65	2.84	150.10	-
	4	101.15	2.82	-	-
	5	101.20	2.76	-	-
			2.95	-	-
			2.92	-	-
	Mean value	100.79	2.86	150.60	77.57
	St. Deviation	0.36	0.06	0.46	

> **INT specimens**

INT	n° measure	Width [mm]	Thickness [mm]	Length [mm]	Mass [g]
	1	97.10	2.87	150.75	-
	2	97.20	2.97	150.45	-
	3	97.20	2.96	150.00	-
	4	97.10	2.94	-	-
Specimen 1	5	97.00	2.94	-	-
	6		2.97	-	-
	7		2.93	-	-
	Mean value	97.12	2.94	150.40	76.03
	St. Deviation	0.08	0.03	0.38	
	1	97.15	2.96	151.10	-
	2	97.30	2.97	150.80	-
	3	97.35	2.98	150.00	-
	4	97.50	2.98	-	-
Specimen 2	5	97.60	2.94	-	-
	6		3.01	-	-
	7		2.95	-	-
	Mean value	97.38	2.97	150.63	77.5
	St. Deviation	0.18	0.02	0.57	
	1	100.25	2.94	150.45	-
	2	99.55	2.94	150.15	-
	3	99.10	2.96	149.80	-
	4	99.05	2.95	-	-
Specimen 3	5	99.20	2.91	-	-
	6		2.94	-	-
	7		2.88	-	-
	Mean value	99.43	2.93	150.13	77.6
	St. Deviation	0.50	0.03	0.33	